small method
www.small-methods.com

A Chronicle Review of Nonsilicon (Sn, Sb, Ge)-Based Lithium/Sodium-Ion Battery Alloying Anodes

Suzhe Liang, Ya-Jun Cheng, Jin Zhu, Yonggao Xia,* and Peter Müller-Buschbaum**

Since the commercialization of lithium-ion batteries (LIBs) in the early 1990s, tin (Sn), antimony (Sb), and germanium (Ge)-based anodes have attracted considerable research interest as promising candidates for next-generation LIBs due to their high theoretical capacities, suitable operating voltages, and natural abundance. Additionally, the awareness of limited global lithium sources promoted the renaissance of sodium-ion batteries (SIBs) in recent years. Sn, Sb, and Ge can electrochemically alloy with sodium and are regarded as promising anode candidates for high-performance SIBs. However, these alloying/dealloying anodes suffer severe volume expansion during lithiation or sodiation processes, which is one of the biggest obstacles toward practical applications. In order to solve this problem, several strategies are developed including reducing the absolute size of particles, creating interior void space, and introducing buffer media. After more than two decades' efforts, the electrochemical performance of Sn, Sb, and Ge-based anodes is significantly improved. Considerable studies about Sn, Sb, and Ge-based anodes are summarized in a chronicle perspective and the brief development histories of the three anodes are outlined. With this unique review, light will be shed on the future trends of the studies on the Sn, Sb, and Ge-based anodes for advanced rechargeable batteries.

1. Introduction

In modern life, portable digital products are indispensable, e.g., mobile phones, laptops, digital cameras, which are not only personal entertainment media but also significant productivity tools for the society.[1,2] Additionally, in recent years, electric vehicles (EV) and hybrid electric vehicles (HEV) have become the most popular and fascinating types in the market, due to their advanced driving technologies, fuel economy and zero emission.[3–5] Both traditional and emerging automobile enterprises are investing considerable resources to develop the new-energy vehicles. Moreover, the imminent exhaustion of fossil fuel resources and increasing environmental problems influence every corner of the Earth, which needs clean energy to improve such predicament.[6,7] At present, solar and wind energy have been developed to a mature stage and applied globally. However, how to integrate these renewable but inconstant energies into electrical supply grids smoothly and safety is still a big challenge.[8] Therefore, developing low-cost, large-scale electrical energy storage (EES) is considered as the necessary strategy and key enabler for future smart and green grids.[9,10] All these products need a high energy density power source for longer endurance time and better efficiency. The invention of the lithium-ion battery (LIB) in the 1990s started a new era, and a better portable power source has always been the persistent pursuit for both academic and industrial worlds in the following years. The birth of LIB endured several tens of years coupled with the efforts from top scientists all over the world.

1.1. Emergence of lithium-Ion Batteries and Sodium-Ion Batteries

Lithium (Li), the first metal element on the periodic table of elements, has a low atomic weight (6.941 g mol^{-1}), a small ionic

S. Liang, Prof. P. Müller-Buschbaum
Lehrstuhl für Funktionelle Materialien
Physik-Department
Technische Universität München
James-Franck-Str. 1, Garching 85748, Germany
E-mail: muellerb@ph.tum.de

The ORCID identification number(s) for the author(s) of this article can be found under https://doi.org/10.1002/smtd.202000218.

DOI: 10.1002/smtd.202000218

S. Liang, Prof. Y.-J. Cheng, Prof. J. Zhu, Prof. Y. Xia
Ningbo Institute of Materials Technology & Engineering
Chinese Academy of Sciences
1219 Zhongguan West Rd, Zhenhai District, Ningbo, Zhejiang Province 315201, P. R. China
E-mail: chengyj@nimte.ac.cn; xiayg@nimte.ac.cn
Prof. Y.-J. Cheng
Department of Materials
University of Oxford
Parks Rd, Oxford OX1 3PH, UK
Prof. Y. Xia
Center of Materials Science and Optoelectronics Engineering
University of Chinese Academy of Sciences
19A Yuquan Rd, Shijingshan District, Beijing 100049, P. R. China
Prof. P. Müller-Buschbaum
Heinz Maier-Leibnitz Zentrum (MLZ)
Technische Universität München
Lichtenbergstr. 1, Garching 85748, Germany

radius (0.76 Å), a low density (0.53 g cm^{-3}) and a low redox potential (E° = −3.04 V vs standard hydrogen electrode).[11,12] Due to these characteristics, lithium has a great potential to realize high energy-density electricity storage systems. U.S. military and National Aeronautics and Space Administration (NASA) started to investigate Li-based rechargeable batteries since the 1960s.[13–18] These batteries used Li metal anode, transition metal halide cathode such as CuF_2, $CuCl_2$, $AgCl_2$, etc., and nonaqueous electrolytes. Various battery systems had been studied. However, their electrochemical performance and operation life were far from satisfying practical applications due to an unstable lithium anode and irreversibility of cathode materials. Until the 1970s, the primary lithium battery was successfully commercialized after a huge number of investigations, using solid cathodes (such as CuO and V_2O_5).[19–22] Primary lithium batteries were applied in various fields because of high energy density, long shelf life, and lightweight. However, how to make lithium recycle efficiently was still a big challenge at that time. In the middle of the 1970s, the concept of electrochemical intercalation and its potential applications were firstly proposed.[23,24] Based on this concept, a new secondary lithium battery was developed by Exxon with a TiS_2 cathode, which presented a good reversibility. However, uncontrollable growth of lithium dendrites at the interface between metallic Li and the liquid electrolyte could lead to severe safety problems. In 1977, researchers from Exxon used lithium–aluminum (Li–Al) anodes to replace Li metal, fabricating the Li–Al/TiS_2 battery without the Li dendrite problem.[25] Unfortunately, the volume change of Al during charge and discharge cannot be alleviated effectively at that time.

In the following years, the development of cathode materials of lithium batteries gained great progress based on the intercalation concept.[26–31] Transition metal oxides were demonstrated to have good stability and high potentials toward lithium, such as $LiCoO_2$ (LCO), which were regarded as promising cathode candidates for lithium batteries. However, the development of anodes encountered many difficulties.[12] Until the mid-1980s, carbonaceous materials were proved to accommodate Li ions with a high reversibility.[32–38] Besides, with other advantages of low reaction potential (<1.0 V vs Li/Li^+) and small volume change during cycling, carbon materials were considered as an ideal choice of anodes which was researched for many years by countless researchers. The discovery of intercalation carbon material could be regarded as a milestone in the history of LIBs. In 1986, Yoshino and his colleagues created a new battery system, using $LiCoO_2$ as the cathode and carbonaceous material as the anode, and named after LIB.[39–41] Based on the prototype by Yoshino, Sony successfully commercialized the LIB in the 1990s.[42] Until now, various types of LIB have been applied in different fields all around the world. Especially consumer electronics, assisted with advanced batteries, are changing human life nowadays.

Similar to the LIB, the evolution of the sodium-ion battery (SIB) is also based on the sodium metal battery. Early in the 1960s, studies on high-temperature Na-based batteries started. A kind of ceramic material, sodium β-alumina ($Na_2O \cdot 11Al_2O_3$), was found to present high ionic conductivity for Na ions at high temperature in 1976.[43] This discovery indicated that sodium β-alumina could act as a promising solid electrolyte in high-temperature electrochemical cell. Based on this finding, two kinds of high-temperature sodium batteries, Na–S[44,45] and Na–metal chloride,[46,47] were developed in the following years and successfully commercialized in utility-based load-leveling and peak-shaving applications.[9] The more widespread civilian application requires a Na-based battery operating at ambient temperatures. Using Na ions as charge carriers for electrochemical energy storage at normal temperature emerged in

Ya-Jun Cheng is a professor in the Institute of Materials Technology in Ningbo Institute of New Energy Technology and Engineering, Chinese Academy of Sciences. He received a B.S. degree from Peking University, China, followed by a Master degree from the University of Siegen, Germany, and completed Ph.D. studies at the Max-Planck Institute for Polymer Research in Mainz, Germany. From 2015 to 2017, he conducted research at the Department of Materials at the University of Oxford sponsored by the Marie Sklowdowska-Curie Fellowship from the EU. His research interests focus on polymer/inorganic nanohybrids for advanced battery applications.

Yonggao Xia is a professor in the Institute of New Energy Technology in Ningbo Institute of Materials Technology and Engineering, Chinese Academy of Sciences, heading the research group of Novel Organic Electrolyte and Its Devices. He received his Ph.D. in energy and materials science from Saga University, Japan, in 2008. His research interests focus on advanced materials and technologies for lithium-ion batteries.

Peter Müller-Buschbaum is a full professor in the Physics Department of Technical University of Munich, Germany, heading the Chair of Functional Materials. Moreover, he is the scientific director of the Munich neutron source FRM-II and scientific director of the Heinz Maier Leibnitz Zentrum MLZ. His research interests cover polymer and hybrid materials for energy and sensing applications with a special focus on thin films and nanostructures, including kinetic, in situ, and in operando experiments.

the 1980s, following the research wave of LIBs.[48] Similarly, the sodium insertion materials (such as TiS_2, $TiSe_2$, ZrS_2, VS_2), sodium-containing layered oxides (such as Na_xCoO_2), and 1D chain-type compounds (such as NbS_2Cl_2, MoS_2Cl_2) were discovered and investigated as cathode materials for sodium batteries since the 1980s.[49–52] It seemed that the real SIB would be developed and could realize commercialization soon, synchronized with the LIB. However, in the following decades, related studies about SIBs almost disappeared from mainstream sights. This could be attributed to the lower energy of SIB (compared to LIB) and a lack of appropriate anode materials for SIBs.[48] The flourish of investigations about LIBs is mainly caused by the discovery of carbonaceous material-based anodes (especially graphite). However, graphite was found to be no good insertion host for sodium ions.[53,54] Due to the awareness of the limit of lithium resources globally, the number of the related reports about SIBs started to increase from the 2010s.[7,55–57] However, the commercialization of the SIB is still under way.[58]

1.2. Development and Challenges of Anode Materials for Lithium-Ion Batteries and Sodium-Ion Batteries

Although graphite anodes promoted LIBs into a fast development stage, it is not an ideal anode candidate due to a relatively low specific capacity and safety concerns.[59–61] Because of high specific capacities and safety characteristics, alloy-type LIB anodes attracted much attention since the 1990s. Different from insertion/desertion mechanism of carbon-based anodes, some metal and metalloid materials can react electrochemically with lithium to from alloys.[62] A number of metal materials are reactive toward lithium and have been studied as LIB anodes, such as Si, Sn, Sb, Ge, Al, Mg, and Bi.[61,63] Among these, silicon anodes gained the most attention due to the highest gravimetric capacity (4200 mAh g^{-1}) and appropriate discharge voltage (≈0.4 V in average).[64] Moreover, a few main group metals (Sn, Sb, Ge), and metal oxides (or sulfides, phosphides) can also react with Li and present high specific capacities.[65,66] However, all these anode materials suffer from the same drawback of large volume change during charge and discharge, leading to pulverization of the electrode material, a repeated growth of the solid electrolyte interface (SEI) film, and a rapid capacity fading.[67,68] Until now, three main strategies have been developed to overcome the adverse effects originating from the volume expansion of the alloy-type anodes: i) reducing the absolute size of the active material particles;[69] ii) compositing active materials with carbonaceous materials (or noncarbonaceous materials) or forming alloys to provide a cushion matrix to buffer the volume change;[70–73] iii) creating void space inside the active materials to accommodate the volume change.[74,75] In most reports, combining two or all of these three strategies is applied to gain a better electrochemical performance.

With the renaissance of research about SIBs, studies of anode materials for SIBs were also restarted and gradually reached a peak point since 2010s.[48] Similar to those in LIBs, alloy-type anodes are also in the main focus for achieving high-performance SIBs. However, the "crown" anode material for LIBs, silicon, cannot form a Na-rich phase when it electrochemically reacts with sodium.[76–78] Therefore, nonsilicon (especially

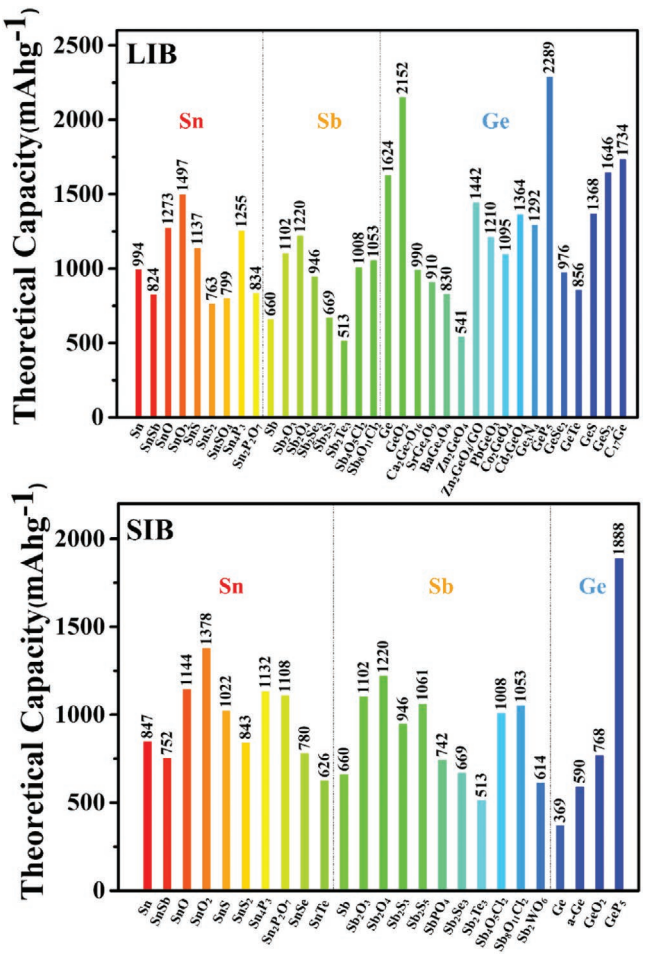

Figure 1. Various anode materials for LIBs and SIBs addressed in this review and their corresponding theoretical capacities.

Sn, Sb, Ge)-based anode materials for SIBs embraced a golden development period in the past ten years.[79] The alloy-type anodes for SIBs also encountered the big challenge of volume change during cycling, which is even worse than that in the LIBs due to a larger radius of the Na ions (1.02 Å)[66]. With abundant experience from LIBs, a large number of alloy-type anodes for SIBs were synthesized and good results were generated.[79,80]

For both, LIBs and SIBs, nonsilicon (Sn, Sb, Ge)-based anodes are promising candidates for achieving high energy density electrochemical energy storage in the future. As claimed by the Emperor Taizong of Tang Dynasty, "History is a mirror that can reflect the vicissitude of society," retrospective and introspection of history benefit us to explore the unknown and create new things in the future. Previously, silicon-based LIB anodes have been reviewed in a chronicle perspective by our groups[64] In the present review, the development history of nonsilicon (Sn, Sb, Ge)-based anodes for both LIBs and SIBs will be reviewed. The review is divided into three parts: Sn, Sb, Ge-based anodes for rechargeable batteries. In every single part, various types of anodes will be systematically reviewed according to a chronological order. Different active materials of LIBs and SIBs anodes will be discussed later and corresponding theoretical capacities are summarized in **Figure 1**.

2. Tin-Based Anodes for Rechargeable Batteries

Tin or Stannum (Sn), which belongs to IVA, can electrochemically react with lithium to form various alloys. In 1971, Dey found that lithium metal can alloy with various metals including Sn, Pb, Al, Au, Pt, Zn, Cd, Hg, and Mg in an organic electrolyte electrochemical cell at ambient temperature, and systematically analyzed the products of cathodic reactions.[81] This research built the foundation of an implement of alloy-type anodes for LIBs. The reacting behavior of Li and Sn was studied as early as 1910, where the existence of compounds such as Li_4Sn, Li_3Sn_2, Li_2Sn_5 was identified.[82] In the following years, various physical and electrochemical parameters of Li_xSn ($0.4 \le x \le 4.4$) were systematically investigated.[83–86] Particularly, when $x = 4.4$, the formation of the lithium-rich phase $Li_{22}Sn_5$ generates a total theoretical capacity of 994 mAh g^{-1}, which is the highest among various Li–Sn alloys.[87] The reaction equation between Sn and Li is as followed

$$5Sn + 22Li^+ + 22e^- \leftrightarrow Li_{22}Sn_5 \quad (1)$$

Moreover, Sn could also electrochemically react with Li to form a Na-rich phase $Na_{15}Sn_4$ according to Equation (2), exhibiting a theoretical capacity of 847 mAh g^{-1}[88]

$$4Sn + 15Na^+ + 15e^- \leftrightarrow Na_{15}Sn_4 \quad (2)$$

Due to high theoretical capacity, Sn and Sn-based anode materials for LIBs and SIBs received particular attention. However, volume expansion of Sn in during cycling LIB and SIB could reach 259% and 423%, respectively.[48,89] Volume expansion has been the core point of the investigations about Sn-based anodes since the original stage.

2.1. Tin Alloy-Based Anodes for Lithium-Ion Batteries

After the birth of LIBs, several methods had been developed for synthesizing Sn alloys based anodes, such as electroplating or electrolytic deposition,[90,91] chemical reaction[92] and mechanical alloying by ball-milling.[93,94] Generally, the tin alloy-based anode consisted of an active phase (Sn) and an inactive phase (M). In the process of charging and discharging, Sn plays an active site to react with Li according to Equation (1), while the inactive phase could act as a cushion for accommodating volume change of Sn.[92] It was demonstrated that the cyclic stability of the electrode can be improved significantly, if the active phase was finely mixed with an inactive phase in a composite matrix.[90,92,95] Since the 1990s, a large number of reports about Sn alloy-based anodes has been published.[89,96–98]

2.1.1. Emergence Stage: Before 2000

Initially, limited by technology and technics, the electrochemical performance of the tin alloy-based anodes was not good. In 1990s, studies focused on Sn alloy-based anodes emerged and gained some progress. Although to some extent an alloy material can accommodate the volume expansion of Sn in the charging/discharging process, its electrochemical performance was still not good enough for applications. Therefore, researchers proceeded with their efforts to improve the performance of Sn alloy-based anodes.

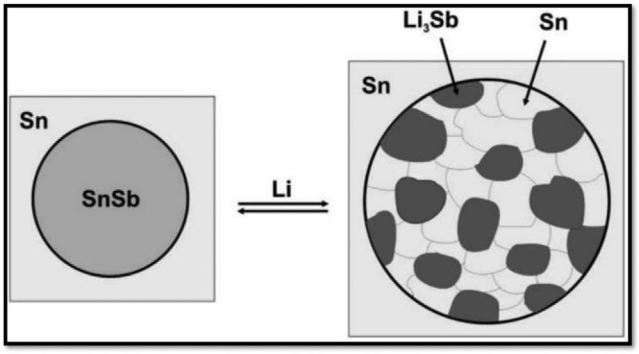

Figure 2. Model showing the lithiation of a sub-microstructured multiphase material, which contains an intermetallic, for the example of Sn/SnSb. Reproduced with permission.[100] Copyright 2001, Elsevier Science B.V.

When alloying and dealloying with lithium, some properties of the host metal, such as particle size, morphology, porosity etc., can affect the structural stability and cycling behavior of the cells.[90,95] In 1996, Besenhard and co-workers for the first time investigated the influence of tin and the tin-alloy particle size on the cycling behavior in standard organic solvent Li^+-electrolytes.[90] Although the small particle size of the tin-alloy anode exhibited a better electrochemical performance than that of a larger one, it still suffered from a few drawbacks, such as moderate cycling stability and low initial Coulombic efficiency (ICE). Before long, Besenhard's group synthesized a new "Sn/SnSb" composite as LIB anode, and analyzed its properties in details in a series of reports.[99–101] In terms of cycling stability, the Sn/SnSb composite anode outperformed the pure Sn anode. According to an explanation of Besenhard, the single-phase host (Sn), which is completely wetted by the electrolyte in cells, begins to react with lithium at the same potential. However, in a multiphase Sn/SnSb, each phase has a different reaction activity with lithium under different potentials. The more-reactive phase (SnSb) can react with lithium first at 800–850 mV, whereas the subreactive phase (Sn) does not react at this potential. Thereby, the unreacted Sn can act as a matrix and buffer expansion of the first generated phase (Li_3Sb). With a generation of Li_3Sb, Sn segregates from SnSb. After continuous alloying/dealloying and segregation, the original SnSb domain is converted into a nanostructured "mosaic" of Li_3Sb and Sn domains, which is displayed in **Figure 2**. Besides, the continuous phase segregation and restoration during cycling can restrain the aggregation of Sn, which alleviates volume expansion and improves cycling stability. In 2001, Besenhard's team synthesized a Sn/SnSb composite electrode (82 wt% Sn/SnSb, 10 wt% Ni, 8 wt% polyvinylidene difluoride (PVDF)), which can remain a reversible capacity of about 450 mAh g^{-1} after 50 cycles.[100]

2.1.2. Preliminary Stage: 2000–2006

At the beginning of the new century, the study of Sn alloy-based anodes also entered a new period. The number of the published studies increased compared with those in the 1990s. Before

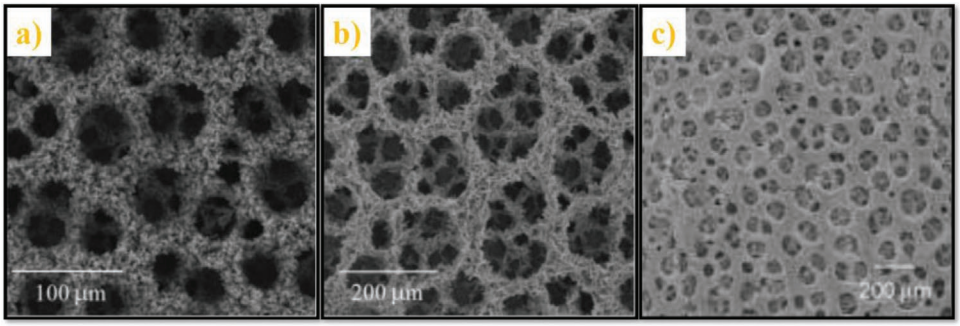

Figure 3. Typical SEM images of 3D porous a) Cu and b) Sn. Reproduced with permission.[129] Copyright 2003, Wiley-VCH. Typical SEM image of 3D porous c) Cu-Sn alloy. Reproduced with permission.[114] Copyright 2005, Wiley-VCH.

2000, most studies about Sn alloy-based anodes chose the SnSb alloy as the active material. After 2000, the type of the Sn alloy was diversified, and some novel Sn alloys emerged, such as Sn–Ca,[102] Sn–Mg,[103] Sn–Cu,[104–115] Sn–Ni,[116–120] Sn–Ag,[73] Sn–Zn,[72] and Sn–Co.[121–124] Besides, various ternary alloys also gained more attention in the new century.[125–128] With new materials and strategies better performance was achieved than before in terms of either reversible capacity or cycling stability.

Copper (Cu), as an inactive phase in the Sn–Cu alloy, can reduce the damage of the electrode due to the volume expansion of Sn and improve reversible capacity. Additionally, Cu has excellent electrical properties and also a low oxidation potential, which are beneficial for the electrochemical performance.[92] Therefore, the Sn–Cu system received much attention in this period. In 2003, Shin reported a unique method to synthesize 3D free-standing foams of metal (such as Cu and Sn) with highly porous ramified (dendritic) walls,[129] as shown in **Figure 3**a,b. This method combined electrochemical deposition with hydrogen evolution. By 2005, Shin and his colleges applied this technique to 3D porous Cu_6Sn_5 intermetallic as anodes for LIBs.[114] As presented in Figure 3c, the unique structure of the Cu_6Sn_5 alloy could not only accelerate the transport of Li ions between the electrolyte and the electrode, but also speed up electrochemical reactions. As a result, this porous Cu_6Sn_5 alloy anode delivered a reversible capacity of about 400 mAh g^{-1} up to 30 cycles and maintained capacity retention of about 50% of the capacity of 1C (1C = 0.5 mA cm^{-1}) (in this review, we try to report the current density by the international system of units (mA g^{-1} or mA cm^{-1}) as possible as we can. If there is vacancy, it indicates that we do not find the relative description in the original reports) rate when tested at a high current density of 20C.

Nickel (Ni), the neighbor of Cu in the periodic table of elements, also received attention as an electrochemical-inactive phase in Sn alloys. Different groups developed various methods to synthesize Sn–Ni alloy anodes, such as high-energy ball-milling,[117–119] chemical synthesis,[130] and electrodeposition.[131,132] In 2005, Cheng prepared Ni_3Sn_4 alloy through high-energy ball-milling, and the alloy was further electroless plated with Cu to form a composite.[117] The Ni_3Sn_4 alloy featured irregular particles of less than 2 μm size, and small Cu particles were plated on the surface of Ni_3Sn_4 the alloy. In 2004, Dong et al. synthesized Ni_3Sn and Ni_3Sn_2 by altering the molar ratio of the reactants in a hydrogen reduction process.[130] In 2003, Osaka's team prepared a series of Sn–Ni thin film anodes with different Sn/Ni ratios by using a different ratio of the reactants when electrodepositing.[132] In 2005, based on their previous work, Osaka's team further investigated structural changes during charge–discharge cycling of Sn–Ni alloys with different compositions.[131] All these Sn–Ni alloy anodes exhibited an enhanced electrochemical performance.

In contrast to Cu and Ni, which act as inactive phases in Sn alloy-based anodes, silver (Ag) is active toward Li. From 2003 to 2005, a series of studies about Sn–Ag system were made by Sakai's team.[126,127,133–135] It was found that the Sn–Ag composite system with suitable composition presented high capacity and long cycle life. In 2003, new Sn–Ag alloys were prepared by Sakai's group through mechanical alloying technique (high-energy ball-milling).[73] After optimizing compositions, it was found that the $Ag_{46}Sn_{54}$ and $Ag_{52}Sn_{48}$ alloy anodes exhibited the best capacity retention, maintaining a reversible capacity of above 350 mAh g^{-1} after more than 50 cycles.

2.1.3. Fast Development Stage: 2007–2011

In this period, the development of nanotechnology and material science provided new strategies and buffering materials to tin-based alloy anodes. It has been demonstrated that decreasing particle sizes into the nanoscale or creating hollow structures inside materials are effective to accommodate the volume change. Since 2007, this strategy has gained much progress, and various nanoscale and nanostructured (3D, porous, core–shell structures and others) Sn alloy-based anodes were synthesized. In this stage, carbon material also gained increasing popularity, and some novel carbon materials (carbon nanotube (CNT), graphene (G)) appeared. Besides, investigations on the microstructured materials, mechanism, improvement and optimization for traditional Sn-alloy materials also attracted much attention.

Nanostructured Tin Alloy-Based Anodes: Various methods have been developed for obtaining Sn alloy nanoparticles (NPs), such as high-energy ball-milling,[119,136,137] electrodeposition,[138,139] vapor deposition,[140] reductive precipitation,[100,108,128,141] and hydrothermal or solvothermal synthesis.[142] In this period, nanoscale Sn alloy-based anodes were still highlighted by researchers. In 2007, Ren's team synthesized nanometer Cu–Sn alloy anodes for LIBs by a reverse microemulsion technique.[143] Microemulsion synthesis, based on a microemulsion solution consisting of a hydrophilic phase, a hydrophobic phase, and stabilizing surfactants, is a simple and useful method for adjusting and controlling particle size. In a reverse microemulsion solution, water is the dispersed phase in a continuum of oil. Various reactants could be restrained by individual reverse

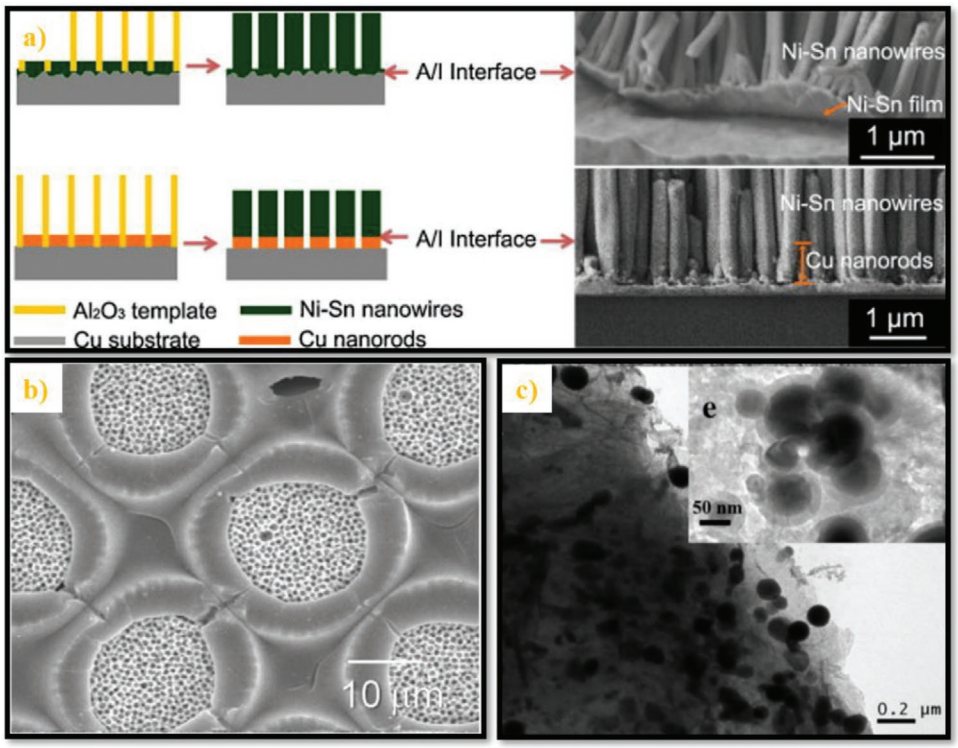

Figure 4. a) Schematics and FE-SEM images of Ni–Sn nanowire arrays with different bonding materials at base: Ni—Sn bonding and Cu bonding. Reproduced with permission.[146] Copyright 2011, Elsevier B.V. b) SEM image of highly patterned cylindrical Ni–Sn alloys with 3DOM structure prepared by colloidal crystal templating method combined with electroplating method using photoresist substrate. Reproduced with permission.[150] Copyright 2010, Elsevier Ltd. c) TEM image of GNS-supported Sn–Sb@carbon particles. Reproduced with permission.[151] Copyright 2010, Elsevier Ltd.

micelles and acting as microscopic reactors, the controllable nanosized particles may be obtained due to exchange reactions between different micelles. Particularly, in this study, the prepared Cu–Sn alloy with the particle size of 50–60 nm displayed a reversible capacity of 300 mAh g^{-1} after 50 circles at a current density of 0.3 mA cm^{-2}.

Using various templates is a usual way to build 3D nanostructured materials, such as Cu/Al_2O_3 nanoarrays, Ni nanocones and so on.[144,145] In 2011, Tian et al. fabricated Ni–Sn nanowire arrays directly on current collectors with the assistance of porous anodic alumina (PAA) templates.[146] The authors focused on the different active/inactive interfaces (A/I interfaces) of Ni–Sn nanowire arrays and investigated the effect of A/I interfaces on electrochemical performance. Two different samples with different A/I interface were synthesized through altering electrodeposition conditions. As shown in **Figure 4**a, Ni–Sn alloy or Cu served as different bonding materials for different Ni–Sn nanowire on Cu substrate samples. The first sample had a large continuous A/I interface, while the A/I interface of the second one was reduced to nanoscale islands on top of Cu nanorods. In terms of cycling performance, the sample with Cu bonding outperformed the one with Ni—Sn bonding. In case of the sample with Cu bonding, the A/I interface area was decreased to nanoscale, which could significantly reduce large strain mismatch result from the continuous Ni–Sn A/I interface and thus improved the electrochemical performance. In addition, the influences of Ni–Sn nanowire diameter and composition on the electrochemical performance were also investigated in this report.

In 2010, Zhang et al. developed a novel nickel nanocone-array (NCA) as a template for building nanostructured anode materials.[147] In 2011, the NCAs were introduced in Sn-based anode systems.[144,148] The nanoarchitectured Sn–Co alloy electrode was prepared by electrodepositing Sn–Co alloy onto the nickel nanocone-array.[148] Core–shell Sn alloy-based anodes with noncarbon-based shell also appeared during this period. In 2010, Cho's team synthesized 10 nm sized core–shell Sn–Cu nanoalloys as anodes for LIBs via redox transmetalation reactions.[149] The Sn@Cu core–shell electrode presented a good rate performance due to its highly conductive copper shell. It could reach a specific capacity of about 680 mAh g^{-1} at 5C (1C = 660 mA g^{-1}), corresponding to ≈94% capacity retention based on the capacity of the first cycle. During the cycling test, this anode could keep capacity retention of 84% after 170 cycles, under a rate of 0.8C. The inactive copper shell could not only improve the conductivity of electrode but also act as a strong constraint to volume change from the active tin.

Microstructured Tin Alloy-Based Anodes: Compared to nanosized materials, micrometer scale anode materials have some advantages, such as simpler synthesis and fewer side reactions. Generally, the methods for preparing micrometer-sized Sn alloys include melting-alloying process, carbothermal reduction of metal oxides and others.[152,153] In 2008, Simonin et al. prepared micrometer-sized SnSb particles with a simple method including melting tin and antimony ingots and casting them together.[154] Micrometer-sized Sn–Cu alloy thin film anodes were prepared through electron-beam evaporation by Zhu's

group.[155] The stable cycling performance of this anode could be only obtained within first 30 cycles. The electrochemical performance of the micrometer-sized Sn alloy-based anodes was not comparable to that of nanosized anodes.

However, creating some microstructures inside anode materials is effective for improving the electrochemical performance of the Sn alloy-based anodes. Copper and nickel foams are favorable skeletons to build 3D porous materials.[145,156–159] The foam not only acted as a template but also served as the current collector. In 2009, Sun' team prepared a 3D porous Sn–Ni alloy anode with reticular structure through electroplating on Cu foam.[156] In 2011, Sun's team upgraded the method for synthesizing the copper foam and prepared a 3D porous Sn–Co alloy anode.[158] According to this work, an electroless plating method was developed for the first time to produce 3D porous Cu film with pore size ranging from nanoscale to microscale. Compared to the electroplating method, this way produced 3D porous Cu foam owning good adhesion to the substrate, but without thermal treatment. At the same year, Goodenough's group prepared a Sn–Co alloy film anodes supported by a Ni foam.[145] Like copper foam, the foamed nickel had a 3D porous structure and presented a high specific surface area.

Except for metal-based materials, nonmetallic materials were also used as the templates to build microstructured anodes, such as polystyrene (PS) beads.[150,160,161] In 2010, highly patterned cylindrical Ni–Sn alloy anodes with 3D ordered macroporous (3DOM) structure were prepared using monodispersed polystyrene bead and photoresist substrate as templates,[150] as presented by Figure 4b. Photoresist substrates had highly patterned holes within a circular region of 1 cm diameter, and the PS beads with the size of 1.0 μm diameter were injected into these holes on the photoresist substrate under pressure. During this process, the PS spheres assembled spontaneously into an ordered lattice in the holes of the photoresist substrate. The void space between the PS beads was 26%. Then, the Sn–Ni alloy was electroplated into the void space, and the PS templates were removed by immersing in toluene. The 3DOM cylinder structure of Ni–Sn alloy electrode was effective for buffering large volume expansion and keeping electrodes intact during the charge and discharge processes, leading to enhanced cycling stability.

Tin Alloy/Carbonaceous Material Composite Anodes: Using carbon materials to buffer a large volume expansion of tin is not new in the Sn alloy-based anode studies. As early as 2002, Sn-alloy/graphite composites were prepared and explored as anodes for LIBs.[162,163] However, the combination of Sn-alloys and a carbon matrix, as well as a variety of carbonaceous materials became diversified in this period. Sn-alloy/carbon composites could be obtained by coating carbon layers onto the Sn alloys[164–166] or encapsulating Sn-alloy particles into carbon matrix.[167–169] Various carbon-based materials were applied to prepare such composites, such as amorphous carbon,[170–172] graphite,[173,174] graphene,[151] carbon nanofibers (CNFs) or carbon nanotubes,[175–178] and so on.

In 2009, Xia's team synthesized core–shell carbon-coated nanoscale Cu_6Sn_5 anodes via an in situ polymerization method combined with surface modification.[166] Firstly, the nanosized Cu_6Sn_5 particles were synthesized through a sodium borohydride reduction method as a starting material. After the surface modification process and carbonization at high temperature, the carbon-coated Cu_6Sn_5 nanoparticles were obtained. The final particle size of Cu_6Sn_5 was ≈20–30 nm and the thickness of the carbon layer was ≈5 nm. This Cu_6Sn_5/C composite electrode exhibited good cycling performance, which maintained a reversible capacity of 405 mAh g^{-1} after 50 cycles at a current density of 100 mA g^{-1}. The well-coated carbon layer played a key role for improving the electrochemical performance of this composite anode. It could not only protect the low melting point tin–copper alloy but also prevent aggregation and pulverization of nanoparticles during the lithiation/delithiation process. Encapsulating Sn alloy nanoparticles into a continuous carbon matrix is another effective way to obtain high-performance Sn-alloy/carbon composite electrodes. In 2009, a SnSb/C nanocomposite anodes were synthesized by the Hassoun's group, where SnSb alloy nanoparticles were embedded into an amorphous carbon matrix.[170] The nanostructured composite was prepared by a sol–gel method followed by calcination under an inert atmosphere, which had been reported by Hassoun's team in earlier time.[179]

Most of carbon layers and matrices mentioned in the above studies were amorphous carbon, which mainly originated from pyrolysis of polymers. Other kinds of carbonaceous materials were also applied as buffer matrix during this period. Graphene, a single atomic layer of graphite with 0.34 nm in thickness, has various outstanding properties such as great electrical conductivity, large surface area, good thermodynamic stability and so on.[180–182] It has been demonstrated that those properties of graphene are beneficial to improve the electrochemical performance of LIB anodes.[183–185] In 2010, Wang's group prepared graphene nanosheets (GNS) supporting Sn–Sb alloy and Sn–Sb@carbon nanoparticles, and studied their electrochemical performance as the anodes of LIBs.[151] The GNS was obtained by reducing graphite oxide (GO) under high temperature in nitrogen atmosphere. The GNS-supported Sn–Sb nanoparticles were synthesized through a chemical reduction in the solution containing $SnCl_4 \cdot 5H_2O$, $SbCl_3$, and GNS. The GNS-supported Sn–Sb@C nanoparticles were fabricated by similar reduction process in a solution containing $SnCl_4 \cdot 5H_2O$, $SbCl_3$, and GO, followed by a thermal treatment (Figure 4c). Due to assistance of an extra carbon layer, the Sn–Sb@C/GNS anode exhibited better electrochemical performance.

CNFs and CNTs also attracted much attention in this period because of their good properties and application in LIBs. Carbon nanofibers usually own high surface area, high electrical conductivity, and good mechanical property, which could improve the electrochemical performance of electrode when they are combined with intermetallic materials.[186,187] In 2011, Jung and Lee prepared Ni–Sn/CNFs composite anodes, where Ni–Sn alloy nanoparticles were embedded onto carbon nanofibers.[177] Carbon nanotubes, including single-walled carbon nanotubes (SWCNTs) and multiwalled carbon nanotubes (MWCNTs), are considered as a great nanoscale framework material for electronic devices due to their outstanding mechanical and thermal stability and high electronic conductivity.[188–190] In 2007, Park et al. coated SnSb alloy nanoparticles on the surface of MWCNTs to prepare nanostructured SnSb/CNT composite anodes.[176] This SnSb/CNT nanocomposite anode gained a stable capacity over 480 mAh g^{-1} after 50 cycles

at a current density of 100 mA g^{-1}. The network structure formed by CNTs could not only anchor SnSb nanoparticles to prevent them from agglomeration but also maintain the electrical connection around the SnSb nanoparticles.

Other Studies about Tin Alloy-Based Anodes: Through a large number of studies for many years, it has been demonstrated that unique microscopic morphology and structure can significantly improve the electrochemical performance of anode materials for LIB. However, there are still various issues worthy of further investigation, except for those focused on morphology and structure. During this period, such studies of Sn alloy-based anodes also attracted much attention, i.e., new synthesis methods for traditional tin-alloy materials,[191–195] electrochemical reactions or mechanisms investigations,[196–200] and kinds of tin-based alloys.[201–203]

Among these studies, the investigations about electrochemical reactions or mechanisms not only provided important complements to the normal researches but also contributed to deeply understand the role and effect of these anode materials in the battery system. In 2008, Lee et al. fabricated Sn–Co/C composite anodes by mechanochemical synthesis and studied its reaction mechanism with lithium through ex situ X-ray diffraction (XRD), high-resolution transmission electron microscopy (HRTEM), and Co–K edge X-ray absorption spectra (EXAFS).[199] It was found that the Co_3Sn_2 phase of the Sn–Co alloy remained during the first cycle but transformed into $CoSn_2$ during the second cycle. In 2010, Sun's group investigated the interfacial processes and reactions of the Sn–Co thin film anode by X-ray photoelectron spectroscopy (XPS) and time-of-flight secondary ion mass spectrometry (ToF-SIMS) measurements.[200] By XPS measurements, the chemical components of the SEI layer were confirmed as a mixture of Li_2Co_3, $ROCO_2Li$, lithium oxalates, and/or ROLi (R refers to alkyl). In addition, an incomplete initial alloying process between Li and Sn was evidenced by ToF-SIMS, which divided the electroplated layer into a highly lithiated outer part (Li_xSn) and an essentially nonlithiated inner part.

2.1.4. Steady Development Stage: Since 2012

Since 2012, the investigation activity about Sn alloy-based anode materials stepped into a steady development period. Constructing nano and microstructures and combining alloys with various carbon materials were still the mainstream strategies for improving the electrochemical performance of these anode materials. Although no distinctly new strategy emerged in this period, more delicate and complicated structures were synthesized to achieve better electrochemical performance.

Nanostructured Tin Alloy-Based Anodes: Nanowire or nanowire-like structure arrays exhibit various advantages when applied as the anode materials for LIBs. In 2012, Yang's team developed a novel Ni–Sn anodes with 3D nanowire networks for LIB, assisted by a defect-containing PAA templates.[204] The straight vertical nanowires were connected with each other by horizontal "bridges" due to nanoindentations of the defect-containing PAA templates (**Figure 5**a), leading to an effective elimination of agglomeration. Particularly, the 40 μm long 3D Ni–Sn nanowire network electrode retained a reversible capacity of about 450 mAh g^{-1} after 60 cycles at 0.2C, whereas the capacity of the 40 μm long straight Ni–Sn nanowire electrodes decreased to lower than 50 mAh g^{-1} after 40 cycles at 0.2C. As discussed above, compared with the structure constructed by isolated 2D materials (i.e., nanowire arrays), continuous 3D framework construction was more to keep electrode intact and finally improved the electrochemical performance. In 2016, Braun' group reported a 3D nickel scaffold supported Ni–Sn alloy structure with good electrochemical performance.[205] Improved cycling stability and rate performance were obtained which were mainly attributed to the firm network structure of the electrode and fast-diffusion pathways of electrons and Li-ions supported by the 3D network. After several-year investigation by Braun's team, building 3D network structure electrode assisted with opal/inverse opal templates has evolved into a universal method to synthesize various high-performance electrodes for LIBs.[206–209]

Compared to the last period, hollow-structured anode materials have gained more popularity since 2012 and various methods have been developed for fabricating hollow structures,[210–219] including template-directed synthesis, chemical reactions and Kirkendall effect-based synthesis. The Kirkendall effect, named after Ernest Kirkendall, refers to the motion of the interface between two metals derived by the different diffusion rates of the metal atoms, which has been widely applied to synthesize hollow-structured materials.[212,220–222] In 2018, micrometer-sized spherical aggregates of Sn and Co components containing core–shell, yolk–shell, hollow nanospheres were synthesized as a high-performance anode material for LIB by Park and Kang, which applied nanoscale Kirkendall diffusion in the large-scale spray drying process.[223] The detailed formation scheme of this unique material is presented in Figure 5b. First, the Co nitrate–Sn oxalate–dextrin composite microspheres were produced through a spray drying process. After heat-treatment at 900 °C under Ar atmosphere, the composite microspheres were reduced into Sn_2Co_3–$Co_3SnC_{0.7}$–C, where ultrafine Sn_2Co_3–$Co_3SnC_{0.7}$ nanoparticles were distributed in an amorphous carbon matrix. Then, the as-prepared samples were treated under different temperatures. When treated at 300 °C in air, the Sn_2Co_3–$Co_3SnC_{0.7}$–C composite was converted into porous microspheres consisting of Sn–Sn_2Co_3@$CoSnO_3Co_3O_4$ core–shell nanospheres. The $CoSnO_3$–Co_3O_4 shell was mainly derived from an oxidation process of $Co_3SnC_{0.7}$. Due to a faster diffusion rate of Co^{2+} than that of Sn^{2+} and O_2, the Co components of Sn_2Co_3 could diffuse into the outer surface of nanoparticles to form Co_3O_4 shell, while the original Sn_2Co_3 components were partially reduced into Sn to form the Sn–Sn_2Co_3 core, corresponding to a typical nanoscale Kirkendall effect. With the temperature continuously increased to 400 and 500 °C, the Kirkendall effect was forced toward the positive shift, leading to formation of Sn–Sn_2Co_3@void@$CoSnO_3$–Co_3O_4 yolk–shell structure (400 °C) and the microspheres with $CoSnO_3$–Co_3O_4 hollow nanospheres (500 °C). In terms of electrochemical performance, the sample treated at 300 °C (denoted as Ar900-O300) exhibited the best record. It maintained a reversible capacity of 1265 mAh g^{-1} after 200 cycles at a current density of 1000 mA g^{-1}. The improved performance of Ar900-O300 electrode was related to the robust core–shell structure of Sn–Sn_2Co_3@$CoSnO_3$–Co_3O_4

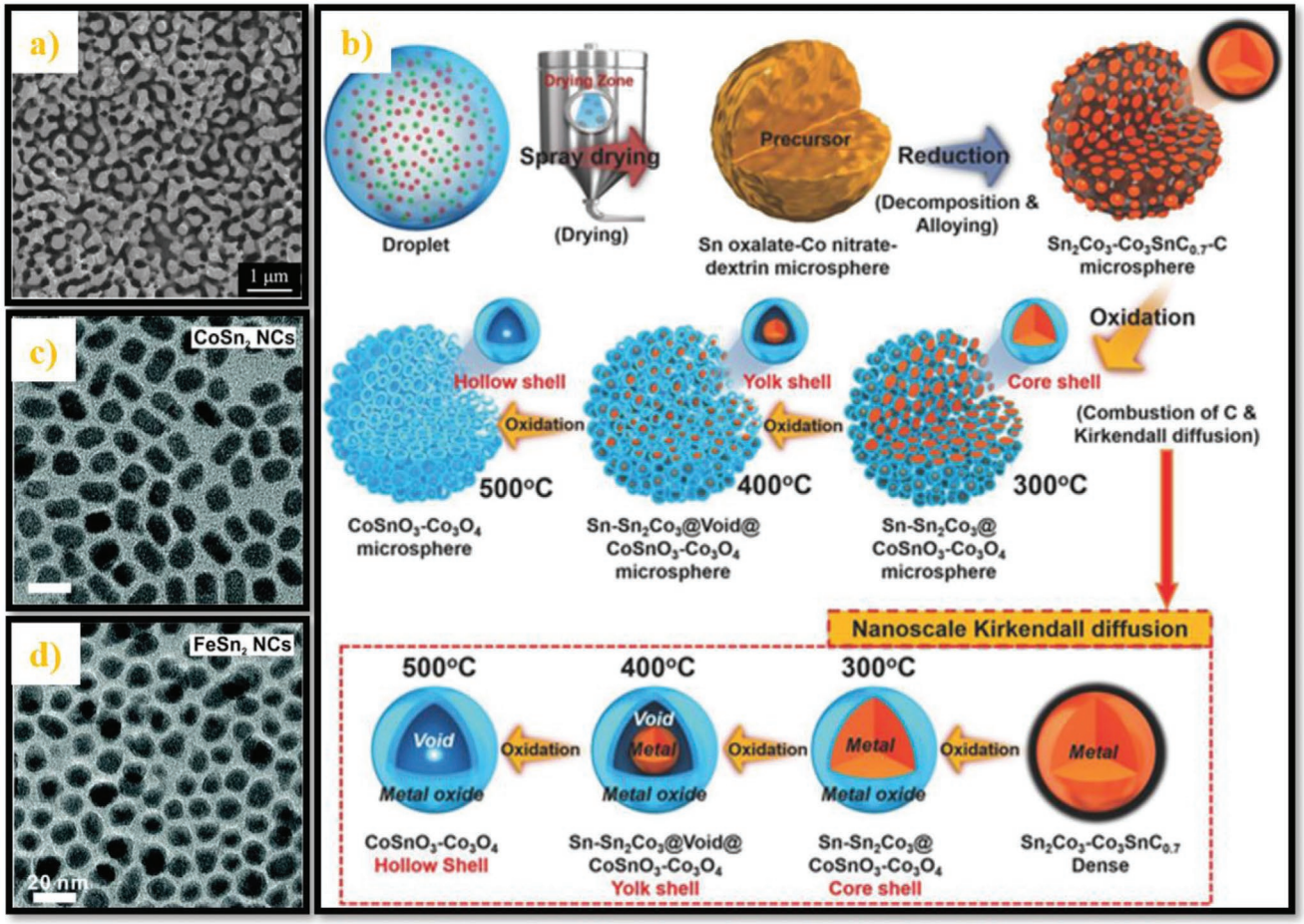

Figure 5. a) Top-view and FE-SEM micrographs of a 20 mm long 3D Ni–Sn nanowire network. Reproduced with permission.[204] Copyright 2012, Elsevier B.V. b) Formation mechanism of the porous microspheres containing Sn–Sn_2Co_3@$CoSnO_3$–Co_3O_4 core–shell, Sn–Sn_2Co_3@$CoSnO_3$–Co_3O_4 yolk–shell, and $CoSnO_3$–Co_3O_4 hollow nanospheres. Reproduced with permission.[223] Copyright 2018, Wiley-VCH. c) TEM images of monodisperse $CoSn_2$ and d) $FeSn_2$ nanoparticles. Reproduced with permission.[224] Copyright 2018, Royal Society of Chemistry.

nanoparticles, which could maintain their primary morphology after numerous lithiation and delithiation cycles. By combing the Ar900-O300 anode with $LiMn_2O_4$ cathode in a full Li-ion battery, a reversible capacity of 482 mAh g^{-1} was achieved after 100 cycles at a current density of 1000 mA g^{-1} based on the anode mass.

Another breakthrough during this period was the successful synthesis of monodisperse Sn alloy nanoparticles, which could effectively limit the agglomeration of nanoparticles and improve performance of the electrode. Since 2012, Kovalenko's team made efforts to synthesize monodisperse Sn-based and Sb-based anode materials.[69,224–231] In 2018, monodisperse $CoSn_2$ and $FeSn_2$ nanocrystals were prepared by them via a facile colloidal synthesis.[224] The as-prepared nanocrystals displayed the monodisperse morphology with size ranged from 5–13 nm, as shown in Figure 5c,d. These nanocrystal electrodes exhibited very stable cycling performance. In addition, the colloidal synthesis has been developed as a universal method by Kovalenko's team, which could be used to prepare various monodisperse inorganic nanoparticles (In, Ga, Bi, Sb, Zn, Cu, Sn, and their alloys) with controllable sizes (5–30 nm).[231]

Microstructured Tin Alloy-Based Anodes: Similar to the last period, studies about microstructured tin alloy-based anodes were still concentrated on porous structure, assisted with Ni or Cu foam frameworks.[232–236] In 2013, Sun's group prepared a 3D-structured Sn–Sb–Co composite where nanoscale alloy particles were deposited on the microporous copper substrate.[237] The porous Cu substrate was fabricated via a typical electroless deposition which had been reported in their previous work.[159] The $C_{14}H_{26}O_2$ (TMDD, 2,4,7,9-Tetramethyl-5-decyne-4,7-diol), as an addition, was added into the electroless deposition solution and played a key role during the formation of the porous copper framework. Hydrogen gas was generated during the deposition process, and the gas bubbles acted as dynamic templates for the formation of porous copper.[238] However, an excess of bubbles could destroy the 3D porous structure. The presence of TMDD was beneficial to sustain the porous structure. Then, the ternary Sn–Sb–Co alloy was electrodeposited on the as-prepared Cu framework, forming the final 3D porous Sn–Sb–Co alloy electrode. The pore size of the alloys could be controlled by changing the electroless deposition time. The shorter time led to a smaller pore size of about 2.3 μm (sample denoted as SnSbCo/Cu–S), while the longer time to the larger

size of around 5.2 µm (sample denoted as SnSbCo/Cu–L). The SnSbCo/Cu–L maintained a stable capacity of 540 mAh g^{-1} after 300 cycles at a 0.2C, corresponding to retention of 79% against the first charge capacity. In contrast, the capacity of SnSbCo/Cu–S faded severely since the 120th cycle, and capacity retention was only 50% after 150 cycles. Such good rate performance was mainly attributed to the 3D network structure and solid adhesion between active materials and copper substrate, which enhanced the diffusion rate of Li-ions.

Tin Alloy/Carbonaceous Material Composite Anodes: Compared with the last timeframe, there was no big breakthrough about the variety of buffering carbon materials after 2012. However, more delicate structures were successfully synthesized, such as encapsulating tin-alloy particles inside carbon nanotubes/nanofibers, which further improved the electrochemical performance of the Sn alloy-based anodes.

Encapsulating active materials inside 2D carbon materials (such as nanotubes and nanorods) has been realized.[239–241] In 2016, Pan and Li synthesized 3D core–shell Sn–Ni–Cu alloy@carbon nanorod anodes for Li-ion battery by pulse nano electrodeposition.[242] The track-etched polycarbonate membranes were used as the template. Firstly, a Cu film was evaporated onto one side of the membrane as the current collector. Then, the Sn–Ni alloy nanorods were electrodeposited into nanosized pores of the membranes, followed by calcination under Ar/H_2 condition. The synthesis process of this core–shell Sn–Ni–Cu alloy@carbon nanorod is presented in **Figure 6**a. During the calcination process, the copper atoms of current collector could react with Sn–Ni alloys to form Sn–Ni–Cu nanorods, while the carbon atoms pyrolyzed from the polycarbonate reacted with Ni atoms to generate NiC_x thin layer around the surface of the nanorods. The Ni and Cu inactive phases in the alloy acted as a buffer matrix for volume change of tin and enhanced the electronic conductivity as well. The carbon shell accelerated the transportation of electrons and Li-ions and further accommodated the volume expansion. Stable cycling performance and good rate performance were exhibited due to dual protection.

Besides amorphous carbon matrices and shells, the graphene was still preferred as a framework material of Sn-based anodes since 2012.[243–247] In 2015, Yu's group synthesized 3D porous graphene network-encapsulated Sn–Co alloy nano architectures (0D-Co-Sn⊂3D-pGN) as anodes for Li storage.[245] As shown by Figure 6b, graphene oxide (GO), PS latex particles and the $CoSn(OH)_6$ nanoparticles were uniformly dispersed into an aqueous solution firstly to form block units. Assisted with cationic surfactant (cetyltrimethyl ammonium bromide, CTAB) solution, these blocks were self-assembled into a continuous matrix. After the reduction of GO and pyrolysis of GN, the final 0D-Co-Sn⊂3D-pGN products were synthesized. This type of anode exhibited good electrochemical performance, including long cycle life and high rate capabilities. In 2017, Tang's group synthesized a Sn–Ni/C composite using dual matrices of porous carbon and graphene.[244] Graphene oxide and cyano-bridged Sn(IV)–Ni(II) coordination polymer aerogel were selected as precursors, and the final Sn–Ni@C/G composite was obtained after a calcination process. The reaction mechanism was similar to their previous work,[248,249] which mainly relied on the ligand-substitution reactions between aqueous solutions of metal chlorides and transition-metal cyanometalates. The coexistence of amorphous carbon and graphene immobilized Sn–Ni nanoparticles efficiently, leading to improved electrochemical performance due to the buffering effect and enhanced conductivity of the dual matrices.

Based on chemical reactions and assistance with templates, sophisticated structures were successfully synthesized and electrochemical performance was significantly improved. However, it is still far away from the real application of these anode materials. Thus, many researchers devoted themselves to making further progress of this ultimate goal. Even though ball-milling is regarded as a traditional technique, it is a very simple solid-state synthetic method, which can produce various nanosized particles.[250] In 2018, Park and Choi reported their new work about Sn-based intermetallic modified by

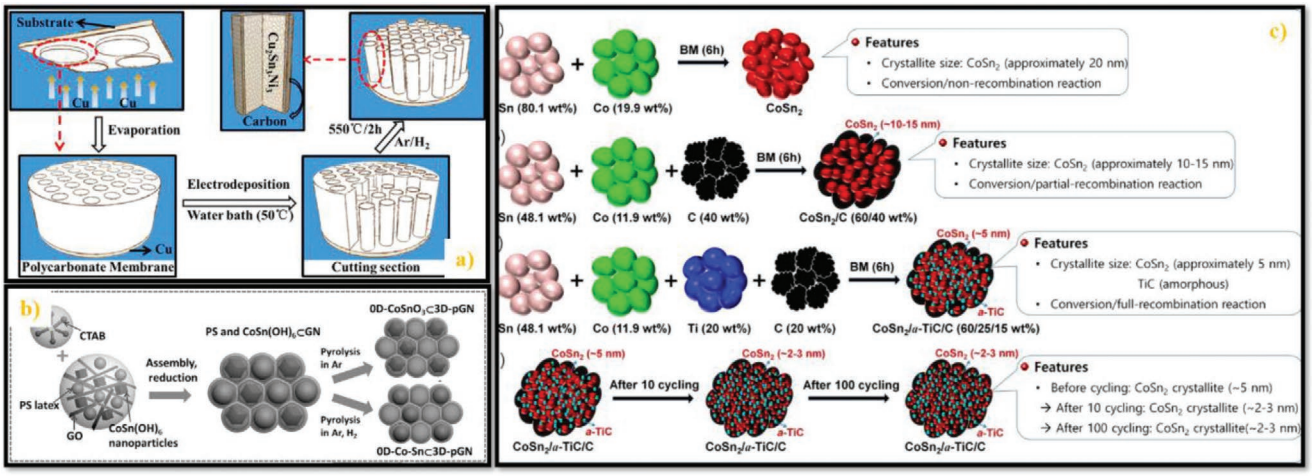

Figure 6. a) Schematic illustration of the preparation of the core–shell Sn–Ni–Cu-alloy@carbon nanorods array. Reproduced with permission.[242] Copyright 2016, American Chemical Society. b) Fabrication of 3D porous graphene network-encapsulated Sn-based nanocomposites. Reproduced with permission.[245] Copyright 2015, Wiley-VCH. c) Schematic of the straightforward preparation method for and features of $CoSn_2$-based materials. Reproduced with permission.[251] Copyright 2018, American Chemical Society.

carbon or titanium carbide (TiC) using ball-milling method.[251] In this work, the microscopic morphologies, electrochemical performance, and behaviors of various Co–Sn alloys were investigated step by step, and the ideal composition of the Co–Sn alloy anode material was identified. With ex situ XRD and Co K-edge EXAFS measurements, the lithiation/delithiation mechanism of the Co–Sn alloys were further investigated in details. The initial $CoSn_2$ electrode gradually evolved into $CoSn_2$/C phase, and finally into $CoSn_2$/a-TiC/C. In addition, the reaction mechanism between active material and lithium was transferred from a conversion/nonrecombination reaction to the conversion/full recombination one. Finally, the best electrochemical performance was achieved, where the $CoSn_2$/a-TiC/C electrode presented an initial insertion/extraction capacity of 576/479 mAh g^{-1} (ICE = 83.2%) and did not exhibit any capacity fading after 100 cycles. It was also found that the particle size of $CoSn_2$ in $CoSn_2$/a-TiC/C was further reduced to 2–3 nm after 10 cycles and maintained this particle size until 100 cycles. Interestingly, the conversion/full recombination reactions and tiny particle size of $CoSn_2$ in $CoSn_2$/a-TiC/C generated a positive feedback and promotion reciprocally, leading to a good electrochemical performance. Furthermore, the $CoSn_2$/a-TiC/C nanocomposite could keep its no-fading reversible capacity until the 180th circle with a good rate performance. The preparation methods and structure features of various Co–Sn alloy-based anode materials in this work are presented in Figure 6c.

Other Studies about Tin Alloy-Based Anodes: Since the 2010s, Sun's team started to investigate the lithium storage properties of Sn alloys with P phase.[252–255] In 2012, they synthesized quaternary Fe–Sn–Sb–P alloy Li-ion battery anodes and achieved good electrochemical performance.[252] This Fe–Sn–Sb–P alloy was prepared by electrochemical deposition and presented a dicranopteris-like structure which was beneficial to accommodate the volume expansion of Sn. In 2017, the ternary Fe–Sn–P alloy anodes were prepared by Sun's team through a similar method and also gained good electrochemical performance.[254] Besides, the effect on cycling performance of various Fe–Sn–P alloy anodes with different components was also investigated in this paper.

Except for explorations of new materials, the research about basic reaction mechanism of Sn-based alloy anodes also gained progress assisted with some in operando characteristic techniques.[256,257] In 2017, Fehse et al. studied the electrochemical reaction of ternary TiSnSb with Li by tracing the physicochemical state of the three elements at the same time with in operando X-ray absorption spectroscopy (XAS).[256] According to their results, TiSnSb reacts with lithium through a conversion reaction. Sn and Sb are electrochemically active, while Ti is inactive from the redox point of view but undergoes reversible structural changes from TiSnSb to Ti nanoparticles. After one complete electrochemical cycle, a ternary "Ti–Sn–Sb-like" compound is formed, which has different structural properties compared with pristine state TiSnSb. Besides, the lithiation and delithiation reactions of Sn and Sb are not simultaneous. Assisted with triple-edge XAS measurement, this study probed many in depth details of the electrochemical reaction mechanism between TiSnSb and Li, leading to a better and more clear understanding of such battery systems.

2.2. Tin Oxide-Based Anodes for Lithium-Ion Batteries

Tin dioxide (SnO_2) can react with lithium by two steps according to the following equation,[258] corresponding to a theoretical capacity (as to the multistep reaction mechanism, we calculate the theoretical capacity based on the total transferred electron numbers in the overall reaction, representing the theoretical first-charge capacity. Due to irreversible reaction, the actual capacity is lower than the theoretical. In some reports, theoretical capacity calculation is based on the reversible reaction, where the corresponding values are therefore lower than those in this review) of 1497 mAh g^{-1}

$$SnO_2 + 4Li^+ + 4e^- \rightarrow Sn + 2Li_2O \quad (3)$$

$$Sn + 4.4Li^+ + 4.4e^- \leftrightarrow Li_{4.4}Sn \quad (4)$$

Besides, tin monoxide (SnO) can also electrochemically react with Li with the similar mechanism and exhibit a theoretical capacity of 1273 mAh g^{-1}[259]

$$SnO + 2Li^+ + 2e^- \rightarrow Sn + Li_2O \quad (5)$$

$$Sn + 4.4Li^+ + 4.4e^- \leftrightarrow Li_{4.4}Sn \quad (6)$$

SnO_2, as an n-type wide-bandgap semiconductor, has been successfully applied in gas sensing as well as biotechnology,[ii260,261] which has also emerged as an important branch of Sn-based LIB anode material since about 2000s.

2.2.1. Preliminary Stage: Before 2000

In 1994, Fuji Photo Film Co., Ltd., Japan, applied for a patent about a new class of LIB with tin-based amorphous oxide (TCO) as the anode.[262] Later in 1997, Idota (Fujifilm Celltec) and Miyasaka (Fuji Photo Film) reported this novel, high-capacity LIB with TCO anodes, which could replace the commercialized LIBs with carbon-based lithium intercalation anode materials at that time.[263,264] The tin-based amorphous oxide contained Sn (II)-O active center, as well as a group of glass-forming metallic elements which comprised of a mixture of B (III), P (V), and Al (III). The Sn (II)-O active center reacts with lithium electrochemically to provide high capacity, while the other glass-forming network elements (B, P, Al) could enhance the mobility of Li-ions. The TCO anode material was prepared through a molten-state reaction where a mixture of SnO, B_2O_3, $Sn_2P_2O_7$, and Al_2O_3 powders were calcined at high temperature under argon atmosphere. In both half and full ($LiCoO_2$ cathode) cell tests, this kind of battery exhibited better electrochemical performance than that of commercial LIBs with carbon-based anodes at that time. This research work demonstrated that the tin oxides can be used as anode materials for LIBs and presented good electrochemical performance, which could be regarded as the beginning of the studies about tin oxides anode materials.

Following the study of TCO, Courtney and Dahn further investigated the reaction mechanisms and electrochemical behaviors of tin oxides with lithium.[265,266] Key factors responsible

for good reversibility of Li/Sn_2BPO_6 cells and Li/SnO_2 were identified, such as an appropriate voltage window and a smaller particle size of SnO_2.[266] A variety of tin oxide-based compounds, SnO, SnO_2, Li_2SnO_3, and $SnSiO_3$ glass, exhibited a similar manner when reacting with lithium. They firstly react with lithium to form amorphous Li_2O and Sn irreversibly, and further undergo a reversible Li-Sn alloying/dealloying process. The formation of matrix-glue Li_2O is beneficial to the reversibility of subsequent alloying/dealloying process by inhibiting agglomeration of tin atoms. However, further lithium insertion could form unlayered structures accompanied by the large volume change, leading to fast capacity fading. After this fundamental research period, various strategies and techniques were established in order to obtain a long cycling life.

2.2.2. Rising Stage: 2000–2009

The tin oxide-based anodes emerged almost at the same time with Sn alloy-based anodes, which also faced similar volume expansion problem during lithiation and delithiation. Mutual inspiration and reference between these two research fields promoted a fast development of tin oxide-based anode materials for Li-ion batteries. Therefore, as for stannic oxide anodes, nanostructure building and carbonaceous material composition are still the most prevalent strategies of improving their cycling stability and electrochemical performance.

Nanostructured Tin Oxide Anodes: During this period, 2D nanostructures (nanowires and nanorods) were the major research directions of the tin oxide anodes, and various synthesis methods were developed. In 2000, Martin's group synthesized SnO_2 nanofiber anodes using a microporous polycarbonate filter as the template.[267–269] The fabricated SnO_2 nanofibers were about 110 nm in diameter and 6.0 μm in length. Extra space among every single SnO_2 nanofiber provided enough room to accommodate volume expansion during cycling, thus this SnO_2 nanofiber-based anodes displayed better cycling stability than that of Sn thin film anodes. In later years, nanofiber and similar structured (nanowire and nanorod) Sn oxide anodes continuously proved their cycling stability.[270–274] In 2005, massive SnO_2 nanowires were synthesized by Feng's group via thermal evaporation of metal Sn based on the Au-catalyzed vapor–liquid–solid (VLS) growth mode.[274] In 2008, Kim and Cho synthesized mesopore and nanowire SnO_2 anode materials via a hard template method using SBA-15 and KIT-6 silica.[270] All these SnO_2 nanowire or nanorod anodes exhibited enhanced electrochemical performance due to their good capability to absorb inner stress caused by the volume changes.

On the other hand, creating hollow structures inside tin oxide materials also emerged at the end of this period.[275–278] Archer's team developed a simple one-pot template-free synthesis method for SnO_2 hollow nanostructures, based on an unusual inside-out Ostwald ripening mechanism.[277] The synthesis proceeded in a solution environment, where the precursor, potassium stannate, was converted into solid SnO_2 nanoparticles due to hydrolysis. These solid nanospheres were affected by the inside-out ripening mechanism, with prolonging hydrothermal treatment. This evacuation process could initiate at regions either near to the surface or around the nano sphere center depending on the ripening characteristics of chemical species, leading to hollow structured nanospheres. The size of the SnO_2 nanosphere could be controlled with their diameter ranging from 50 to 200 nm. When used as anode materials in LIBs, the as-prepared SnO_2 hollow nanospheres exhibited improved electrochemical properties. Moreover, decreasing the absolute size of Sn oxide nanoparticles and building porous structures also gained attention and good results.[279]

Tin Oxide/Carbonaceous Material Composite Anodes: From 2002, Lee's group reported their series of work about tin oxide/graphite composite anode materials for LIBs. They developed various methods to produce SnO_2/graphite nanocomposites, such as Pechini process-derived method,[280] urea-mediated hydrolysis,[281] microemulsion synthesis,[282] and microwave-assisted synthesis.[283] With optimization of the synthesis method and condition, the particle size of SnO_2 was successfully decreased from micrometer scale to about 3 nm. Thus, the corresponding electrochemical performance was also remarkably improved. Compared to graphite, the graphene-based materials exhibit various advantages, such as superior electrical conductivity, high surface area, good chemical tolerance, and broad electrochemical window.[284–286] In later years, SnO_2/graphene nanocomposite anode materials started to emerge and showed their superiority.[287–289] In 2009, Honma's group fabricated SnO_2/graphene nanoporous electrode by assembling graphene nanosheets (GNS) in the presence of tin oxide nanoparticles.[288] In the as-prepared SnO_2/GNS electrode, graphene nanosheets are homogeneously distributed between tin oxide nanoparticles. Due to the inflection of graphene nanosheets and a random stack of SnO_2 nanoparticles, some pore structures were generated. The porous structure provided enough void spaces to buffer volume change and the graphene nanosheets surrounding SnO_2 nanoparticles could also limit the volume expansion upon lithium insertion. Besides, graphene nanosheets could accommodate Li ions and contribute some capacity. Therefore, such SnO_2/GNS nanocomposite anode exhibited both high specific capacity and good cycling stability.

CNT, with good mechanical and electrical properties, not only acts as the conductive additive in electrode materials but also provides certain capacity.[190] The effectiveness of carbon nanotube for improving the electrochemical performance of anodes has been proved by a large number of reports, which also played an important role in high performance SnO_2/carbon composite anodes.[290–295] In the early days, SnO_2/CNTs anodes were mainly prepared by dispersing CNTs into a precursor solution of SnO_2. After a reduction process, SnO_2/CNTs composite was synthesized, where the SnO_2 nanoparticles (or SnO_2 nanoparticle clusters) were nonuniformly distributed on the surface of the CNTs.[294,296] Although such structure could improve the electrochemical performance at a certain extent, the effect was far away from what was expected. In the following years, homogenous dispersion of SnO_2 nanoparticles on CNTs attracted much attention from researchers. Zhang's team synthesized SnO_2/CNTs anode material where SnO_2 nanoparticles were uniformly loaded on carbon nanotube sheets.[295] In order to realize a homogenous distribution of SnO_2 nanoparticles, long-chain poly(vinyl pyrrolidone) (PVP) polymers were used on CNTs as the catcher for the SnO_2 nanoparticles in the sol.

The cross-stacked carbon nanotube sheets could act as not only buffer matrix for volume change but also a good conductive agent. Thus, this binder-free anode exhibited enhanced electrochemical performance, which delivered over 850 mAh g^{-1} of charge capacity with 100% retention for at least 65 cycles when cycled in the potential window of 0.01–3 V versus Li^+/Li. In addition, advanced nanotechnology made it possible to encapsulate foreign matter within the hollow cavity of CNTs.[239,297–302] Lee's team reported a method for synthesizing SnO_2-tube-in CNT nanocomposite anode material for LIB.[240] Particularly, the porous SnO_2 nanotubes were formed first, and a uniform CNT overlayer was grown on the external surface of the SnO_2 nanotubes through a confined-space catalytic deposition process assisted by anodic aluminum oxide (AAO) membranes. This new method ensured the tin oxide species completely covered by carbon nanotubes. This SnO_2/C nanocomposite exhibited good cyclic stability, which only had a 0.0375% capacity loss per cycle after 200 cycles.

2.2.3. Fast Development Stage: Since 2010

After development over ten years, basic strategies toward electrochemical performance improvement of the tin oxide-based anodes have been established and tended to enter into a maturity stage. Since 2010, architecting nanostructures and compositing with carbonaceous materials are still two most favorite and effective ways to obtain high-performance stannic oxide anodes for LIBs. However, SnO_2/carbon nanocomposite anodes obviously attracted much more attention than pure nanostructured SnO_2 electrodes.

Nanostructured Tin Oxide Anodes: Since 2010, Archer and co-workers continued their work on synthesizing hollow nanostructures, where a variety of hollow SnO_2 nanomaterials were fabricated by their team with good electrochemical properties as anodes for LIBs.[258,303–306] In 2011, Luo's group synthesized hollow SnO_2 nanoboxes (**Figure 7**a) by combining controlled hydrolysis of corresponding metal ions and simultaneous coordinating etching of the sacrificial template.[304] Cu_2O nanocubes were selected as templates, where the synthesis process was driven by the interfacial reaction between an aqueous solution of $SnCl_4$ and solid Cu_2O crystal. Due to hydrolysis effect, SnO_2 precipitation layer was formed around Cu_2O template. Moreover, this process generated insoluble CuCl, which could be dissolved simultaneously in an aqueous solution of NaCl by coordinating with Cl^- to form soluble $[CuCl_x]^{1-x}$. Therefore, the continuous outward flow of $[CuCl_x]^{1-x}$ and inward flow of Sn^{4+} and Cl^- led to complete consumption of Cu_2O and final formation of hollow SnO_2 nanobox. The as-prepared SnO_2 nanoboxes exhibited uniform structure and size, with an edge length of hundreds of nanometers and a wall thickness of 10–20 nm, which can be altered by different-sized Cu_2O templates. Moreover, in 2012, they also prepared various hollow SnO_2 nanomaterials,[305] such as nanococoon, nanosphere and nanorings (Figure 7b–d). This synthesis principle was similar to that of SnO_2 nanobox above, which combined controlled deposition of SnO_2 from hydrolysis of $SnCl_2$ and simultaneous acidic etching of α-Fe_2O_3 templates. When applied as anodes of Li-ion batteries, all these hollow SnO_2 nanomaterials presented stable cyclability as well as excellent rate performance. As discussed in Section 2.1.4.1, it has been demonstrated that utilizing the Kirkendall effect was an effective method to produce hollow structured materials. During this period, many efforts were also devoted to fabricating hollow SnO_2 nanostructured anode materials assisted with Kirkendall effect.[307,308] In 2015, Kang and Cho reported their work about producing nanofibers comprising yolk–shell Sn@void@SnO/SnO_2 and hollow SnO/SnO_2 and SnO_2 nanospheres by applying the nanoscale Kirkendall diffusion process to conventional electrospinning process.[307]

Tin Oxide/Carbonaceous Material Composite Anodes: At the beginning of the 2010s, tin oxide/carbonaceous material composite anodes embraced an explosive development. Graphene, carbon nanotubes and amorphous carbon are main carbonaceous materials which are widely used as the carbon matrix for alleviating volume change of tin oxide. Meanwhile, distributing nanostructured SnO_2 on or in carbon matrix and coating or creating carbon shell out of SnO_2 nano architectures are the two major strategies to obtain SnO_2/C composite electrode materials.

Graphene (G) is a good material as a carbon matrix in composite anodes and its effectiveness has been demonstrated by a large number of studies. Preparing SnO_2 nanoparticle/graphene composite anode material became a hotspot in the research field since about 2008. Due to the lack of strong interactions between nanoparticles and graphene layers and the stacking trend of graphene layers, SnO_2/G nanocomposite electrodes cannot exhibit the best performance. In 2010, Guo's team developed a method to synthesize monodispersed SnO_2 nanoparticles on both sides of single-layer graphene sheets as anode materials in Li-ion batteries.[309] The key of this method was to use GO single sheet as the carbon source instead of graphene sheet. Sn^{4+} ions of SnO_2 precursor were selectively bonded with the oxygenated groups (such as hydroxyl and carbonyl groups) through electrostatic force.[310] The SnO_2 nanocrystals were firstly in situ loaded on GO sheets, which

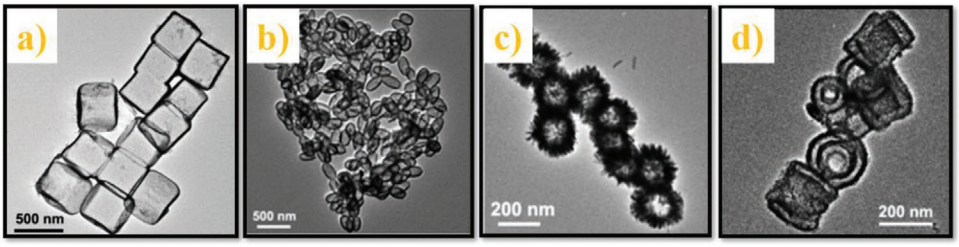

Figure 7. a) TEM image of SnO_2 nanoboxes. Reproduced with permission.[304] Copyright 2011, American Chemical Society. b) TEM images of SnO_2 nanococoons, c) SnO_2 nanospheres and d) SnO_2 nanorings. Reproduced with permission.[305] Copyright 2012, Wiley-VCH.

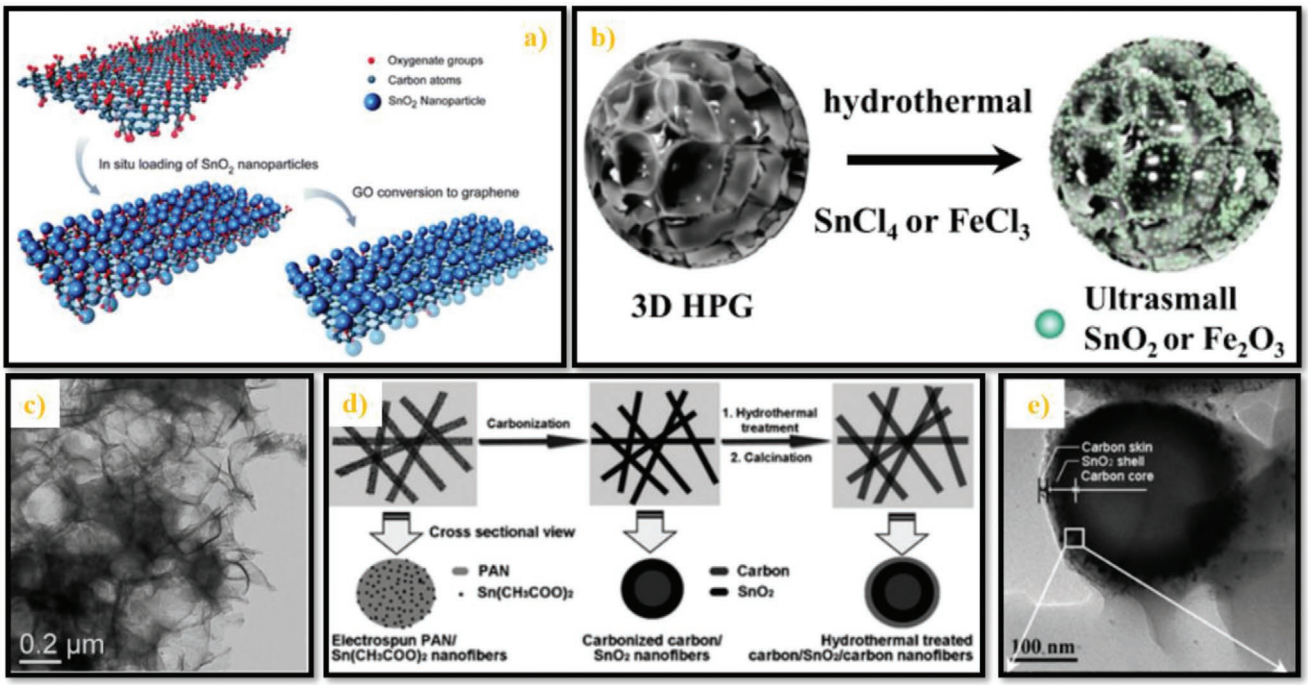

Figure 8. a) A two-step method to load SnO_2 nanoparticles on both sides of single-layer graphene sheets to form a SnO_2/G composite. Reproduced with permission.[309] Copyright 2010, Royal Society of Chemistry. b) Schematic for the synthesis and c) TEM image of MO_x-3D HPG hybrid composites. Reproduced with permission.[316] Copyright 2015, Elsevier Ltd. d) Schematic illustration of the preparation and e) cross-sectional view of TEM image of carbon@SnO_2@carbon–core/shell/shell hybrid nanofibers. Reproduced with permission.[324] Copyright 2012, Royal Society of Chemistry.

were then converted to SnO_2/G composites (**Figure 8**a). A homogeneous distribution (nearly monodispersion) of SnO_2 nanoparticles on graphene could suppress nanoparticle aggregation during cycling, leading to enhanced electrochemical performance.

In the following years, 3D SnO_2/G composite anode materials began to emerge,[311–315] which had better ability to accommodate the volume expansion of SnO_2 compared to previous 2D electrodes. In 2015, Shen's group prepared well-dispersed ultrasmall SnO_2 nanoparticles anchored on 3D hierarchical porous graphene (HPG)-like anode via a hydrothermal process, as displayed by Figure 8b.[316] Synthesis of the HPG material was based on an ion-exchange resin-based technology.[317] The ion-exchange process proceeded between pretreated macroporous acrylic type cation-exchange resin and nickel acetate solution. Then, the nickel ion-exchanged resin was immersed into the KOH/ethanol solution to form nickel ion exchanged resin/KOH mixture. The HPG material was obtained after heat treatment under nitrogen atmosphere. The as-prepared composite material exhibited a hierarchical porous structure (Figure 8c). The interconnected 3D HPG network was mainly derived by resin pyrolysis catalyzed by Ni^{2+} ions, and mesopores on the walls of the 3D HPG were attributed to KOH activation.[317] The ultrasmall SnO_2 nanoparticles (≈3 nm) were nearly monodispersed on walls of 3D HPG. This electrode exhibited both stable cyclability and good rate performance due to its unique hierarchical structure. Especially, it could maintain a reversible capacity of 474 mAh g^{-1} at a high current density of 10 A g^{-1}, with capacity retention of 88% after 1000 cycles against the capacity value of the second cycle.

During the last period discussed in this review (Section 2.2.2.2), a great progress has been made using carbon nanotubes as the buffer for tin oxide's volume change. Several delicate structures, such as encapsulating nanoscale SnO_2 into the hollow cavity of CNTs, have been realized and presented enhanced electrochemical performance. In this period, the studies about SnO_2/CNTs composite anodes stepped into a steady development stage. Many efforts were focused on uniform distribution of SnO_2 nanoparticles on CNTs by functionalizing carbon nanotubes[318] or constructing 3D-structured SnO_2/CNTs composites assisted by template.[319–321] A good development was also demonstrated since 2010 using amorphous carbon as a buffer matrix for the SnO_2/C composite anodes. Carbon nanofiber[322–324] and carbon shell[325–328] were favorable options as carbon cushion during this period. In 2012, Lu's team prepared C@SnO_2@C-core/shell/shell hybrid nanofibers via single spinneret electrospinning followed by carbonization and hydrothermal treatment, where the synthesis process is illustrated in Figure 8d.[324] Firstly, C@SnO_2-core/shell nanofibers were converted from electrospun PAN/$Sn(CH_3COO)_2$ nanofibers through carbonization, where Kirkendall effect was involved. The second amorphous carbon shell was formed around the C/SnO_2-core/shell nanofibers through hydrothermal treatment of an aqueous glucose solution, followed by calcination process, yielding a C@SnO_2@C-core/shell/shell structure (Figure 8e). The morphology of this hybrid nanofiber could be further modified by varying the concentrations of the aqueous glucose solution. When used as the anode of Li-ion battery, this hybrid nanofiber exhibited good electrochemical performance with a

reversible capacity of 837 mAh g^{-1} after 200 cycles at a rate of 0.1C (1C = 522 mAh g^{-1}).

Tin Oxide/Noncarbonaceous Material Composite Anodes: From 2010, various noncarbonaceous materials, such as TiO_2,[329,330] WO_3,[331] ZnO,[332] MnO_x,[333,334] and Fe_2O_3[335,336] were used to form composite anodes with tin oxide. Among those metal oxides, TiO_2 attracted much attention due to its good mechanical property, tiny volume change (less than 4%) and extra capacity contribution.[337,338] In 2010, Liu's group deposited SnO_2 nanocrystals into self-organized TiO_2 nanotube arrays through a solvothermal method, forming a 3D-structured SnO_2/TiO_2 composite electrode material.[330] The TiO_2 nanotube was prepared by a potentiostatic anodization process. At the same year, Oritz's team synthesized 3D SnO_2/TiO_2 composite anode where tin oxide nanowires were grown onto titania nanotubes.[329] The TiO_2 nanotube array was also fabricated via an electrochemical anodization technique. Then the SnO_2 nanowires were grown in the hollow space of TiO_2 nanotubes. These two similar SnO_2/TiO_2 composite electrodes both displayed good electrochemical performance.

2.3. Tin-Based Compound Anodes for Lithium-Ion Batteries

Similar to tin oxide, other Sn-based compounds, such as Sn sulfide, sulfate, phosphide, and phosphate, can also react with lithium based on a two-step process. Therefore, they could be utilized as anodes for LIBs. The reaction equations are as following

Sn sulfide (SnS_2 as example[339])

$$SnS_2 + 4Li^+ + 4e^- \rightarrow Sn + 2Li_2S \quad (7)$$

$$Sn + 4.4Li^+ + 4.4e^- \leftrightarrow Li_{4.4}Sn \quad (8)$$

Sn sulfate ($SnSO_4$ as example[340]):

$$SnSO_4 + 2Li^+ + 2e^- \rightarrow Sn + Li_2SO_4 \quad (9)$$

$$Sn + 4.4Li^+ + 4.4e^- \leftrightarrow Li_{4.4}Sn \quad (10)$$

Sn phosphide (Sn_4P_3 as example[341])

$$Sn_4P_3 + 2Li^+ + 2e^- \rightarrow Li_2Sn_4P_3 \quad (11)$$

$$Li_2Sn_4P_3 \rightarrow Sn + (LiP_5 + LiP_7) \rightarrow Sn + LiP \quad (12)$$

$$Sn + 4.4Li^+ + 4.4e^- \leftrightarrow Li_{4.4}Sn \text{ and } LiP + 2Li^+ + 2e^- \rightarrow Li_3P \quad (13)$$

Sn phosphate ($Sn_2P_2O_7$ as example[342])

$$Sn_2P_2O_7 + 4Li^+ + 4e^- \rightarrow 2Sn + Li_3PO_4 + LiPO_3 \quad (14)$$

$$Sn + 4.4Li^+ + 4.4e^- \leftrightarrow Li_{4.4}Sn \quad (15)$$

According to calculation, the theoretical capacities of SnS_2, $SnSO_4$, Sn_4P_3, and $Sn_2P_2O_7$ are 763, 799, 1255, and 834 mAh g^{-1}, respectively. Due to high theoretical capacities, these Sn-based compounds have attracted great attention.

2.3.1. Preliminary Stage: 1998–2006

During this period, the electrochemical performance of Sn-based compound anodes was investigated. Studies were mainly focused on reaction mechanism and new preparation methods.[265,339–346] In 1998, it was found that $SnSO_4$ could be used as anode material for LIBs at ambient temperature.[340] Commercial $SnSO_4$ was directly used to fabricate anode with conductive agent and binder, where initial discharge capacity could reach 500 mAh g^{-1}. The reaction mechanism between $SnSO_4$ and lithium was confirmed according to XRD and Mössbauer spectra. Early in 1994, Fuji Photo Film Co., Ltd., Japan, filed a patent for nonaqueous Li-ion batteries in which tin composite oxides (TCOs) were used as the active anode material.[262] The Sn (II)-O site of TCOs was the virtual active center for lithium insertion.[263] Inspired by this finding, in 1999, Lee's team selected amorphous and crystalline $Sn_2P_2O_7$ as intrinsic P-doped tin oxide composites for LIB anodes.[346] Crystalline $Sn_2P_2O_7$ was a commercial product, while amorphous $Sn_2P_2O_7$ could be synthesized through a melt-quenching procedure. Both amorphous and crystalline $Sn_2P_2O_7$ anodes exhibited similar capacities and fading characteristics. The first charge capacity reached over 1000 mAh g^{-1}. However, a fast capacity fading was observed in subsequent cycles. In 2001, Osaka's group prepared SnS_2 LIB anode by sonochemistry.[339] The annealed SnS_2 anode showed a capacity of over 600 mAh g^{-1} at the initial stage, while the nonannealed one presented a capacity of about 300 mAh g^{-1}. It was also proved that SnS_2 could work as anode in a full cell using $LiCoO_2$ cathode. From the 2000s, phosphide materials was investigated as the LIB anodes due to their reversibility and a large amount of lithium uptake at relatively low potential.[347–349] In 2004, layer structured tin phosphide (Sn_4P_3) was synthesized by Sohn's team using a mechanochemical technique.[343] As for Sn_4P_3, both Sn and P acted as reactive sites for lithiation at different voltages. At a limited voltage window, the Sn_4P_3 anode displayed a reversible capacity of 370 mAh g^{-1} up to 50 cycles. During the initial stage, these tin-based compound anodes always suffered from moderate cycling stability.

2.3.2. Rising Stage: Since 2007

In order to improve the electrochemical performance of Sn-based compound anodes, many efforts have been made since 2007. In the 2010s, there were countless researches about alleviating volume change of tin. Inspired by other researches, creating nanostructures and introducing matrix materials were also applied in the field of S Sn-S/P compound anodes.

Since 2010, various nanostructured Sn-based compound anodes were synthesized, such as $Sn_2P_2O_7$ nanodisks,[350] SnS_2 nanorods,[351] SnS nanobelts,[352] and Sn_4P_3 hollow spheres.[353] All these electrodes exhibited enhanced cycling stability compared with their non-nanostructured counterparts. Introducing carbonaceous materials into Sn-based compounds to fabricate composite anodes emerged recently.[354–357] In 2018, Hong's group synthesized core–shell Sn_4P_3/C nanospheres as high-performance anode for LIBs, via carbonization/reduction and phosphorization of SnO_2/GCP (glucose-derived, carbon-rich

polysaccharide) nanospheres.[358] This Sn_4P_3/C composite electrode displayed stable cycling performance, which could maintain a reversible capacity of 440 mAh g^{-1} after 500 cycles at a current density of 2000 mA g^{-1}. Cao's team prepared SnS_2 semi-CNT carbon nanotube (SnS_2@CNT) anode material through plasma-assisted fabrication of Sn semi-filled CNT (Sn@CNT) followed by post sulfurization.[356] This SnS_2@CNT anode delivered an initial discharge capacity of 1258 mAh g^{-1} at a current density of 0.3 A g^{-1}, which increased inversely to 2733 mAh g^{-1} after 470 cycles. This inverse capacity growth could be attributed to the pocket effect of CNTs. After numerous cycles, SnS_2 was highly pulverized but SnS_2 granules were confined inside CNTs. The pulverization of SnS_2 actually increased interface and shortened Li-ion diffusion path in SnS_2, leading to increased capacity. It is worth noticing that the studies about the Sn-based compound anodes stepped into a fast development stage since 2010, especially in the field of SIB due to their high reversible capacity. This will be discussed in the following part.

2.4. Tin/Carbonaceous and Other Material Composite Anodes for Lithium-Ion Batteries

Direct using the elemental tin as anodes of LIBs is always hindered by serious volume expansion and agglomeration of tin during lithiation/delithiation process. Compared with tin-alloy and tin oxide anodes, the origin of tin/carbon (others) composite anodes is a little later. Wide application of carbon materials in the energy field and prosperity of nanotechnology promoted tin/carbon (others) anodes into a fast development stage. Generally, the tin/carbon (others) anodes can be divided into two classifications. One is contact type and the other is noncontact type. The contact-type tin/carbon (others) anodes are usually designed by embedding and coating strategies where the tin component direct contacts with carbon matrix.[179,359,360] Alleviation of volume change of Sn mainly relies on the mechanical strength and flexibility of carbon material. As to the noncontact-type anodes, void space between tin and carbon is created in order to accommodate the volume expansion of Sn, such as yolk–shell structure.[241,361,362] Due to the strict requirement of synthesis technique for the noncontact-type tin/carbon (others) composite anodes, most studies are still focused on the contact-type Sn-based composite anodes.

2.4.1. Preliminary Stage: 2000–2005

During the initial stage, most of the Sn/C composite electrodes were simple mixtures of metallic tin and carbon source (most of were graphite),[363–376] which belonged to the contact-type. These Sn/C anodes all had enhanced electrochemical performance, and some electrode could keep stable cycling up to 50 cycles. Despite of the progress, such cyclability still cannot compare with commercialized Li-ion battery with the graphite-based anode. However, in 2003, the first noncontact-type Sn/C composite anode was successfully fabricated by Oh's team where Sn nanospheres were encapsulated in carbon spheres.[377] According to the **Figure 9**a, CTAB was dispersed in deionized water to form spherical micelles firstly. After adding the mixture of resorcinol (R), formaldehyde (F) and sodium carbonate (as a catalyst), surfactant-stabilized RF sols were obtained. Then, tributyl phenyl tin (TBPT), as a precursor of Sn, was added into the solution to form surfactant-stabilized TBPT/RF core–shell colloids because of the hydrophilicity difference between TBPT and RF sol. Through a heat-treatment process, the final Sn-encapsulated spherical hollow carbon was obtained, as presented in Figure 9b. Due to the existence of void space between Sn core and carbon shell, the volume effect was obviously decreased, resulting in improved cycling stability. Although this study opened the gate of noncontact-type Sn/C composite anodes for LIBs, further improvement was still needed for the electrochemical performance. Besides, more nanostructured Sn/C composite anodes were prepared in 2005, such as tin nanoparticles dispersed on cellulose fiber,[365] tin-decorated mesoporous carbon,[368] and Sn/C core–shell nano powder.[369]

2.4.2. Fast Development Stage: 2006–2012

More and more nanostructured Sn/C composite anodes for LIBs appeared in this stage, the contact-type anodes were still the mainstream while the noncontact-type also gained progress.

Contact-Type Tin/Carbonaceous Material Composite Anodes: Assisted by nanotechnology, various strategies to synthesize contact-type Sn/C composites were developed from 2006 to 2012, including embedding Sn nanoparticles into continuous carbon matrix, coating carbon layers on Sn nanostructures and encapsulating Sn nanostructures into carbon nanotubes. In 2007, Scrosati's team synthesized a Sn/C anode where Sn nanoparticles were finely dispersed in a supporting carbon matrix,[179] as displayed by Figure 9c. The synthesis process consisted of the infiltration of an organometallic tin precursor into an organic Resorcinol–Formaldehyde gel, followed by calcination under argon. Most of the generated tin nanoparticles presented tiny size less than 10 nm. This anode exhibited a stable cyclability as well as good rate performance. It could maintain a reversible capacity of about 500 mAh g^{-1} after 200 cycles at 0.8C (1C = 1.25 A cm^{-2} g^{-1}), and reached a capacity of 200 mAh g^{-1} even at a rate of 5C. In 2012, Chiu's group prepared Sn@CNT core–shell nanowires (Figure 9d) as anode for LIBs via a simplified process.[378] The Sn@CNT anode displayed good electrochemical performance. Wang's team also synthesized Sn@CNT nanostructured anode and introduced graphene into the system in order to improve the rate performance.[379]

During this period, graphene has started to be used as both cushion matrix and electrical conductivity booster for Sn/G composite anodes.[380–382] One creative work was reported by Wang's team in 2013. A 3D porous core–shell Sn@C anode on nickel foam substrate was fabricated by electrostatic spray deposition (ESD) technique followed by high-temperature treatment,[360] where the electrode morphology is presented in Figure 9e. During the ESD process, the porous structure was formed due to solvent evaporation (ethanol) and decomposition of inorganic salts (butyl carbitol). Further heat-treatment enabled the PVP surfactant to decompose into carbon, which enlarged the pore diameter and produced more pores at the

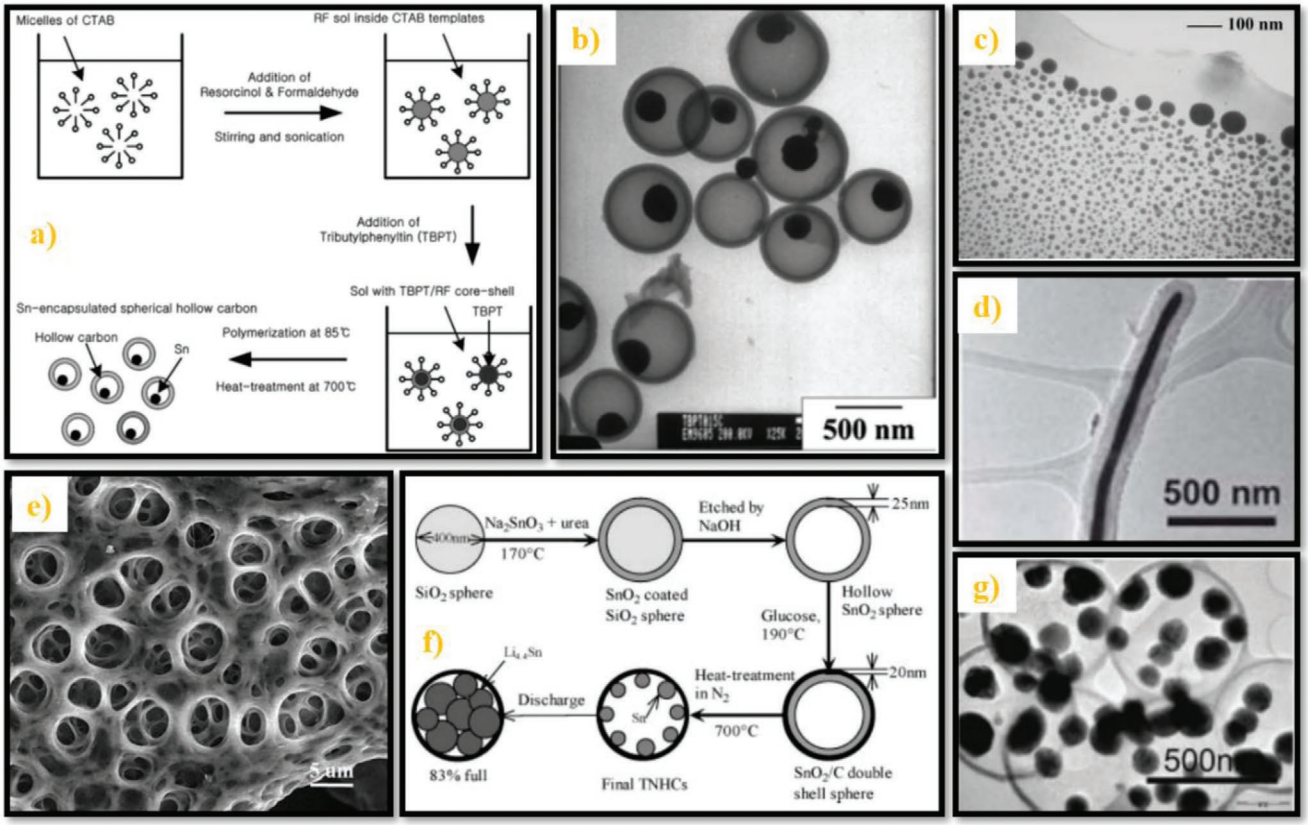

Figure 9. a) Synthetic scheme and b) TEM image for Sn-encapsulated spherical hollow carbon. Reproduced with permission.[377] Copyright 2003, American Chemical Society. c) TEM image of a Sn/C composite material. Reproduced with permission.[179] Copyright 2007, Wiley-VCH. d) TEM image of Sn@CNT core–shell nanowire. Reproduced with permission.[378] Copyright 2012, Royal Society of Chemistry. e) TEM image of 3D porous core–shell Sn@C composite. Reproduced with permission.[360] Copyright 2012, Wiley-VCH. f) Synthetic scheme and g) TEM image of tin nanoparticles encapsulated elastic hollow carbon spheres. Reproduced with permission.[383] Copyright 2008, Wiley-VCH.

same time. This 3D Sn@C anode worked stably with the capacity of 638 mAh g^{-1} after over 300 cycles at 25 mA g^{-1}, corresponding to a capacity loss of 0.11 mAh g^{-1} per cycle on average.

Noncontact-Type Tin/Carbonaceous Material Composite Anodes: In 2008, Wan's team developed a new method to synthesize tin nanoparticles encapsulated in elastic hollow carbon spheres (TNHCs) as anode materials for LIBs.[383] SiO_2 nanospheres, synthesized according to Stöber method,[384] were used as the initial templates to form SnO_2 hollow spheres by hydrolysis of Na_2SnO_3 and an etching process of NaOH solution. Then, carbon precursor layers were coated on the surface of as-prepared hollow SnO_2 spheres via pyrolysis of glucose under hydrothermal conditions. After calcination, the final TNHCs were obtained due to carbonization of carbon precursor shell and reduction of tin oxide. The synthesis route and morphology of the final product are shown in Figure 9f,g. The average diameter of inside tin nanoparticles was less than 100 nm and the thickness of carbon shell was about 20 nm. The void space in carbon was about 70–80% by volume, which provided enough room for accommodating volume change of tin during cycling. Compared with the report by Oh's team in 2003, this study realized encapsulating several Sn nanoparticles into one carbon hollow sphere, resulting in better electrochemical performance. In 2009, Wang and Lee encapsulated Sn nanoparticles into a carbon nanotube to obtain Sn@CNT or Sn@C@CNT anodes with inside hollow structure.[241] This work was supposed to be the first report about CNT-encapsulation of pristine Sn particles as anodes for Li-ion batteries. In the same year, Yu's team continuously reported their work about encapsulating Sn nanoparticles into carbon nanotube or hollow nanofiber.[361,362] Yu utilized coaxial electrospinning technique to produce carbon nanotubes or hollow nanofibers with tin core, which greatly simplified the synthesis process of hollow-structured Sn/C composite anodes.

2.4.3. Explosive Development Stage: Since 2013

Development of Sn/C composite anodes embraced a golden stage since 2013, when the number of the work reported experienced an explosive increase. On the one hand, contact and noncontact-type Sn/C anodes still dominated the major field of Sn-based composite anodes. On the other hand, similar to SnO_2-based anodes (Section 2.2.3.3), some noncarbonaceous or multicomponent mixture materials were used to produce Sn-based composite anodes for Li-ion batteries since 2013.

Contact-Type Tin/Carbonaceous Material Composite Anodes: Compared with the last period, graphene was more widely used as the carbon source of Sn/C composite in this stage. Moreover, utilizing the flexibility of graphene, some 3D network structures were constructed.[385,386] In 2014, Wang's team designed a novel tin-graphene composite anode for LIBs.[385] Sn nanoparticles were encapsulated in graphene shells (Sn@GS), which were homogeneously distributed on vertically aligned graphene nanosheets (Sn@GS-VAGNs). The VAGNs were directly grown on copper current collectors in a microwave plasma enhanced chemical vapor deposition (MPECVD) system. VAGNs formed a 3D network which could not only alleviate volume change of Sn but also fasten electron transportation of the composite material. Then, SnO_2 nanoparticles were homogeneously anchored on VAGNs via a solvothermal process. Finally, the as-prepared SnO_2–VAGNs sample was placed in the MPECVD chamber, where Sn@GS–VAGNs was synthesized after reduction of CH_4 gas. The decomposition of CH_4 enabled coating a thin graphene layer on Sn nanoparticles, which could effectively inhibit agglomeration of the tin nanoparticles during cycling. Due to the double protection (GS and VAGN), this electrode presented a very stable cyclability as well as great rate performance. It could maintain a reversible capacity of over 400 mAh g^{-1} after 5100 cycles at a rate of 6C (1C = 600 mA g^{-1}). Wang's team applied a similar synthesis process to obtain Sn@CNT–VAGNs anode, which also exhibited long-term cycling stability and fast charge–discharge rate.[387]

Encapsulating tiny tin nanoparticles into a continuous carbon matrix (sphere or bulk) gradually attracted attention and acquired good electrochemical performance as anodes for LIBs. In 2013 and 2014, Wang's group[388] and Chen's group[389] used aerosol spray pyrolysis to synthesize Sn/C composite anodes with similar structures, where tiny Sn nanoparticles were embedded uniformly inside the carbon sphere. In a typical aerosol spray pyrolysis process, precursor solution (carbon source and Sn precursor) was atomized into microsized droplets and then swept by a carrier gas consequently through a dryer to form precursor particles. After pyrolysis under high-temperature, final pitaya-like Sn/C composite was obtained. In addition, various methods were successfully developed to prepare Sn/C nanocomposite, such as carbonizing divalent Sn complex (Sn(Salen)),[390] hydrothermal method combined with postcalcination process,[391] and hydrolysis with pyrolysis.[392]

Except for the construction of novel structures, researchers also explored some new materials which could be applied to synthesize Sn/C composite anodes. In 2018, Liu and Lee introduced Fullerene C_{60} into Sn/C composite anode material for the first time.[393] By combining radio frequency plasma-assisted thermal evaporation with chemical vapor deposition (RFPATE-CVD), Sn (coated by a thin amorphous SnO_2 layer)/C_{60} nanocomposite was prepared. An important point in this report was that the Sn–SnO_2–C_{60} ternary interface was composed of a metallic/n-type semiconductor/p-type semiconductor structure. According to semiconductor theory,[394–396] the metallic/n-type semiconductor (Sn/SnO_2) interface formed an Ohmic contact while the n-type semiconductor/p-type semiconductor interface (SnO_2/C_{60}) created a p–n junction to generate a built-in electric field (BEF) effect. The established Ohmic/BEF characteristics could fasten the diffusion rate of lithium ions within the material, leading to enhanced rate performance. This Sn/C_{60} composite anode could maintain a reversible capacity of 834 mAh g^{-1} after 5000 cycles at a current density of 1 A g^{-1} and reached a specific capacity of 544 mAh g^{-1} at 10 A g^{-1}.

Noncntact-Type Tin/Carbonaceous Material Composite Anodes: Compared with the last stage, more yolk–shell Sn/C composite anodes have been synthesized since 2013, accompanied with simplified synthesis methods. In 2013, Ni and Xu fabricated Sn@C yolk–shell nanospheres (**Figure 10**a) as high-performance anode for LIBs, through a catalyzed thermal CVD.[397] Tin oxide hollow nanospheres were produced and used as the original templates. They found that various nanostructures including SnO_2–Sn@C, Sn@C yolk–shell nanospheres, and core–sheath nanowires could be obtained by simply varying the crystallinity of SnO_2 hollow spheres. In 2014, Ni and Wang synthesized Sn@C yolk–shell nanostructure and combined it with a 3D carbon nanofiber conducting network (Figure 10b), in order to further improve the electrochemical performance.[398] The Sn@C yolk–shell nanospheres were prepared with the same method as mentioned above. Carbon nanofibers were obtained by electrospinning and pyrolyzing polyacrylonitrile (PAN) fibers. The final products were synthesized by integrating these two steps into one. The formed 3D carbon nanofiber conducting network not only enhanced the electron transportation but also eliminated the use of polymer binders, conducting carbon black and copper current collectors. In 2015, Sn@C core–shell microspheres (Figure 10c) were prepared by a one-pot spray pyrolysis process, as reported by Kang's team.[399] Firstly, Sn oxalate, Zn nitrate, and PVP were dissolved into an aqueous solution and formed droplets via an ultrasonic nebulizer. After a series of heat treatment process, PVP was carbonized to form outside carbon shell, Sn and Zn salts were reduced into metallic Sn and Zn inside the shell. Meanwhile, the Zn component was evaporated, leaving void space within the microsphere. In 2017, Yu's group also utilized low evaporation temperature of zinc

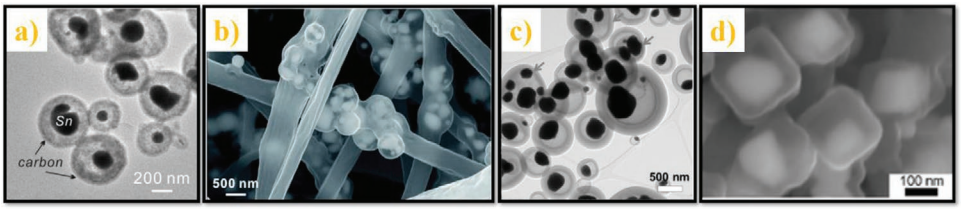

Figure 10. a) TEM image of Sn@C yolk–shell nanospheres. Reproduced with permission.[397] Copyright 2013, Wiley-VCH. b) TEM image of Sn@C yolk–shell nanospheres/3D carbon fiber network. Reproduced with permission.[398] Copyright 2014, Royal Society of Chemistry. c) TEM image of Sn@C core–shell microspheres. Reproduced with permission.[399] Copyright 2015, Wiley-VCH. d) TEM image of yolk–shell Sn@C nanoboxes. Reproduced with permission.[400] Copyright 2017, Wiley-VCH.

to fabricate yolk–shell Sn@C nanoboxes (Figure 10d) for lithium storage.[400] The $ZnSnO_3$ nanocubes were synthesized through a solution process involving the reaction of zinc sulfate and sodium stannate as reported in 2010.[401] Polydopamine (PDA) was selected as a carbon source and coated on the surface of $ZnSnO_3$ nanocubes. In heat treatment, the Zn species also acted the sacrifice to generate hollow structure inside the carbon shell which was converted from PDA. All these yolk–shell Sn/C composite electrodes exhibited good electrochemical performance with a stable cycling over at least 500 cycles.

Tin/Other Material Composite Anodes: Titanium dioxide is a favorable material, which could replace carbonaceous materials as cushion matrix for Sn-based anodes and also provide capacity for batteries. TiO_2 matrix has been widely used in SnO_2-based anode materials (Section 2.2.3.3). In 2014, Liao and Manthiram reported mesoporous TiO_2-Sn/C core–shell nanowire arrays as anodes in LIBs, which were prepared by two hydrothermal processes.[70] Mesoporous TiO_2-based nanowire arrays were fabricated by a hydrolysis process of the $H_2Ti_2O_5 \cdot H_2O$ nanowires.[402] The as-prepared TiO_2 nanowires were then soaked into a solution containing Sn precursor. After a second hydrothermal reaction, TiO_2–SnO_2 nanowire arrays were formed. Finally, additional hydrothermal process and calcination were proceeded to reduce SnO_2 into metallic Sn while coating carbon layer onto the TiO_2–Sn nanowire arrays. The TiO_2–Sn/C core–shell nanowire electrodes presented good electrochemical performance, which could maintain high reversible capacities of 769, 663, 365, 193, and 90 mAh g^{-1} at 0.1C, 0.5C, 2C, 10C, and 30C (1C = 335 mA g^{-1}), respectively. Additionally, silicon oxycarbide (SiOC) fibers[403] and several metallic materials (Cu, Al)[404–406] were also applied to act cushion matrix, aiming to improve the electrochemical performance of tin anodes.

2.5. Elemental Tin Anodes for Lithium-Ion Batteries

Although Sn-based anodes for LIBs have been studied since the 1990s, applying bare Sn material as anode still faced a huge challenge in the following years due to severe volume expansion of Sn during the lithiation process. Without cushion matrix, decreasing Sn particle size into nanoscale or creating porous Sn structures is an effective method to alleviate volume expansion effect. In 2007, Wu's group prepared tin nanoparticles by a laser-induced vapor deposition method and studied its electrochemical performance.[407] The as-prepared Sn nanoparticles were sized in a range from 5 to 80 nm. This anode presented a high initial discharge and charge capacities, which faded nevertheless quickly after a few cycles due to nonuniform particle size and agglomeration. In 2013, Kovalenko's team synthesized monodisperse Sn nanoparticles and achieved good electrochemical performance as LIB anode.[408] The particle sizes of the Sn particles could be tuned from 9 to 23 nm according to different synthesis conditions. Such monodisperse Sn nanoparticle electrode exhibited much better cycling stability compared with commercial Sn nano powders. In 2019, Oh's team used a high-pressure thermal evaporation technique to prepare nanoporous Sn anode material for LIBs.[409] High-pressure thermal evaporation was carried out using a conventional thermal evaporation vacuum chamber with a gas flow system to form nanoporous structures of Sn. The as-prepared nanoporous Sn material had a porosity of over 98%. This anode could keep capacity retention of 63% after 100 cycles without any binders or conducting additive materials.

2.6. Tin-Based Anodes for Sodium-Ion Batteries

In principle, all types of Sn-based anodes for LIBs can be applied in SIBs, because the Sn active site can electrochemically react with Na ions to form alloys.[88] The reaction mechanism of Sn in SIBs and its theoretical capacity are presented in Equation (2) and Figure 1, respectively. In this part, the brief development of tin alloy, tin/carbon composite, tin oxide, and tin sulfide/phosphide anodes will be discussed. Due to a relative short fast development period of Sn-based anodes for SIBs (since the 2010s), the subcategory based on time frame in every single type of anode material will not be created in this part.

2.6.1. Tin Alloy-Based Anodes for Sodium-Ion Batteries

As we discussed in Section 2.1.4, studies about Sn alloy-based anodes for LIBs entered a steady development stage. Due to sharing a large part of attention from LIBs, researches about Sn alloy-based anodes for SIBs started to emerge and gained much progress since 2010s. For alloy anodes, introducing carbonaceous matrixes and creating nanostructures are still effective methods to further improve the electrochemical performance.

SnSb alloy attracted much attention during this period, because of its high capacity, suitable voltage plateaus, and inexpensive price. Although SnSb is regarded as an active/inactive anode material, the inactive phase Sb still can react with sodium to form Na_3Sb alloy and provide capacities (theoretical capacity of SnSb for SIBs: 752 mAh g^{-1}), which is similar with the reaction mechanism toward lithium.[410,411] The reaction process is described as following equations[412]

$$SnSb + 3Na^+ + 3e^- \leftrightarrow 3Na_3Sb + Sn \quad (16)$$

$$Na_3Sb + Sn + 3.75Na^+ + 3.75e^- \leftrightarrow Na_3Sb + Na_{3.75}Sn \quad (17)$$

In 2015, SnSb nanoparticles were loaded onto reduced graphene oxide (RGO) sheets to form SnSb/RGO nanocomposite and applied as anode for SIBs.[413] The particle size of SnSb could be controlled at 20–30 nm, and the SnSb nanoparticles were uniformly dispersed on RGO sheets due to bonding effect between functional groups of RGO and precursors of Sn and Sb. The presence of RGO played a key role in alleviating volumetric effects of SnSb alloy as well as increasing electrical conductivity, leading to enhanced electrochemical performance. In 2017, Zhang and Ma synthesized a 3D-nanostructured SnSb alloy electrode via electrodeposition, assisted with porous nickel scaffold.[414] When applied as anode for Na-ion battery (in this review, a number of anode materials were investigated for both LIBs and SIBs. In this case, we only discuss their electrochemical performance for SIBs in the corresponding parts), it could keep a reversible capacity of about 247 mAh g^{-1} after 1000 cycles at a current density of 1 mA g^{-1}. In 2018, Zhang's team fabricated

a bimetallic nanoporous SnSb (NP-SnSb) alloy anodes for SIB through the compositional design of ternary Mg–Sn–Sb precursor and subsequent dealloying,[415] as shown in **Figure 11**a. The specific surface area of the NP-SnSb was 16.97 m^2 g^{-1} derived from BET method. This SnSb exhibited good electrochemical performance for SIBs in both half cells and full cells. Especially, the full cell, using $Na_3V_2(PO_4)_3$ cathode, maintained capacity retention of 86.2% after 200 cycles with a discharge capacity of 388.6 mAh g^{-1}, at a current density of 500 mA g^{-1}.

In addition, several studies have been published which aimed to gain insights into the alloying mechanism of SbSb anode for SIBs.[410,412,416] As we mentioned in Section 2.1.4, Fehse et al. have investigated the electrochemical reaction mechanism of TiSnSb alloy as anode of LIBs.[256] In 2018, they revealed the sodiation/desodiation mechanisms of the SnSb anode via in operando XRD, XAS and Mössbauer spectroscopy, and explained the reason why SnSb can exhibit better performance in SIB than in LIB in spite of its even larger volume expansion[416] The results indicated that SnSb undergoes a two-step alloying reaction upon sodiation in which Sb is firstly sodiated, ensuring the sodiation of Sn. The sodiated phases are confirmed as Na_3Sb and $Na_{15}Sn_4$ as well as an amorphous Sn metal intermediate phase α-Sn. Different from the lithiation process of SnSb, the sodiation process of SnSb alloy exhibits a gradual and decoupled way by firstly sodiating Sb and subsequently Sn. Therefore, the volume change of SnSb when sodiating is a stepwise and steady increase, which is less harmful to the electrode structure than an abrupt formation of lithiated compounds in LIBs. Besides, the strong amorphization upon sodiation of SnSb could provide a cushion for the volume change, leading to a better electrochemical performance than SnSb during lithiation–delithiation cycles.

Moreover, Kovalenko's team brought the advantage of nanoparticle synthesis to SIB domain.[230,417] Monodisperse SnSb nanocrystals were prepared by a facile colloidal method. The as-prepared SnSb nanoparticle anodes exhibited stable cyclability and good rate performance in both LIBs and SIBs. Additionally, various Sn alloys were also studied as anodes for SIBs, such as Sn–Cu,[418] Sn–Ni,[419] Sn–Fe,[420] Sn–Co,[421] Sn–La,[422] and Sn–Mn[423] alloys.

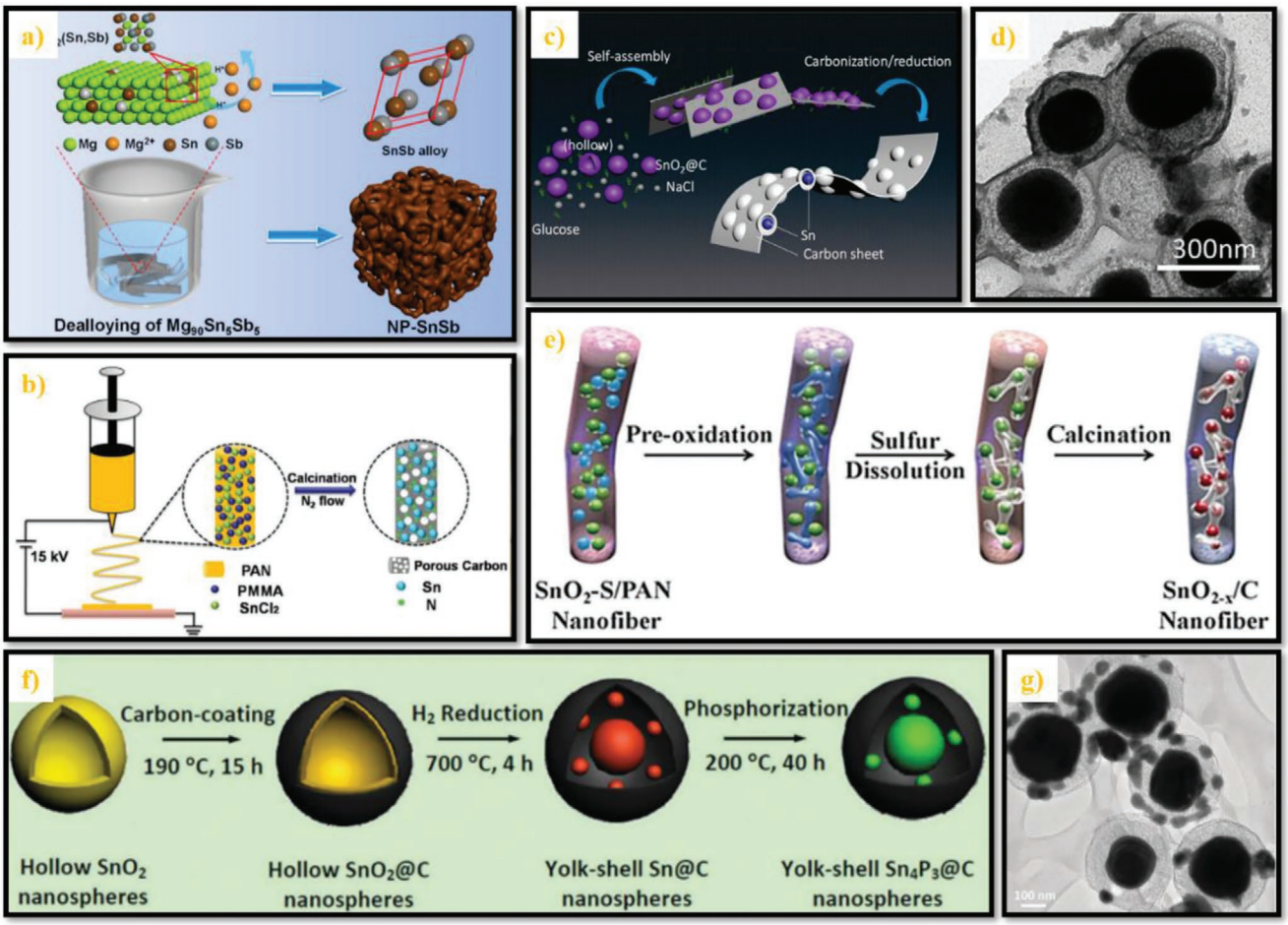

Figure 11. a) Schematic illustration of the one-step dealloying process for NP-SnSb alloy. Reproduced with permission.[415] Copyright 2018, Elsevier Ltd. b) Schematic illustration of the preparation process for Sn NDs@PNC nanofibers. Reproduced with permission.[429] Copyright 2015, Wiley-VCH. c) Synthetic procedure and d) TEM image of yolk–shell Sn@C eggette-like compounds. Reproduced with permission.[430] Copyright 2016, American Chemical Society. e) Schematic illustration of the formation of SnO_{2-x}/C nanofibers. Reproduced with permission.[434] Copyright 2018, Wiley-VCH. f) Schematic illustration of the fabrication and g) TEM image of uniform yolk–shell Sn_4P_3@C nanosphere anodes. Reproduced with permission.[435] Copyright 2015, Royal Society of Chemistry.

2.6.2. Tin/Carbonaceous and Other Material Composite Anodes for Sodium-Ion Batteries

With the existence of carbonaceous and other materials, more possibilities are generated toward high-performance Sn-based anodes for SIBs. Compared with the contemporary in Li-ion battery studies, researches of Sn/C (other materials) composite anodes for Na-ion batteries presented similar design principle and synthesis method.[424–428] Actually, most of these anode materials were double-functional, which could be applied in both LIBs and SIBs.

Both contact-type and noncontact-type structures were constructed with respect to the Sn-based anodes for SIBs. In 2015, Jiao and Chen reported a high-performance Sn/C composite anode for SIBs, where Sn nanodots were finely encapsulated in porous N-doped carbon nanofibers through an electrospinning technique and subsequent thermal treatment,[429] as presented in Figure 11b. Due to an appropriate selection of calcination temperature, ultrasmall Sn nanodots (1–2 nm) and high Sn content (about 63%) were obtained, leading to an effective reduction of absolute volume change from the tin as well as high specific capacity. After 1300 cycles at 2000 mA g^{-1}, this Sn/C anode only lost 10% of capacity, which maintained at 483 mAh g^{-1}. Regarding the noncontact-type electrode, Liu and Wang prepared a yolk–shell Sn@C anode material in 2016. The work was inspired by a Hong-Kong snack-eggette in which the cream was poured into the mold to form a sphere-sheet bread with cheese in the core.[430] The hollow SnO_2 nanospheres coated with carbon shell were homogeneously dispersed in NaCl/glucose solution. Then, SnO_2@C nanospheres with glucose were formed through a self-assembly process templated by NaCl.[431,432] The final product was obtained by carbonization and reduction process. The preparation process and morphology are presented by Figure 11c,d. Such yolk–shell structure could effectively improve the electrochemical performance when applied in SIBs.

In 2017, Zhang and co-workers introduced TiO_2 into the Sn/C system, in order to further improve cycling stability and high-rate performance of the anode for rechargeable batteries.[433] A pipe-wire TiO_2-Sn@CNFs anode material was synthesized via electrospinning and atomic layer deposition (ALD), where the nano-Sn was uniformly dispersed in carbon nanofibers and covered by thin TiO_2 film. The subsequent calcination process created vacant space between TiO_2 pipe and Sn@ CNFs, resulting in good absorption of tin expansion and integrity of SEI. When used as an anode in SIB, reversible capacities of 490 and 413 mAh g^{-1} were achieved at the end of 10 and 400 cycles (at a current density of 100 mA g^{-1}), respectively, with 15.7% capacity loss over 400 cycles. The performance was much better than the electrode without void space design.

2.6.3. Tin Oxide-Based Anodes for Sodium-Ion Batteries

Studies about the application of tin oxide anodes for SIBs appeared since around 2013.[436,437] Both SnO and SnO_2 can electrochemically react with Na ions based on following equations,[438,439] corresponding to theoretical capacities of 1144 mAh g^{-1} and 1378 mAh g^{-1} respectively

sodiation:

$$SnO + 2Na^+ + 2e^- \rightarrow Sn + Na_2O \quad (18)$$

$$Na_2O + Sn + 0.5Na^+ + 0.5e^- \rightarrow Na_2O + 0.5NaSn_2 \quad (19)$$

desodiation:

$$Na_2O + 0.5NaSn_2 \rightarrow xSnO + (1-x)Sn + yNa^+ + ye^- \quad (20)$$

and

sodiation:

$$SnO_2 + 4Na^+ + 4e^- \rightarrow Sn + 2Na_2O \quad (21)$$

$$2Na_2O + Sn + 2.25Na^+ + 2.25e^- \rightarrow 2Na_2O + 0.25Na_9Sn_2 \quad (22)$$

desodiation:

$$2Na_2O + 0.25Na_9Sn_2 \rightarrow SnO_2 + 6.25Na^+ + 6.25e^- \quad (23)$$

However, the actual reversible capacities of SnO and SnO_2 are much lower than the theoretical values, due to irreversible generation of Na_2O and formation of different Sn–Na alloy phases at different cathodic potentials.[436,437] For tin oxide-based electrodes, the large volume expansion and low intrinsic conductivity are major obstacles to impede their practical application in SIBs. Various high-performance tin oxide-based anodes for SIBs were synthesized recently, assisted with cushion materials and nanosturctures.[434,440,441]

In 2017, Varzi and co-workers fabricated tetrahedral SnO micro flowers as anode material for SIB, through an ultrafast ionic liquid-assisted microwave synthesis.[440] The SnO micro flowers were synthesized (5 min) at a low temperature (120 °C). According to the explanation of authors, this process could be ascribed to excellent microwave absorption capability of the ionic liquid-based solution. This heating process was not only very effective due to interaction between ionic liquid and microwaves,[442] but also economic and safe. Besides, this electrode exhibited good electrochemical performance in SIBs. In 2018, Zhang and Lin reported a strategy to produce oxygen-vacancy-containing SnO_{2-x}, as advanced anode material for Na-ion battery.[434] According to the route in Figure 11e, SnO_2 nanoparticles, sulfur nanoparticles and polyacrylonitrile (PAN) were used as raw materials for fabricating nanofibers via electrospinning technique. After drying, removing residual sulfur and carbonization process, the final SnO_{2-x}/C nanofibers were obtained, which could be directly used as electrode without any binder and electron conductive agent. The sulfur nanoparticles played a key role in well-defined void surrounding the SnO_2 anodes, which could effectively buffer the volumetric expansion during cycling. Additionally, the transform form SnO_2 to SnO_{2-x} was able to introduce oxygen vacancies, which reduced reaction energy barrier and enhanced intrinsic electronic conductivity. Therefore, this anode exhibited good electrochemical performance, which could maintain a reversible capacity of 565 mAh g^{-1} after 2000 cycles at a high current density of 1000 mA g^{-1}. Besides, this free-standing electrode showed a potential application for flexible SIBs.

2.6.4. Tin-Based Compound Anodes for Sodium-Ion Batteries

Since the middle of the 2000s, Sn-based compound (mainly Sn sulfide, sulfate, phosphide, and phosphate) started to become favorable as anode materials for LIBs, as discussed in Section 2.4. Until about 2014, studies on these materials were extended to SIB anodes. Especially, Sn phosphide (or phosphate)[443–446] and Sn sulfide,[447,448] including Sn_4P_3, $Sn_2P_2O_7$, SnS_2, and SnS, attracted much attention. The reaction mechanism with Na ions can be described as following.

Sn phosphide (Sn_4P_3 as example[446])

$$Sn_4P_3 + 24Na^+ + 24e^- \leftrightarrow Na_{15}Sn_4 + 3Na_3P \quad (24)$$

Sn phosphate ($Sn_2P_2O_7$ as example[449])

$$Sn_2P_2O_7 + 4Na^+ + 4e^- \rightarrow 2Sn + Na_4P_2O_7 \quad (25)$$

$$2Sn + 4.5Na^+ + 4.5e^- \leftrightarrow 0.5Na_9Sn_4 \quad (26)$$

Sn sulfide (SnS_2 as example,[450] SnS has a similar reaction mechanism.)

$$SnS_2 + 2Na^+ + 2e^- \leftrightarrow Sn + Na_2S_2 \quad (27)$$

$$Sn + 3.75Na^+ + 3.75e^- \leftrightarrow Na_{3.75}Sn \quad (28)$$

According to calculation, the theoretical capacities of Sn_4P_3, $Sn_2P_2O_7$, SnS_2, and SnS for SIBs are 1132, 1108, 843, and 1022 mAh g^{-1}, respectively.

In 2014, tin phosphide (Sn_4P_3) was firstly studied as a promising anode material for Na-ion battery. The electrode was prepared by simple ball-milling and exhibited high specific capacity and good electrochemical performance.[446] Because of its high specific capacity, the related investigations of Sn_4P_3 anodes were pushed to a climax at a short time. As to Sn_4P_3 anodes, however, the major problem was still the enormous volume change during cycling, leading to electrode structure pulverization, rapid capacity fading and repeated SEI formation.[444] Both tin and phosphorus could react with sodium to form alloys, and the total volumetric expansion after full sodiation were about 420% and 590%, respectively.[451–453] Besides, the poor electrical conductivity of P also influences the final performance of batteries. In 2015, Yu's team synthesized yolk–shell Sn_4P_3@C nanospheres as anode for Na-ion battery, which largely enhanced cycling stability of this anode material.[435] Monodisperse well-defined SnO_2 hollow nanospheres were fabricated and used as templates. After carbon-coating, reduction of SnO_2 and phosphorization, the final products were synthesized. The fabrication method and morphology of this yolk–shell electrode are shown in Figure 11f,g. The as-prepared yolk–shell Sn_4P_3@C nanospheres presented a high reversible capacity of 790 mAh g^{-1} at 100 mA g^{-1} and kept a capacity of 360 mAh g^{-1} at 1500 mA g^{-1} after 400 cycles. In 2018, tin pyrophosphate ($Sn_2P_2O_7$) was demonstrated as a promising candidate of Na-ion battery anode due to its high theoretical capacity.[449,454] Du's group synthesized amorphous $Sn_2P_2O_7$/rGO nanocomposite by a simple two-step ball-milling process and reported its electrochemical performance for SIBs for the first time.[449] The nanohybrid electrode exhibited a capacity of 480 mA h g^{-1} at 50 mA g^{-1} and maintained 70% capacity after 15 000 cycles. Moreover, two prototype full cells were assembled with $Na_3V_2(PO_4)_2F_3$/C and $Na_3V_2(PO_4)_2F_3$/C cathodes, respectively. Both full cells could keep a long cycle life over 1000 cycles with an energy density of more than 140 Wh kg^{-1}.

Almost at the same time, tin sulfides also emerged as high-performance anodes for SIBs. Graphene-based materials were widely used to improve the electrochemical properties of the tin sulfides in SIBs.[447,450,455] To our best knowledge, Lee's team was one of the first groups to apply tin sulfide as anode material for Na-ion battery.[447] In 2014 they fabricated SnS_2–rGO nanocomposite through a hydrothermal route from a mixture of tin (IV) chloride, thioacetamide (TAA) and graphene oxide. The as-obtained SnS_2–rGO anode could reach a high specific capacity of 630 mA h g^{-1} at 200 mA g^{-1}, and present a long cycle life (500 mAh g^{-1} at 1000 mA g^{-1} for 400 cycles). Besides, the full Na-ion cell consisting of $Na_{0.80}Li_{0.12}Ni_{0.22}Mn_{0.66}O_2$ cathode and SnS_2–RGO anode also showed good performance. In addition, other types of tin sulfide-based high-performance anodes of SIBs were also reported recently, such as SnS 3D nanoflowers,[448] SnS@SPC (S-doped porous carbon)[456] and SnS/CNTs@S-CNFs (SnS/CNTs encapsulated by S-doped CNFs hybrids).[457]

Besides tin–sulfur compounds, other tin–chalcogenide group element compounds such as SnSe and SnTe were also demonstrated to have sodium-storage properties and studied as anode materials for Na-ion batteries since about 2015.[458–464] SnSe, known as a p-type semiconductor, was firstly applied as anode for SIB by Lee's team in 2015.[461] The reaction mechanism between SnSe and Na ions is presented as following, corresponding to a theoretical capacity of 780 mAh g^{-1}

$$4SnSe + 23Na^+ + 23e^- \leftrightarrow Na_{15}Sn_4 + 4Na_2Se \quad (29)$$

The SnSe/C anode fabricated by Lee's team exhibited a reversible capacity of 707 mAh g^{-1} at a current density of 143 mA g^{-1} over 50 circles. Tellurium (Te) can alloy with lithium and sodium to form Li_2Te and Na_2Te and has been applied as anode materials for both LIBs and SIBs.[465,466] SnTe is a semiconductor and has been utilized in diverse electronic devices, such as infrared detectors, and insulators.[467–469] Due to its high density of 6.445 g m^{-3}, SnTe is regarded as a good anode candidate with large volumetric capacity for LIBs and SIBs. In 2017, the Li/Na-storage properties of SnTe were reported by Park for the first time.[458] As an anode for Na-ion batteries, SnTe showed a theoretical capacity of 626 mAh g^{-1}, and the reaction mechanism is summarized by the following chemical formulas

$$4SnTe + 23Na^+ + 23e^- \leftrightarrow Na_{15}Sn_4 + 4Na_2Te \quad (30)$$

According to the report by Park, SnTe/C was synthesized via a solid-state ball-milling process. Assisted with carbon matrix, SnTe/C presented good cycling stability in SIBs, which could remain reversible gravimetric and volumetric capacities of 316 mAh g^{-1} and 639 mAh cm^{-3}, respectively, after 100 cycles at 50 mA g^{-1}. Moreover, it also exhibited a rapid C-rate characteristic, reaching a volumetric capacity of 430 mAh g^{-1} at a 3C rate (1C = 320 mA g^{-1}).

2.7. Temporary Summary of Tin-Based Anodes

Since the 1990s, Sn-based anodes have evolved into various types and tremendous progress has been made. During the

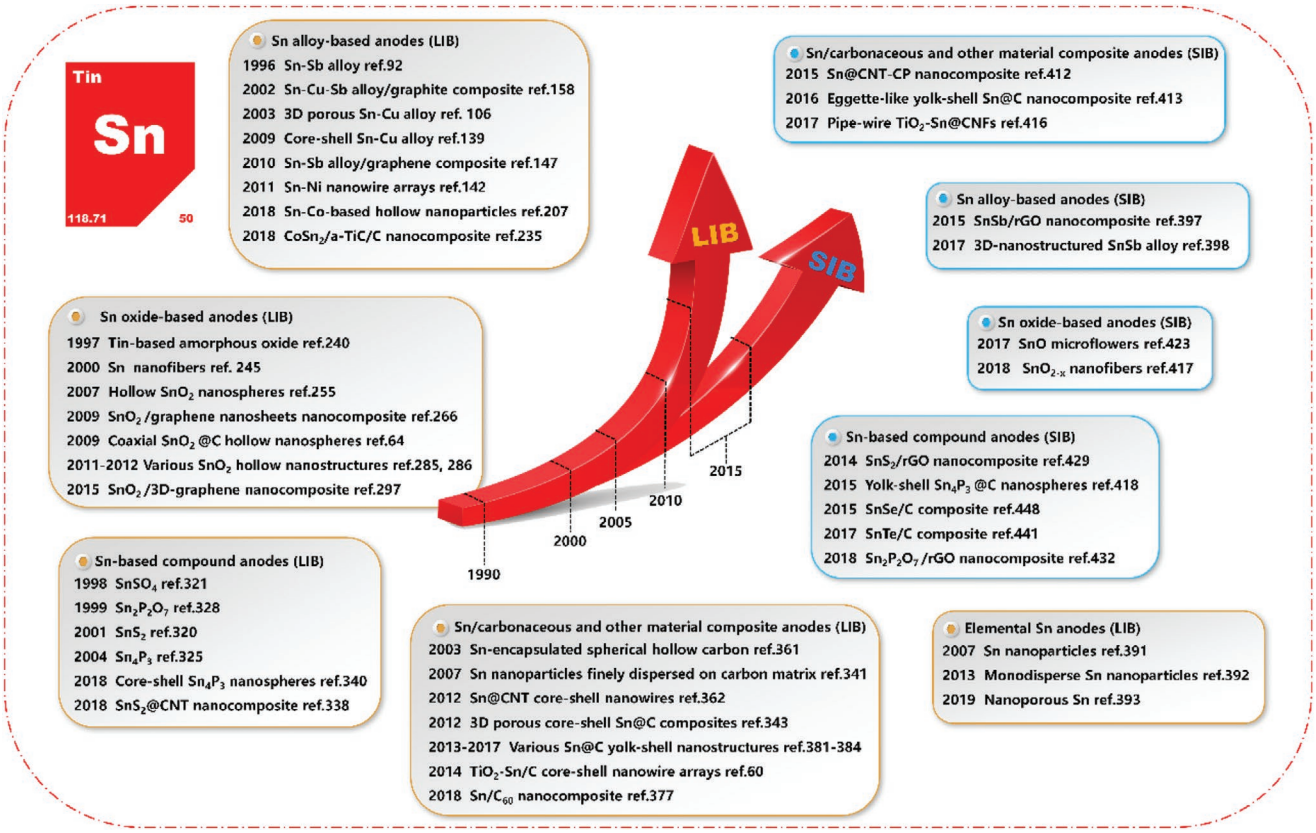

Figure 12. A brief illustration of the development history of tin-based anodes.

last 30 years, the development of Sn-based anodes could be regarded as a fighting against the huge volumetric effect of Sn. Tin alloys, tin oxides, tin-based compounds, tin/carbon (or noncarbon) composites, and element tin materials all can be applied as anodes for LIBs. Most of them could also be used in SIBs. Three mainstream strategies for alleviating volume expansion, decreasing particle size, creating void space and introducing cushion matrix, have entered a mature stage and achieved promising results. A brief development history of Sn-based anodes is illustrated in **Figure 12**, and some representative Sn-based anodes of every type mentioned above are also listed in the Figure 12. With a panoramic perspective, the origin of the Sn-based anodes was derived from a large number of basic studies from the 1960s to 1990s. In the last 10 years of the 20th century, Sn-based anodes gradually attracted attention and evolved into several classifications. From 2000 to 2010, studies about Sn-based anodes stepped into a fast-developing period, the electrochemical performance of the Sn-based anodes were obviously enhanced. The year 2010 can be considered as a watershed, when the renaissance of SIBs promoted the researches about Sn-based anodes to a great mass fervor. Due to this divergence of research attention from LIB to SIB, the rising trend of Sn-based anodes for LIBs started to become relative gentle since 2015. Moreover, in order to accelerate the practical application of Sn-based anodes, studies have been performed to develop facile and scalable methods to synthesize Sn-based anode materials with high tap density in recent years. Generally, Sn-based anodes presented a relative balance development in both LIB and SIB domains. The synthetic methods and electrochemical performance of representative studies about tin-based anodes for LIBs and SIBs are summarized in **Table 1**.

3. Antimony-Based Anodes for Rechargeable Batteries

Antimony (Sb), the neighbor of tin in the periodic table of the elements, is also a promising anode candidate for rechargeable batteries. Sb can electrochemically react with lithium or sodium to form alloys based on following equations, presenting a theoretical capacity of 660 mAh g^{-1} in both LIBs and SIBs.[470–472] Due to this reason, almost all Sb-based anode materials exhibit the same theoretical capacity whatever in LIBs or SIBs

$$Sb + 3Li^+ + 3e^- \leftrightarrow Li_3Sb \quad (31)$$

$$Sb + 3Na^+ + 3e^- \leftrightarrow Na_3Sb \quad (32)$$

Similar to the Sn-based anodes, the origin of the Sb-based anode studies could also be traced back to 1970s.[473,474] Weppner and Huggins studied kinetic parameters and thermodynamic properties of Li–Sb system through electrochemical galvanostatic intermittent titration technique (GITT) and calculations of Gibbs free energy of formation, corresponding enthalpies, and entropies of the alloying system, respectively.[473,474]

Table 1. Summary on representative studies about tin-based anodes for LIBs and SIBs (ICE: initial coulombic efficiency; *n*: the *n*th cycle).

Material type	Development stage	Representative anode	Synthetic method	ICE	Charge capacity [mAh g^{-1}] (*n*, rate)	Rate capacity [mAh g^{-1}] (rate)	Ref.
			LIBs				
Tin alloy	Emergence stage	SnSb alloy	Electroplating method	\	\	\	[90]
	(before 2000)						
	Preliminary stage	3D porous Cu_6Sn_5	Electrochemical deposition	\	400 (30, 0.5 mA cm^{-2})	200 (10 mA cm^{-2})	[114]
	(2000–2006)	Ni_3Sn_4	Ball-milling method	46%	≈180 (100, 0.2 mA cm^{-2})	\	[117]
		Sn–Ag alloy	Ball-milling method	\	350 (50, 0.2 mA cm^{-2})	\	[73]
Nano-tin alloy	Fast development stage	Ni–Sn nanowires	PAA templating method	\	250 (60, 50 mA g^{-1})	\	[146]
	(2007–2011)	Core–shell Sn–Cu	Redox transmetalation reactions	82%	600 (170, 0.48 A g^{-1})	620 (3.6 A g^{-1})	[149]
Micro-tin alloy		3D porous Sn–Co	Electroplating method	83%	511 (70, 0.1 A g^{-1})	200 (5 A g^{-1})	[158]
		3DOM Ni–Sn	PS templating method	84%	500 (200, 0.1 mA cm^{-2})	360 (1 mA cm^{-2})	[150]
Tin alloy/C		Core–shell Cu_6Sn_5@C	In situ polymerization	55%	430 (50, 0.1 A g^{-1})	\	[166]
		Sn/Sb/C	Sol–gel method	≈40%	300 (100, 100 mA cm^{-2})	100 (440 mA cm^{-2})	[170]
		SnSb@C/GNS	Chemical synthesis	87%	896 (30, 88 mA g^{-1})	668 (4000 mA g^{-1})	[151]
Nano-tin alloy	Steady development stage	3D Ni–Sn NW network	PAA templating method	\	450 (50, 0.2C)	≈400 (6C)	[204]
	(since 2012)	Core–shell Sn–Co alloy	Kirkendall effect-derived method	≈80%	1265 (200, 1 A g^{-1})	608 (10 A g^{-1})	[223]
		Monodisperse $CoSn_2$	Colloidal synthesis	\	750 (500, 992 mA g^{-1})	650 (1984 mA g^{-1})	[224]
Micro-tin alloy		3D Sn–Sb–Co alloy	Electrodeposition	83%	549 (300, 130 mA g^{-1})	500 (16 A g^{-1})	[237]
Tin alloy/C		3D Sn–Ni–Cu@C	PC membrane templating method	≈45%	≈450 (400, 0.45 A g^{-1})	≈150 (4.5A g^{-1})	[242]
		0D-Co–Sn⊂3D-pGN	Surfactant-assisted assembly method	63%	925 (200, 1 A g^{-1})	432 (10 A g^{-1})	[245]
		$CoSn_2$/a-TiC/C	Ball-milling method	83%	≈480 (180, 0.1 A g^{-1})	380 (1.5 A g^{-1})	[251]
Tin oxide	Preliminary stage	TCO	Molten-state reaction	≈63%	≈580 (100, 0.5C)	\	[262]
	(before 2000)	SnO_2	Commercial material	\	≈600 (2, \)	\	[266]
Nano-tin oxide	Rising stage	SnO_2 nanofibers	PC filter templating method	\	600 (1400, mA cm^{-2})	500 (2.6 mA cm^{-2})	[267]
	(2000–2009)	SnO_2 hollow nanosphere	Ostwald ripening mechanism	\	≈480 (40, 0.2C)	\	[277]
Tin oxide/C		SnO_2/GNS	Solvothermal method	\	570 (30, 50 mA g^{-1})	\	[288]
		SnO_2/CNTs	Chemical synthesis	≈60%	850 (65, 40 mA g^{-1})	\	[295]
		SnO_2 nanotube@CNTs	Confined-space catalytic deposition	\	542 (200, 0.3 mA cm^{-2})	\	[240]
Nano-tin oxide	Fast development stage	Hollow SnO_2 nanoboxes	Hydrolysis and etching	45%	570 (40, 0.2C)	470 (0.5C)	[304]
	(since 2010)	Sn@void@SnO/SnO_2	Kirkendall effect-derived electrospinning	47%	630 (250, 2 A g^{-1})	553 (8 A g^{-1})	[307]
Tin oxide/C		SnO_2/G	Chemical synthesis	≈61%	558 (50, 0.2C)	\	[309]
		SnO_2/3D-HPG	Hydrothermal method	58%	986 (100, 0.1 A g^{-1})	507 (10 A g^{-1})	[316]
		C@SnO_2@C nanofibers	Single spinneret electrospinning	95%	837 (200, 52 mA g^{-1})	180 (5220 mA g^{-1})	[324]
Tin oxide/ noncarbon		SnO_2/TiO_2	Solvothermal method	\	625 (50, 50 μA g^{-1})	\	[329]
Tin-based compound	Preliminary stage	$SnSO_4$	Commercial material	\	≈380 (20, 0.1 mA cm^{-2})	\	[340]
	(1998–2006)	a-$Sn_2P_2O_7$	Melt-quenching procedure	49%	487 (5, 20 mA g^{-1})	\	[346]
		c-SnS_2	Sonochemistry	\	400 (10, 50 mA g^{-1})	\	[339]
		Sn_4P_3	Mechanochemical technique	79%	370 (50, \)	\	[343]
	Rising stage	Core–shell Sn_4P_3/C	Chemical synthesis	\	440 (500, 2 A g^{-1})	380 (4 A g^{-1})	[358]
	(since 2007)	SnS_2/CNTs	Plasma-assisted fabrication	≈70%	2377 (470, 0.3 A g^{-1})	200 (5 A g^{-1})	[356]
Tin/carbon	Preliminary stage	Core–shell Sn@C	Chemical synthesis	49%	≈250 (10, 50 mA g^{-1})	\	[377]

Table 1. Continued.

Material type	Development stage	Representative anode	Synthetic method	ICE	Charge capacity [mAh g^{-1}] (*n*, rate)	Rate capacity [mAh g^{-1}] (rate)	Ref.
	(2000–2005)	Sn/CNFs	Chemical reduction	≈54%	≈600 (40, 0.25C)	\	[365]
Contact-type	Fast development stage	Fine-dispersed Sn/C	R–F gel method	≈70%	500 (200, 1 A cm^{-2})	200 (6.25 A cm^{-2})	[179]
	(2006–2012)	Sn@CNT nanowires	Chemical growth method	80%	490 (100, 0.1 A g^{-1})	270 (3 A g^{-1})	[378]
		3D porous Sn@C	Electrostatic spray deposition	74%	672 (200, 25 mA g^{-1})	350 (300 mA g^{-1})	[360]
Noncontact-type		Sn@TNHCs	Hydrothermal method	≈78%	550 (100, 0.2C)	\	[383]
Contact-type	Explosive development stage	Sn@GS–VAGNs	MPECVD method	54%	400 (5000, 3.6 A g^{-1})	151 (166.2 A g^{-1})	[385]
	(since 2013)	Pitaya-like Sn/C	Aerosol spray pyrolysis	69%	710 (130, 0.2 A g^{-1})	600 (16 A g^{-1})	[388]
		Sn/C_{60}	RFPATE–CVD method	64%	834 (5000, 1 A g^{-1})	544 (10 A g^{-1})	[393]
Noncontact-type		Yolk–shell nanospheres	Catalyzed thermal CVD method	66%	430 (800, 0.2 A g^{-1})	\	[397]
		Yolk–shell nanoboxes	Coating and heat treatment	61%	810 (500, 0.2 A g^{-1})	350 (2 A g^{-1})	[400]
Elemental tin	since 2007	Sn NPs	Laser-induced vapor deposition	91%	479 (10, 0.2 mA cm^{-2})	\	[407]
		Monodisperse Sn NPs	Chemical synthesis	\	1000 (100, 1 A g^{-1})	\	[408]
			SIBs				
Tin alloy	2010s	SnSb/rGO	Chemical synthesis	80%	361 (80, 0.1 A g^{-1})	85 (15 A g^{-1})	[413]
		NP-SnSb alloy	Dealloying method	≈60%	506 (100, 0.2 A g^{-1})	458 (10 A g^{-1})	[415]
Tin/carbon (/other)	2010s	Eggette-like Sn@C	Self-assembly process	≈90%	200 (1000, 1 A g^{-1})	160 (5 A g^{-1})	[430]
		TiO_2–Sn@CNFs	Electrospinning and ALD	58%	413 (400, 0.1 A g^{-1})	\	[433]
Tin oxide	2010s	SnO micro flowers	Ionic liquid-assisted microwave synthesis	≈90%	470 (50, 0.1 A g^{-1})	359 (0.25 A g^{-1})	[440]
		SnO_{2-x}/C nanofibers	Electrospinning	55%	565 (2000, 1 A g^{-1})	340 (5 A g^{-1})	[434]
Tin-based compound	2010s	Yolk–shell Sn_3P_4@C	Coating and phosphorization	44%	360 (400, 1.5 A g^{-1})	421 (3 A g^{-1})	[435]
		$Sn_2P_2O_7$/rGO	Two-step ball-milling	52%	≈200 (15 000, 2 A g^{-1})	170 (10 A g^{-1})	[449]
		SnS_2/rGO	Hydrothermal method	75%	500 (400, 1 A g^{-1})	544 (2 A g^{-1})	[447]
		SnTe/C	Solid-state ball-milling	86%	316 (100, 50 mA g^{-1})	234 (960 mA g^{-1})	[458]

According to the results, Sb exhibited high chemical diffusion coefficient and each mole of antimony could react with three moles of lithium, which indicated a great potential as anode for LIBs. However, the huge volume change of Sb during lithiation (147%) and sodiation (293%) is still the largest barrier to realize practical applications.[79,471,475] Compared to Sn-based anodes, the types of materials and strategies of improving the electrochemical performance of Sb-based anodes are not distinctly different. However, different evolution trends are displayed, especially when the interests in Na-ion batteries were renewed after 2010.

3.1. Antimony Alloy-Based Anodes for Lithium-Ion Batteries

Similar to tin alloy-based anodes, antimony alloy-based anodes also mainly relied on the simple "active/inactive" mechanism to mitigate the volume effect of Sb. With continuous development, nanostructured Sb alloys and Sb alloy/carbonaceous material composites appeared as anodes for LIBs in the following years, leading to improved electrochemical performance.

3.1.1. Emergence Stage: Before 2006

Since the last few years of 1990s, studies on electrochemical reactions between lithium and Sb alloys were initiated, such as Co–Sb,[476,477] In–Sb,[478] Ti–Sb,[479] Zn–Sb,[480] Cr–Sb,[481] Mg–Sb,[482] Ag–Sb,[483] and Co–Fe–Sb.[484] These fundamental studies paved a way for developing Sb-based alloy anodes for LIBs. In 2004, Striebel's team prepared Cu_2Sb thin film electrode by a pulsed laser deposition technique at room temperature and tested its electrochemical performance in Li-ion batteries.[485] When cycled over a limited voltage window (0.65–1.4 V vs Li/Li^+), this alloy anode presented a relative stable cyclability within 50 cycles. During this period, Sb-alloy anodes generally relied on the "active/inactive" principle to alleviate volume change of Sb. As discussed in Section 2.1, the capability

of inactive phase in alloys to enhance cycling stability was very limited, thus most of Sb-alloy anodes for LIBs only exhibited moderate performance before 2006.

3.1.2. Rising Stage: 2006–2011

After fundamental research on electrochemical property of Sb, it was natural to develop effective strategies to improve electrochemical performance of antimony alloys anodes for LIBs. In this period, nanostructures and carbonaceous materials exhibited their advantages and became the mainstream strategies to improve performance of Sb alloy anodes. Various nanostructured Sb alloy anodes were synthesized during this timeframe, such as 3D porous Fe–Sb–P amorphous alloy,[486] $CoSb_3$ nanoparticle chains,[487] Zn–Sb alloy nanoflakes,[488] and so on. In 2011, Yan's team reported a template-free single-step synthesis process to fabricate nanostructured Zn–Sb alloys by electrochemical deposition.[488] Particularly, Zn–Sb nanoflakes, nanowires, and nanoparticles could be prepared based on different deposition parameters. The as-deposited Zn–Sb nanoflakes showed a porous morphology with a wide pore-size range from 100 to 800 nm. This open porous structure not only benefited lithium ion diffusion but also buffered volume expansion of Sb during lithiation process. Therefore, the Zn–Sb nanoflakes electrode exhibited the highest specific capacity and best cycling stability, compared with Zn–Sb nanowires and nanoparticles.

Moreover, Sb alloy/C composite anodes also emerged in this stage. In 2010, Park and Sohn prepared ZnSb/C electrode material with simple methods such as heat-treatment and high energy mechanical milling (HEMM) technique.[489] What's more, a "quasi-intercalation'' concept was proposed and applied to guide the synthesis of high-performance anodes for LIBs. According to this report, quasi-intercalation was a process in which a layered structure transformed into another layered structure of host atoms and periodic Li arrays through electrochemical recrystallization upon lithiation. A quasi-intercalation anode material could embrace various advantages, such as small electrochemical energy for recrystallization, fast Li mobility, and limited volume expansion. The orthorhombic ZnSb had a crystalline structure with both layers and channels, and it was demonstrated that ZnSb crystals followed the quasi-intercalation mechanism during lithiation. Under a voltage range of 0.8–2.0 V, ZnSb electrode exhibited a stable cyclability, which kept capacity retention of about 80% after 1000 cycles at a current density of 100 mA g^{-1}. Introducing carbon matrix into ZnSb system could further enhance the electrochemical performance. The as-prepared ZnSb/C composite anode maintained a reversible capacity of ≈520 mAh g^{-1} after 200 cycles at a cycling rate of 100 mA g^{-1}, and also obtained a stable capacity of ≈480 mAh g^{-1} when tested at 1800 mA g^{-1}.

3.1.3. Steady Development Stage: Since 2012

Compared with Sn alloy-based anodes, related studies about Sb alloy-based anodes for LIBs looked like underpowered at the same period (since 2012). Such trend was mainly attributed to the renaissance of SIBs, and similar development trend also presented in other types of Sb-based anodes for LIBs. Although the number of the studies on Sb alloy anodes was relative less during this period, some of them were still worthy of attention. In 2013, Zheng's group reported their work about the CVD growth of several 1D-nanostructured Zn_4Sb_3 alloys, including nanotubes, nanowires, and nanorods.[490] When applied as anodes for Li-ion batteries, the Zn_4Sb_3 nanotube exhibited the best cycling stability due to existence of inner void space. Since about 2008, Prieto's group was always focusing on high-performance Cu–Sb alloy LIBs anodes prepared with an electrodeposition method.[491–494] In 2018, they investigated the correlation between the electrochemical performance of thin-film Cu–Sb alloy anode and film composition or film–substrate interface.[494] In order to achieve extended cycle life, various Cu_xSb ($0 < x < 2$) thinfilm anodes and different film–substrate interfaces (with or without Ni blocking layer) were built and the electrochemical performance was tested as anodes in LIBs. When $x = 1$, the Cu_xSb@Cu thin film anode exhibited the best cycling stability. This off-stoichiometric composition was beneficial to access of Li–Cu–Sb ternary phases, which improved cycling stability and minimized the amount of Cu causing excessive SEI growth. Moreover, with Ni blocking layer, the Cu_xSb@Ni@Cu thinfilm anode presented a better cycling performance than that of Cu_xSb@Cu electrode. In the case of Cu_xSb@Cu anode, voids could form at the interface between Cu–Sb alloy and Cu foil substrate because of the Kirkendall effect.[495] The presence of the voids could weaken the interfaces and exacerbate film delamination, leading to diminished cycling stability of any film composition on a Cu substrate. The Ni blocking layer between Cu–Sb alloy and Cu substrate could prevent the film–substrate interdiffusion as well as the formation of voids, resulting in enhanced cycle life.

3.2. Antimony/Carbonaceous and Other Material Composite Anodes for Lithium-Ion Batteries

Besides antimony-based alloys, antimony/carbonaceous and other material composite anode was another main branch of Sb-based anodes for LIBs. Buffering matrix can effectively improve electrochemical performance of Sb-based anodes for Li-ion batteries, which has been demonstrated as a successful strategy in the studies on the Sn-based anodes. In this part, most of studies focused on contact-type Sb-based anodes for LIBs.

3.2.1. Rising Stage: 2004–2010

To our best knowledge, researches about Sb/C composite anodes for LIBs started from about 2004.[363,496] From 2004 to 2010, most researchers tried to embed Sb nanoparticles into continuous graphite or amorphous carbon matrix. In 2004 and 2005, Billaud's group prepared antimony–graphite composite anodes via chemical reduction process, using $SbCl_5$–graphite intercalation compounds and antimony chloride/KC8 graphite intercalation compound as precursors, respectively.[496,497] In 2008, Hassoun et al. synthesized Sb/C composite anode where Sb nanoparticles were uniformly distributed in carbon matrix,[498] which could be regarded as extension of their

previous work about Sn/C composite.[179] In addition, other matrix materials were also applied in Sb-based composite anodes, such as aluminum carbide (Al_3C_4),[499] MO_x–C ceramic (M = Al, Ti, Mo),[500] silicon carbide (SiC),[501] and TiC.[502] Single use of these materials or compositing with carbon materials also gained good results for buffering volumetric effect of Sb.

3.2.2. Steady Development Stage: Since 2011

Since 2011, new types of matrix materials, such as graphene and TiO_2, and nanostructured Sb/C composite anodes for LIBs were reported. In 2016, Han and co-workers reported fabrication of 1D Sb@TiO_2 composite anodes for LIBs.[503] Sb_2O_3 nanorods were prepared and used as the initial templates, which were coated with TiO_2 layers thereafter via a sol–gel method. After the reduction process, the final Sb@TiO_2 nanocomposite was synthesized. The as-prepared Sn-based electrode material possessed not only uninterrupted TiO_2 shell but also void space inside the nanorods, leading to good electrochemical performance. In 2018, Wang and Zhang proposed a "silica reinforcement" concept and fabricated silica-reinforced carbon nanofibers encapsulating Sb nanoparticles (SiO_2/Sb@CNFs) through an electrospinning method.[504] Silica has been demonstrated as an alternative anode material for LIBs and exhibited a theoretical specific capacity as high as 1965 mAh g^{-1}.[505,506] The existence of silica could not only enhance the overall structure of the electrode but also provide additional capacity. Encapsulating Sb and SiO_2 nanoparticles into porous carbon fibers could efficiently buffer the volumetric effects during alloying/dealloying processes. In addition, the different work potentials of Sb, silica, and carbon established a stepwise mechanism of volume change. Thus, the unreacted components could accommodate the strain yielded by the reacted phase. In half-cells, this SiO_2/Sb@CNF electrode delivered reversible capacities of 700 mAh g^{-1} at 200 mA g^{-1}, and 468 mAh g^{-1} at 1000 mA g^{-1}, respectively, each after 400 cycles. With $LiCoO_2$ as the cathode, the SiO_2/Sb@CNF//$LiCoO_2$ full cell also presented a good performance, which reached a reversible capacity of about 336 mAh g^{-1} at 1000 mA g^{-1} after 500 cycles.

Recently, in order to promote Sb-based anodes into practical application, developing scalable methods to produce high-performance anodes began to attract increasing attention. In 2018, Cheng's group explored a facile scalable synthesis of hierarchical Sb/C micro/nanohybrid anode for LIBs.[507] Difunctional methacrylate monomers (Bis-GMA and TEGDMA) and liquid antimony (III) n-butoxide were selected as carbon source and Sb precursor, in order to form a uniform mixture. A fast photopolymerization process was measured to instantly polymerize the methacrylate monomers, while antimony species were homogeneously integrated into the crosslinked methacrylate network at a molecular level. After calcination, antimony nanoparticles were in situ formed and embedded homogeneously in the carbon matrix. The as-prepared Sb/C electrode with high mass-loading density could keep a reversible capacity of about 362 mAh g^{-1} at 66 mA g^{-1} after 300 cycles, corresponding to capacity retention of 79%. With reduced the mass-loading density, the anode could reach a reversible capacity of about 793 mAh g^{-1} after 100 cycles, at the same current density.

3.3. Antimony Alloy-Based Anodes for Sodium-Ion Batteries

As discussed above, related studies of Sb-based anodes for LIBs did not present a similar fast-developing trend with those of Sn-based anodes, since about 2010. This phenomenon was mainly ascribed to a shift of research focus from LIBs to SIBs, due to good performance of Sb-based anodes in SIBs. Since about 2013, various Sb-based anodes for SIBs gained great progress, and the Sb alloy-based anodes will be discussed in this part first.

Nanostructure construction and application of buffer matrix are still the most effective strategies to gain better electrochemical performance of SIB Sb alloy-based anodes. In 2015, Yu's team fabricated novel 3D nanoarchitectured Ni–Sb intermetallic anodes for SIBs composed of monodisperse 0D hollow nanospheres units.[508] Nickle solid nanospheres were firstly synthesized as templates by a solvothermal method, and Ni–Sb alloy hollow nanospheres were formed through a galvanic replacement process. These hollow nanospheres were interconnected with each other, forming a continuous 3D structure. This Sb alloy electrode displayed both high rate capability and stable cyclability in half and full cell tests, due to its unique structure. During this period, graphene-based materials were very popular as buffer matrix for Sb-alloy anodes.[509,510] In 2018, Yu's team developed a cyanogen-enabled methodology for fabricating homogeneous Sb–M–C (M = Ni, Cu, Fe, etc.) ternary anodes.[510] According to their report, 3D Sb–Ni alloy framework was prepared by reducing the Sb–Ni cyanogel, and rGO was introduced into this system to finally obtain the Sb–Ni–C trinary anodes for Na-ion batteries. By varying the rGO content, the optimized sample delivered good electrochemical performance, which maintained reversible capacities of 468 and 210 mAh g^{-1} at current densities of 1000 and 5000 mA g^{-1}, respectively, after 500 cycles.

3.4. Antimony/Carbonaceous and Other Material Composite Anodes for Sodium-Ion Batteries

Antimony crystalline as an active site, assisted with cushion matrix (both carbon and noncarbon materials), is doubtlessly the most favorite and successfully type of Sb-based anodes for SIBs since about 2013.

3.4.1. Fast Development Stage: 2013–2015

During this stage, Sb/C composite fiber attracted much attention and displayed good Na-storage property. In 2013 and 2014, Wang[511] and Cao[512] led their respective team to fabricate Sb/C nanofibers as high-performance anodes for SIBs using electrospinning technique. The nanofibers showed similar morphology under TEM, where Sb nanoparticles were homogeneously encapsulated in carbon fibers. Due to a smaller size of Sb nanocrystalline, the Sb/C nanofiber electrode prepared by Cao's team exhibited better electrochemical performance, which maintained a reversible capacity of 446 mAh g^{-1} after 400 cycles at 200 mA g^{-1}, corresponding to capacity retention of 90%. Using amorphous carbon derived from the organic

source could also create more possibilities of nanostructured Sb/C composite anodes for SIBs, e.g., Sb/N-doped porous carbon nanosheet composite,[513] 3D-nanostructured Sb/C composite,[417,514] and pitaya-like Sb@C spheres.[515,516] Besides, graphene-based materials also found wide applications in Sb/C composite anodes during this timeframe.[517–519] In 2015, Hu's group synthesized flexible and binder-free Sb/rGO nanocomposite anode for SIBs by reducing $SbCl_3$/GO thin films.[519] Additionally, they also prepared $Na_3V_2(PO_4)_3$/rGO thin film cathode without binder with a similar technique. Both Sb/rGO and NVP/rGO cathode exhibited good electrochemical performance in half-cell tests. Sodium-ion full cells were then assembled by coupling Sb/rGO anode with NVP/rGO cathode. The reversible capacity of the full cell could maintain at about 400 mAh g^{-1} after 100 cycles at 100 mA g^{-1}. Besides, due to flexibility of electrodes, the full cell also displayed good flexibility and it could work properly under a curved status.

3.4.2. Explosive Development Stage: Since 2016

Since 2016, the quantity of the studies about Sb/C (or other materials) composite anodes realized further development and witnessed fruitful progress. Compared with the last stage, various contact-type Sb-based nanocomposites with hollow structures made a splash due to effective accommodation of volume change and good electrochemical performance, when applied as anode materials for SIBs. In 2016, Luo and Paik synthesized unique Sb@C coaxial nanotubes as SIB anodes through a template-derived method.[520] Sb_2S_3 nanorods were selected as templates, then coated with PDA to generate Sb_2S_3@PDA core–shell nanorod, as shown by **Figure 13**a. The final Sb@C coaxial nanotubes (Figure 13b) were obtained after reduction and carbonization processes under high temperature. The as-prepared anodes could keep reversible after 2000 cycles at 1000 mA g^{-1}. At the same year, Yang's team fabricated Sb-based anodes with a similar structure following a similar synthesis route, where the shell material was changed from carbon to titanium oxide.[521] The Sb@TiO_{2-x} anode also exhibited stable cyclability, which maintained a reversible capacity of about 300 mAh g^{-1} after 1000 cycles at 2640 mA g^{-1}. Besides, due to good electrochemical/thermal stability of TiO_2 and enhanced charge-transfer kinetics of TiO_{2-x} assisted with oxygen vacancies, the Sb@TiO_{2-x} nanotubes (Figure 13c) exhibited better rate performance as anodes for sodium-ion half cells. Moreover, the full cells assembled by this Sb@TiO_{2-x} nanocomposite (anode) and $Na_3V_2(PO_4)_3$/C (cathode) also presented stable cyclability and good rate performance. In 2018, Sb_2S_3 nanorods were also used as templates by Mai and co-workers, to fabricate Sb@C nanocomposite anodes for SIBs.[522] Discontinuous short Sb nanorods were encapsulated within continuous carbon shell (Figure 13d), leading to a good electrochemical performance.

In addition, noncontact-type Sb/C (other) composite anodes also attracted much attention. Particularly, various yolk–shell structured Sb-based SIB anodes with different "shell" materials based on different synthetic methods appeared since 2016. In 2017, hollow Sb@C yolk–shell spheres were prepared by Yu and co-workers and applied as SIB anode.[523] As presented in Figure 13e, hollow SnO_2 nanospheres were prepared as the initial templates via a hydrothermal route, which were then coated with carbon to form SnO_2@C hollow nanospheres. Hollow Sb@C yolk–shell nanospheres were realized through

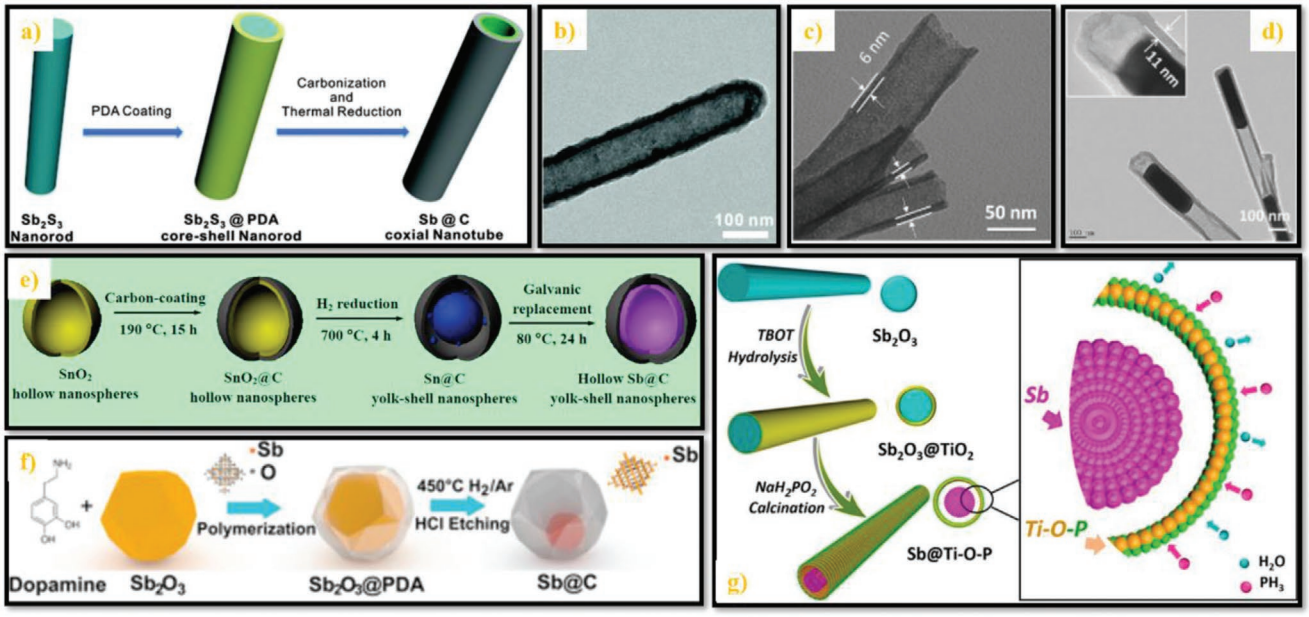

Figure 13. a) Schematic illustration of the formation and b) TEM image of Sb@C coaxial nanotubes. Reproduced with permission.[520] Copyright 2016, Royal Society of Chemistry. c) TEM image of Sb@TiO_{2-x} nanotubes. Reproduced with permission.[521] Copyright 2016, Wiley-VCH. d) TEM image of peapod-like Sb@N–C hybrid. Reproduced with permission.[522] Copyright 2018, Wiley-VCH. e) Schematic evolution of hollow Sb@C yolk–shell nanospheres. Reproduced with permission.[523] Copyright 2017, American Chemical Society. f) Schematic synthesis process of Sb@C yolk–shell structure. Reproduced with permission.[524] Copyright 2017, Elsevier Ltd. g) Formation process of 1D yolk–shell Sb@Ti–O–P nanostructures. Reproduced with permission.[525] Copyright 2016, American Chemical Society.

a nanoconfined galvanic replacement, due to a stronger oxidation capability of antimony compared to tin. Wang and co-workers used Sb_2O_3 nanoparticles as precursors to create yolk–shell Sb-based SIBs anodes.[524] Generally the synthesis route of this work was similar to that of Yu and Zhu, where Sb_2O_3/Sb@C yolk–shell nanospheres were obtained after coating and reduction processes. The Sb_2O_3 phase was finally removed by HCl etching, and the detailed route is shown in Figure 13f. In 2018, Yang's team also selected Ti-based material as a shell to fabricate 1D yolk–shell Sb@Ti–O–P nanostructures as SIB anodes.[525] As displayed by Figure 13g, coating and reduction were still the main strategies. The major difference was addition of NaH_2PO_2 during the calcination process, which allowed TiO_2 to form a unique Ti–O–P shell. Due to extra capacity contribution from TiO_2 and P as well as good mechanical and electrochemical properties of TiO_2, the Sb@Ti–O–P nanocomposite anode achieved better electrochemical performance than its counterpart with bare carbon shell. The void space between yolk and shell could effectively accommodate volume change of antimony during sodiation/desodiation, while the shell could keep structure stable and prevent particle aggregation. Therefore, all these yolk–shell Sb-based anodes delivered good electrochemical performance, even in the full-cell tests.

3.5. Antimony Oxide-Based Anodes for Sodium-Ion Batteries

Antimony oxides have been studied as anode materials for Li-ion batteries as early as 1999.[526] However, only a few related studies were reported in the last decades.[527–531] Until the 2010s, the seemingly forgotten antimony oxides began to attract attention as SIB anodes, due to high theoretical capacities (1102 mAh g^{-1} for Sb_2O_3, 1220 mAh g^{-1} for Sb_2O_4).[532–544] Similar to tin oxides, antimony oxide could also electrochemically react with sodium based on a two-step mechanism, as presented by Equations (33) to (36).[535]

$$Sb_2O_3 + 6Na^+ + 6e^- \leftrightarrow 2Sb + 2Na_2O \quad (33)$$

$$2Sb + 6Na^+ + 6e^- \leftrightarrow 2Na_3Sb \quad (34)$$

and

$$Sb_2O_4 + 8Na^+ + 8e^- \leftrightarrow 2Sb + 4Na_2O \quad (35)$$

$$2Sb + 6Na^+ + 6e^- \leftrightarrow 2Na_3Sb \quad (36)$$

Although the in situ generated Na_2O could buffer volume change of Sb during cycling at some extent, antimony oxide-based anodes still suffered this problem. Besides, the poor conductivity also limited the performance in Na-ion batteries.[535,536] Therefore, combination of nanostructured antimony oxides and carbon materials exhibited great advantages for improving electrochemical performance of antimony oxide-based anodes in SIBs since 2010s.

In 2015, Wang's group synthesized novel Sb_2O_3/Sb@G nanocomposite SIBs anode, which was anchored on carbon sheet network (CSN).[536] The antimony acetate was firstly spread on Al substrate to form Sb_2O_3/Sb–CNS composite with simultaneous heating process via MPECVD. Then, CH_4 was used to grow graphene shell outside Sb_2O_3/Sb nanoparticles. The final Sb_2O_3/Sb@G–CNS nanocomposite anode displayed a 3D hierarchical nanostructure, resulting in good electrochemical performance. This anode exhibited a stable cyclability with 92.7% capacity retention after 275 cycles (100 mA g^{-1}), which maintained reversible capacity of about 480 mAh g^{-1}. Good rate performance was also obtained, which reached capacity of 221 mAh g^{-1} even at 5000 mAh g^{-1}. In 2017, Han and Cheng fabricated 1D Sb_2O_4 sub-micrometer tubes from bulk Sb material via a two-step oxidation route.[542] Bulk Sb powder was firstly oxidized in oxygen-dissolved water to form solid Sb_2O_3 sub-micrometer wires, where ethylenediamine acted as a catalyst and poly(vinyl pyrrolidone) as a surface stabilizer. A secondary oxidation was then applied to prepare the final tube-like Sb_2O_4 sub-micrometer structure. As a result, hollow structure ensured a good electrochemical performance of Sb_2O_4 anode in Na-ion batteries.

3.6. Antimony-Based Compound Anodes for Sodium-Ion Batteries

Inspired by antimony oxides, other antimony–chalcogen compounds were also investigated as anode materials for SIBs and gained good results since the 2010s. Actually, antimony sulfide (Sb_2S_3),[545–547] selenide (Sb_2Se_3),[548] telluride (Sb_2Te_3)[549,550] were also applied as LIB anodes. However, only the applications as SIBs anode will be addressed in this part. These antimony–chalcogen compounds follow similar reaction mechanism with sodium (here taking Sb_2S_3 as an example),[551] and present relatively high theoretical capacities of 946 mAh g^{-1} (Sb_2S_3), 669 mAh g^{-1} (Sb_2Se_3), and 513 mAh g^{-1} (Sb_2Te_3), respectively

$$Sb_2S_3 + 6Na^+ + 6e^- \leftrightarrow 2Sb + 2Na_2S \quad (37)$$

$$2Sb + 6Na^+ + 6e^- \leftrightarrow 2Na_3Sb \quad (38)$$

Similar to Sb oxides, these anode materials also need assistance of nanostructures and buffer matrix to improve their electrochemical performance in SIBs.

In 2013, Yu et al. prepared Sb2S3/rGO nanocomposite anodes for SIBs for the first time, via a chemical synthesis route.[551] This Sb_2S_3/rGO anode could maintain a reversible capacity of 670 mAh g^{-1} after 50 cycles (at 50 mA g^{-1}), reaching capacity retention over 95%. In the following years, other Sb_2S_3-based anodes with structure modifications were synthesized and gained good performance in SIBs, such as 1D Sb_2S_3 nanorods[552] and Sb_2S_3 hollow microspheres.[553] As for Sb selenide-based anodes, Mai's team fabricated a free-standing Sb_2Se_3 ultralong nanowire-based membrane which delivered good electrochemical performance as anodes for SIBs.[554] Sb_2Se_3 nanowires were obtained through a hydrothermal process and the free-standing membrane was fabricated through a suction process. In 2017, Zhao and Li introduced N-doped graphene (NG) into Sb_2Se_3 nanorod system to prepareSb_2Se_3/NG composite anode material which also presented good Na-storage property.[555]

In addition to these antimony–chalcogen compounds, other Sb-based compounds were also found capable of being applied as anodes for Na-ion batteries. Antimony oxychloride ($Sb_4O_5Cl_2$),[556] antimony phosphate ($SbPO_4$),[557] antimony–niobium pentoxide ($SbNb_2O_5$),[558] and antimony tungstate (Sb_2WO_6)[559] were discovered to exhibit Na-storage properties. These materials further enlarged the category range of anode candidates for SIBs.

3.7. Elemental Antimony Anodes for Lithium and Sodium-Ion Batteries

Applying pure alloy-type anode materials (Sn, Sb, Ge) for rechargeable batteries is always a huge challenge. Without the assistance of cushion materials, constructing nanostructures is the only way to solve the volume-expansion problem of antimony during charge/discharge processes. To our best knowledge attempts of using bare Sb materials as anodes for LIBs started from 2004. Cao's team fabricated Sb thin films by magnetron sputtering and electrodeposition and investigated their electrochemical performance as anodes for LIBs.[560] In 2008, Kim and Cho made a breakthrough on elemental Sb anodes. They synthesized hollow Sb nanoparticles via a template-assistance method,[561] where the preparation process is presented as **Figure 14**a. This anode could cycle over 100 cycles with reasonable cycling stability and capacity retention of 94%, where good rate performance was also demonstrated. Recently, Huo and co-workers reported a tailoring engineering method that could tailor natural layered β-phase Sb in both vertical direction and omni direction, which generated 2D antimonene and 0D Sb nanoparticles,[562] as shown in Figure 14b. The exfoliation and tailoring processes were realized by ultrasonic technique. The as-prepared antimonene was stacked by a few layers with a monolayer thickness of about 2 nm, and the average diameter of Sb nanoparticles was about 24 nm. Compared with the bulk antimony, these nanosized Sb anodes exhibited enhanced lithium storage performance.

Since the 2010s, more elemental Sb anodes were designed pertinently for application of SIBs.[69,563–570] In 2014, Kovalenko's team fabricated monodisperse antimony NPs for the first time via one-pot colloidal synthesis, which demonstrated good Li^+/Na^+ storage performance.[69] The particle size could be controlled by different synthesis conditions, where 10 and 20 nm sized Sb NPs were prepared as presented in Figure 14c. When applied as anodes for Na-ion batteries, this anode (20 nm Sb NPs) exhibited both stable cyclability and good high-rate performance, which could reach a capacity of over 500 mAh g^{-1} at a high rate of 20C (1C = 660 mA g^{-1}). From 2014 to 2015, Ji and co-workers continuously reported their work about pure Sb anodes for SIBs, including Sb hollow nanospheres (Figure 14d),[564] Sb porous hollow microspheres (Figure 14e),[565] and cypress leaf-like Sb (Figure 14f).[566] Recently, porous elemental Sb anodes for SIBs attracted much attention.[569,570] In 2016, Feng

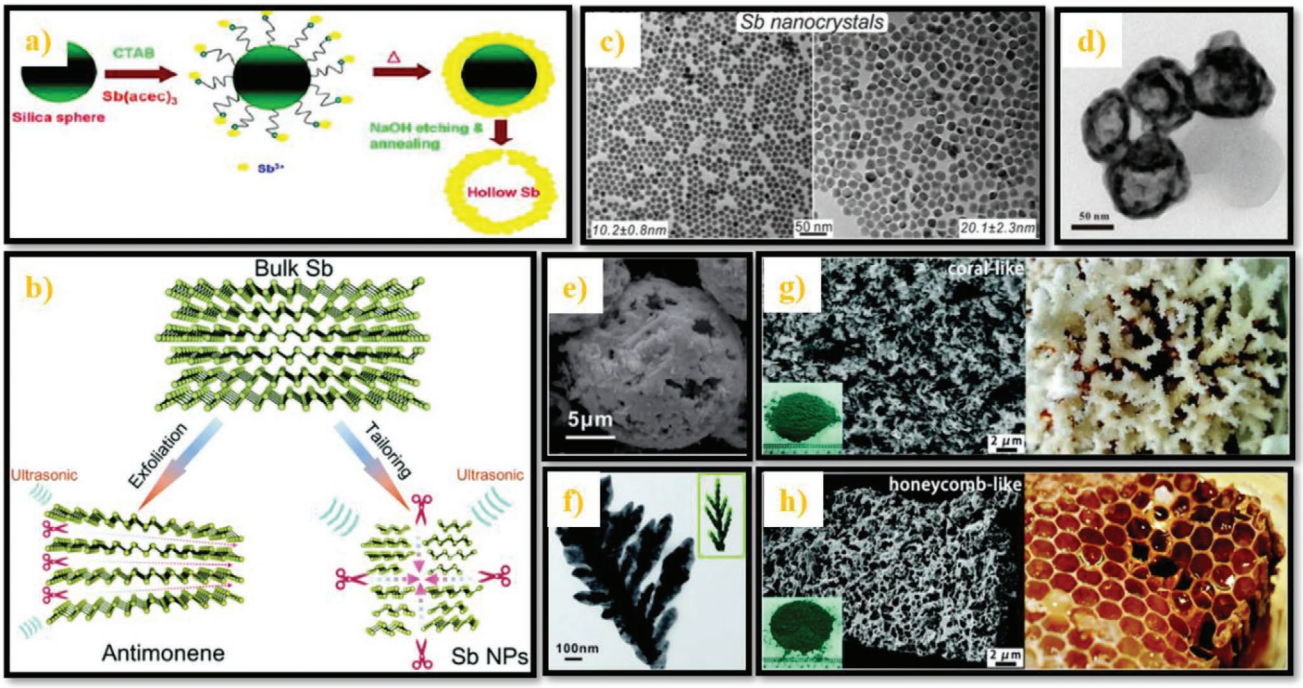

Figure 14. a) Schematic illustration of the formation of hollow Sb nanoparticles. Reproduced with permission.[560] Copyright 2008, American Chemical Society. b) Schematic diagram of sonication assisted tailoring engineering for β-phase antimony. Reproduced with permission.[562] Copyright 2019, Royal Society of Chemistry. c) TEM images of monodisperse Sb nanoparticles. Reproduced with permission.[57] Copyright 2014, American Chemical Society. d) TEM image of Sb hollow nanospheres. Reproduced with permission.[564] Copyright 2014, American Chemical Society. e) SEM image of Sb porous microspheres. Reproduced with permission.[565] Copyright 2015, Royal Society of Chemistry. f) TEM image of cypress leaf-like Sb nanostructure. Reproduced with permission.[566] Copyright 2015, Royal Society of Chemistry. SEM images of the g) coral-like Sb with a coral picture on the right and h) the honeycomb-like Sb with a honeycomb picture on the right. Reproduced with permission.[569] Copyright 2016, Royal Society of Chemistry.

and co-workers synthesized nanoporous-Sb anode using Al–Sb alloy as precursor.[569] Al–Sb alloys (with different element ratios) were prepared by melting pure Al and Sb blocks under high temperature. The sacrificial element Al was then removed by NaOH etching, and porous Sb materials were obtained. Besides, the morphology of the final porous Sb materials could be controlled by different elemental ratios in the Al–Sb alloys. Coral-like Sb ($Al_{30}Sb_{70}$) and honeycomb-like Sb ($Al_{20}Sb_{80}$) were obtained as displayed in Figure 14g,h respectively. Particularly, the coral-like Sb anode delivered a reversible capacity of 574 mAh g^{-1} after 200 cycles (100 mA g^{-1}), which was better than that of honeycomb-like Sb. According to this work, the enhanced performance of coral-like Sb anode could be attributed to its large porosity which was able to accommodate the volume change more effectively.

With increasing cycling stability of the Sb anode for SIBs, some questions remained about sodiation and desodiation processes of antimony, such as the intermediate regions of antimony.[563,571,572] In 2016, Grey and co-workers studied Sb anodes for SIBs by a pair distribution function (PDF) and high-resolution ^{23}Na magic-angle spinning solid-state nuclear magnetic resonance spectroscopy (MAS ssNMR).[572] Assisted with these measurements, the amorphous and crystalline phases in the antimony electrode can be isolated, leading to clear understanding of their transformations during sodiation and desodiation processes. Based on the experimental results and data analysis, the separation of amorphous and crystalline phases formed in SIBs was demonstrated for the first time and a detailed sodiation/desodiation mechanism of Sb with several intermediate phases was also presented as following (a and c refer to amorphous and crystalline respectively)

$$\text{First sodiation: } \text{c-Sb} \rightarrow \text{a-Na}_{3-x}\text{Sb} + \text{c-Na}_3\text{Sb} \rightarrow \text{c-Na}_3\text{Sb} \quad (39)$$

$$\text{First desodiation: } \text{c-Na}_3\text{Sb} \rightarrow \text{a-Na}_{1.7}\text{Sb} \rightarrow \text{a-Na}_{1.0}\text{Sb} \rightarrow \text{a-Na}_{1.0}\text{Sb} + \text{c-Sb} \quad (40)$$

$$\text{Second sodiation: } \text{a-Na}_{1.0}\text{Sb} + \text{c-Sb} \rightarrow \text{a-Na}_{1.7}\text{Sb} + \text{c-Sb} \rightarrow \text{a-Na}_{1.7}\text{Sb} + \text{a-Na}_{3-x}\text{Sb} \rightarrow \text{c-Na}_3\text{Sb} \quad (41)$$

After desodiation, networks consisted of amorphous and crystalline antimony are formed, which is beneficial to enhance the cyclability of antimony anode due to the buffer effect of the "inactive" component.

3.8. Temporary Summary of Antimony-Based Anodes

The history review told that the antimony-based anodes almost emerged at the same time with tin-based anodes. However, they presented different development trends during the last 30 years. As for Sn-based anodes, most of studies focused on their applications in LIBs. In contrast, various Sb-based materials were investigated and applied as high-performance anodes for SIBs. In the first ten years of the new century, Sb-based anodes for LIBs embraced their golden period and gained much progress. Sb-based alloys and Sb/C (or other materials) composites were the most two favorite types of Sb-based anodes for Li-ion batteries. The year 2010 could be considered as a turning point in the development history of Sb-based anodes. After that, the research focus of Sb-based anodes was shifted to the application of SIBs due to the lack of appropriate anode materials for Na-ion batteries. Traditional materials, Sb alloys, and Sb/C (or other materials) composites, still maintained their advantages and promoted the fast development of Sb-based anodes for SIBs. In addition, other Sb-based materials, which were less of a concern in LIBs domain, gained much attention when applied as anodes for SIBs. Both antimony oxides and other antimony-based compounds exhibited great competitiveness in terms of sodium storage performance. Particularly, the performance of elemental Sb anodes was obviously enhanced in both LIBs and SIBs, compared with that of pure Sn anodes. A profile of the development process of Sb-based anodes is also presented in **Figure 15**. Compared to a "balance-type" development history of Sn-based anodes, the development of Sb-based anodes appeared a polarization phenomenon which is more emphasized on SIB applications since the 2010s. In **Table 2**, we summarize the fabrication methods and electrochemical performance of representative studies about antimony-based anodes for LIBs and SIBs.

4. Germanium-Based Anodes for Rechargeable Batteries

Germanium (Ge), an element of group IVA, displays the highest LIB specific capacity (1624 mAh g^{-1}) among these three anode materials in this review, due to the formation of $Li_{22}Ge_4$ phase with lithium (based on the following equation)[573–575]

$$4\text{Ge} + 22\text{Li}^+ + 22\text{e}^- \leftrightarrow \text{Li}_{22}\text{Ge}_4 \quad (42)$$

In terms of volumetric capacity, Ge exhibits the second highest value of 7366 Ah L^{-1} in all anode materials, which is only inferior to that of Si (8334 Ah L^{-1}).[576] Additionally, both lithium ion diffusivity and electronic conductivity of germanium are higher (in order of magnitude) than those of silicon.[577,578] Therefore, Ge-based materials have been considered as promising alternative anodes for LIBs. The origin of the Ge-based anodes could be dated back to the 1980s,[579–581] where fundamental research about Li–Ge alloys system established theoretical ground for later application studies in LIBs. Besides, similar to Sn and Sb, Ge can also electrochemically alloy with sodium and can be used as anode for Na-ion batteries. However, one mole Ge can only react with one mole Na to form NaGe alloy at potentials ranging from 0.15 to 0.6 V versus Na/Na^+, corresponding to a theoretical capacity of 369 mAh g^{-1} (reaction equation shown as following)[582]

$$\text{Ge} + \text{Na}^+ + \text{e}^- \leftrightarrow \text{NaGe} \quad (43)$$

Despite of the relatively low capacity limiting their applications in SIBs, Ge-based anodes were still regarded as having great potential as anodes for rechargeable batteries in the last ten years. It is a key point to limit huge volume expansion of Ge during lithiation (272%) and sodiation (126%) for promoting Ge-based anodes into practical applications.[583,584]

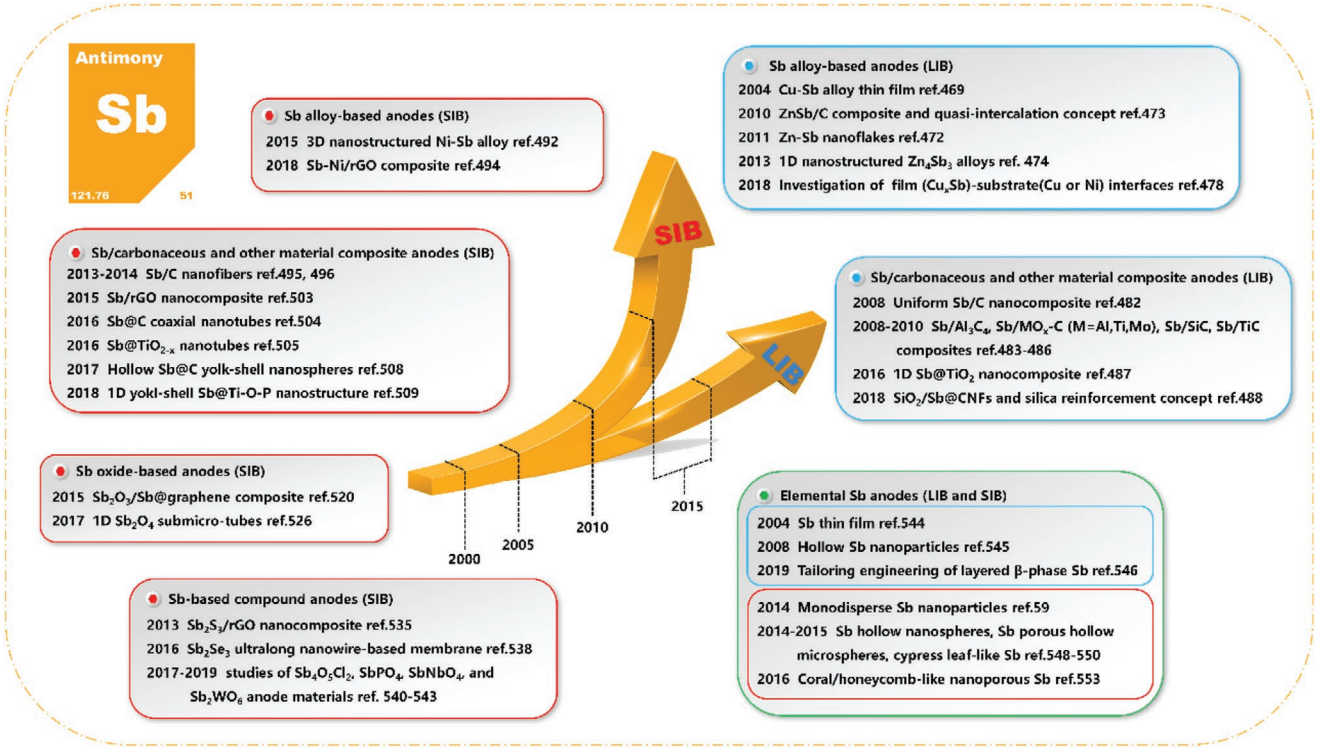

Figure 15. A brief illustration of the development history of antimony-based anodes.

4.1. Elemental Germanium Anodes for Lithium-Ion Batteries

Compared with tin and antimony-based anodes, the development duration of Ge-based anodes is the shortest. However, this inversely becomes an advantage which allows researchers to gain a large amount of experience from Sn and Sb anode systems to benefit the germanium anode studies. This has promoted pure Ge as one of the most important branches in Ge-based anodes, which is distinct compared to the other two counterparts.

4.1.1. Rising Stage: 2004–2011

In 2004, Graetz et al. prepared nanocrystalline and amorphous thin film germanium electrodes for LIBs,[585] which could be regarded as pioneering work of pure germanium anodes. The Ge nanocrystal anode exhibited a specific capacity of ≈1400 mAh g^{-1} and maintained 60% capacity after 50 cycles, at a rate of 0.25C (1C = 1500 mA g^{-1}). In contrast, amorphous thin film Ge electrode retained a stable reversible capacity of ≈1400 mAh g^{-1} after 60 cycles at 0.25C. This work not only demonstrated the great potential of Ge-based anodes for LIBs but also opened a new gate of nanostructured elemental Ge anodes. In the following years, various nanostructured germanium materials were synthesized and studied as high-performance anodes for Li-ion batteries, such as Ge nanowires,[586,587] Ge nanotubes,[588] and porous Ge materials.[589,590] In 2011, Zhu and Huang fabricated Ge nanowires by CVD method based on the VLS mechanism, and their lithiation/delithiation behavior was investigated through in situ TEM technique.[588] During lithiation process, the initial crystalline germanium was firstly converted into an intermediate, amorphous Li_xGe, and finally into the crystalline $Li_{15}Ge_4$ phase. After Li de-insertion, the crystalline $Li_{15}Ge_4$ nanowires were converted to a porous sponge-like segment composed of interconnected ligaments of amorphous Ge. The Ge nanowires could realize a fast cycle process completely within 1 min. Reversible porous structures, coupled with fast cycling, indicated that Ge was a promising anode candidate for high-performance LIBs.

4.1.2. Explosive Development Stage: Since 2012

In previous years, the great lithium storage property of germanium had been proved by several studies, as discussed in the last part. Since 2012, studies of pure germanium anodes embraced an explosive development period. Various nanostructured Ge anodes were fabricated and exhibited good electrochemical performance, including Ge nanowires,[591,592] Ge nanotubes,[593,594] Ge nanoparticles,[595,596] and porous Ge materials.[597,598]

During this period, Ge nanowires anodes have already been synthesized with different methods, such as colloidal solution-phase process,[591] electrochemical liquid–liquid–solid (es-LLS) mechanism,[599] metal-seed growth,[592,600] solvent–vapor growth,[601,602] and electrodeposition or electrospinning.[603–605] In 2012, Tuan and Yuan fabricated Ge nanowires as LIB anode and emphatically studied the effect of chemical surface functionalization on final electrochemical performance.[600] The as-fabricated Ge nanowires were functionalized with dodecanethiol monolayers at 80 °C under Ar atmosphere, generating dodecanethiol-passivated Ge nanowires. In terms

Table 2. Summary on representative studies about antimony-based anodes for LIBs and SIBs (ICE: initial coulombic efficiency; *n*: the *n*th cycle).

Material type	Development stage	Representative anode	Synthetic method	ICE	Charge capacity [mAh g^{-1}] (*n*, rate)	Rate capacity [mAh g^{-1}] (rate)	Ref.
			LIBs				
Antimony alloy	Emergence stage	Cu_2Sb thin film	Pulsed laser deposition	\	200 (50, \)	\	[485]
	(before 2006)						
	Rising stage	Zn–Sb nanoflakes	Electrochemical deposition	85%	500 (70, 0.1 A g^{-1})	\	[488]
	(2006–2011)	ZnSb/C	High energy mechanical milling	85%	520 (200, 0.1 A g^{-1})	480 (1.8 A g^{-1})	[489]
	Steady development stage	Zn_4Sb_3 nanotubes	CVD growth	52%	450 (100, 0.1 A g^{-1})	\	[490]
	(since 2012)	Cu_xSb@Ni@Cu	Electrodeposition	≈65%	≈400 (100, 0.2C)	\	[494]
Antimony/carbon (/other)	Rising stage	Uniform-dispersed Sb/C	R–F gel method	≈36%	200 (100, 0.1 A cm^{-2} g^{-1})	\	[498]
	(2004–2010)						
	Steady development stage	1D Sb@TiO_2	Coating and reduction	67%	450 (100, 0.1 A g^{-1})	340 (1 A g^{-1})	[503]
	(since 2011)	SiO_2/Sb@CNFs	Electrospinning method	66%	700 (400, 0.2 A g^{-1})	520 (2 A g^{-1})	[504]
Elemental antimony	since 2004	Hollow Sb NPs	Template-assisted method	83%	615 (100, 0.6 A g^{-1})	570 (4.2 A g^{-1})	[561]
		Antimonene	Ultrasonication-tailored method	≈87%	584 (100, 0.66 A g^{-1})	410 (6.6 A g^{-1})	[562]
			SIBs				
Antimony alloy	since 2013	3D hollow Ni–Sb	Galvanic replacement reaction	38%	400 (150, 0.6 A g^{-1})	230 (6 A g^{-1})	[508]
		Sb–Ni/rGO	Cyanogel-enabled method	60%	468 (500, 1 A g^{-1})	\	[510]
Antimony/carbon (/other)	Fast development stage	Sb/C nanofibers	Single-nozzle electrospinning	≈50%	446 (400, 0.2 A g^{-1})	337 (3 A g^{-1})	[512]
	(2013–2015)	Binder-free Sb/rGO	Chemical reduction	≈57%	581 (100, 0.2 A g^{-1})	237 (20 A g^{-1})	[519]
Contact-type	Explosive development stage	Sb@C coaxial nanotubes	Template-derived method	50%	407 (240, A g^{-1})	310 (20 A g^{-1})	[520]
	(since 2016)	Sb@TiO_{2-x} nanotubes	Coating and hydrolysis	\	300 (1000, 2.64 A g^{-1})	312 (13.6 A g^{-1})	[521]
Noncontact-type		Yolk–shell Sb@C spheres	Galvanic replacement reaction	60%	400 (100, 0.05 A g^{-1})	279 (2 A g^{-1})	[523]
		Yolk–shell Sb@Ti–O–P	Coating and reduction	72%	760 (200, 0.5 A g^{-1})	360 (10 A g^{-1})	[525]
Antimony oxide	2010s	Sb_2O_3/Sb@G–CNS	MPECVD technique	72%	480 (275, 0.1 A g^{-1})	221 (5 A g^{-1})	[536]
		Sb_2O_4 sub-micrometer wires	Two-step oxidation route	≈63%	382 (100, 0.1 A g^{-1})	\	[542]
Antimony-based compound	2010s	Sb_2S_3/rGO	Solution-based synthesis	69%	670 (50, 0.05 A g^{-1})	520 (3 A g^{-1})	[551]
		Sb_2Se_3/NG	One-pot hydrothermal reaction	\	548 (50, 0.1 A g^{-1})	337 (1.5 A g^{-1})	[555]
		$Sb_4O_5Cl_2$/GA	Solvothermal synthesis	60%	400 (50, 0.03 A g^{-1})	100 (2 A g^{-1})	[556]
		$SbPO_4$/rGO	Solvothermal synthesis	40%	280 (100, 0.5 A g^{-1})	214 (5 A g^{-1})	[557]
		$SbNb_2O_5$	Controllable decomposition	≈59%	200 (500, 5 A g^{-1})	190 (10 A g^{-1})	[558]
		Sb_2WO_6	Microwave-hydrothermal method	51%	350 (100, 0.2 A g^{-1})	285 (2 A g^{-1})	[559]
Elemental antimony	2010	Monodisperse Sb NPs	One-pot colloidal synthesis	≈50%	600 (100, 0.66 A g^{-1})	≈500 (13.2 A g^{-1})	[69]
		Coral-like Sb	Alloying and etching	≈67%	574 (200, 0.1 A g^{-1})	420 (3.3 A g^{-1})	[569]

of electrochemical performance, the passivated anodes maintained a reversible capacity of 1130 mAh g^{-1} after 100 cycles at 0.1C, which was much better than that of the unpassivated counterpart. Moreover, the functionalized Ge nanowires also displayed good rate performance and thermal stability at high working temperatures (55 °C). Through investigation with TEM and XPS, it was found that the passivated Ge nanowires could form a robust nanowire/PVDF network via strong C—F bonding, which benefited structure integrity during lithiation/delithiation process (as shown in **Figure 16**a). Compared with nanowires, nanotubes could accommodate the volume change of Ge more effectively due to their inside hollow structures. In 2015, Zhao and Li reported their work about the preparation of Ge nanotube arrays via template-assisted electrodeposition from ionic liquid at room temperature.[594] As presented in Figure 16a,b commercial poly carboxylate (PC) nanofiltration membrane was used as a template and sputtered with a gold layer on one side before electrodeposition. Ge was

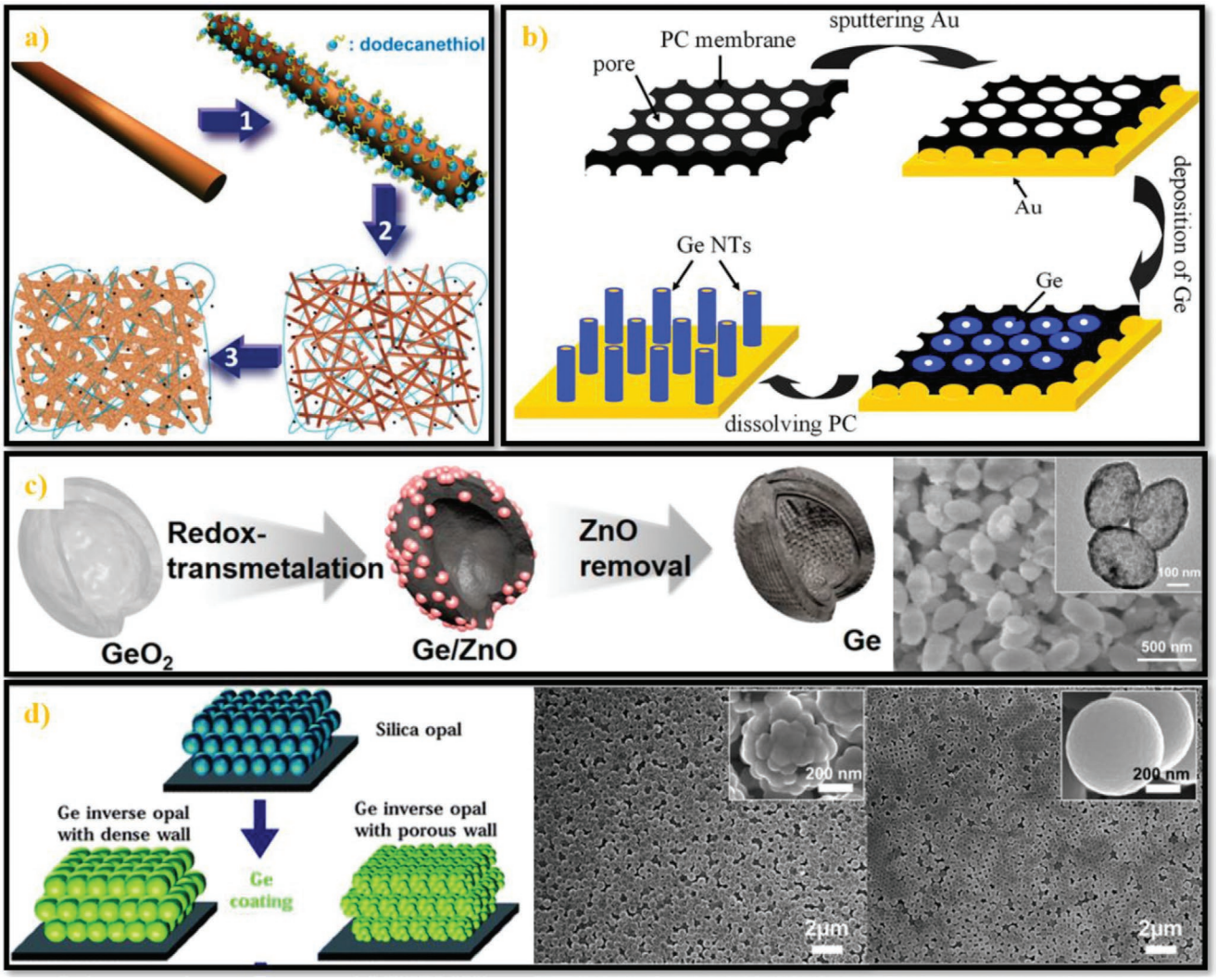

Figure 16. a) Scheme of dodecanethiol-passivated Ge nanowires as anode materials for LIBs. Reproduced with permission.[600] Copyright 2012, American Chemical Society. b) Schematic diagram for the preparation of Ge NT arrays. Reproduced with permission.[594] Copyright 2015, Royal Society of Chemistry. c) Schematic illustration of the method for synthesizing mesoporous Ge materials and their morphology. Reproduced with permission.[606] Copyright 2015, American Chemical Society. d) Schematic illustration of both Ge inverse opals with porous walls and dense walls, and SEM images of the Ge inverse opal with porous walls and dense walls. Reproduced with permission.[612] Copyright 2012, Royal Society of Chemistry.

deposited into pores on PC membrane and Ge nanotube arrays were obtained after dissolving the PC template. The Ge nanotube anode exhibited stable cycling performance as well as high reversible capacity.

In 2015, Park and Kim developed a simple and cost-effective technique to produce mesoporous hollow Ge particles based on a redox-transmetalation reaction.[606] Firstly, hollow GeO_2 nanoparticles were prepared by hydrolysis of $Ge^{4+}$and Sn^{4+} precursors.[607] Mesoporous hollow Ge nanoparticles were obtained via a reaction between Zn^0 (Zn vapor) and Ge^{4+} (GeO_2) known as zincothermic reduction reaction (ZRR). A schematic illustration of synthesis and morphology of final Ge nanoparticles are displayed in Figure 16c. In addition, 3D porous germanium materials also attracted much attention in this time frame. Inspired by inverse opal structures demonstrated in other applications,[608–611] Paik's team synthesized Ge inverse opals with unique wall structures as anodes for LIBs.[612] As shown in Figure 16d, germanium was deposited on the silica opal template using the CVD method. After removing templates, inverse-opal structured porous Ge material was synthesized. As displayed in Figure 16d, morphology of walls could be adjusted by tuning deposition parameters, leading to smooth and uniform surfaces (dense wall) and nanocluster-networked surfaces (porous) wall. When applied as anodes for LIBs, the Ge inverse opal with porous walls delivered enhanced performance compared to those with dense walls, which was mainly attributed to the large free surface of porous structures.

Since 2014, Toney and his co-workers reported a series of studies about lithiation/delithiation mechanisms of germanium anodes via in operando experiments.[583,613,614] They combined in operando XRD with XAS measurements to track the amorphous and crystalline phases of micrometer-sized germanium anode during electrochemical cycles.[583]

According to the results, the proposed reaction mechanism is presented as below

$$\text{Lithiation: c-Ge} \rightarrow \text{c-Ge} + \text{a-Li}_9\text{Ge}_4 \rightarrow \text{a-Ge} + \text{a-Li}_x\text{Ge} \rightarrow \text{c-Li}_{15}\text{Ge}_4 \quad (44)$$

$$\text{Delithiation: c-Li}_{15}\text{Ge}_4 \rightarrow \text{a-Li}_x\text{Ge} \rightarrow \text{a-Ge} \quad (45)$$

In the subsequent study, they investigated the effect of cycling rate and capacity on germanium phase transformation during lithiation/delithiation process, which was also assisted with in operando XRD and XAS measurements.[614] When cycled at different C-rates, the crystalline germanium of electrode exhibited different phase transformation pathway due to the varied (de)lithiation time. The detailed phase transformation pathways are expressed as following

at very low C-rate (≈C/21)

$$\text{c-Ge} \rightarrow \text{a-Li}_x\text{Ge} \rightarrow \text{c-Li}_{15}\text{Ge}_4 \rightarrow \text{a-Li}_x\text{Ge} \rightarrow \text{a-Ge} \quad (46)$$

at low C-rate (≈C/10)

$$\text{c-Ge} \rightarrow \text{a-Ge} \rightarrow \text{a-Li}_x\text{Ge} \rightarrow \text{a-Li}_9\text{Ge}_4 \rightarrow \text{c-Li}_{15}\text{Ge}_4 \rightarrow \text{a-Li}_x\text{Ge} \rightarrow \text{a-Ge} \quad (47)$$

at high C-rate (≈1C)

$$\text{c-Ge} \rightarrow \text{a-Li}_x\text{Ge} \rightarrow \text{c-Ge} \quad (48)$$

The Ge anode presented the best electrochemical performance at the at very low C-rate (≈C/21), which is mainly attributed to a complete transformation into c-$Li_{15}Ge_4$. This study not only revealed the relationship between the electrochemical performance and the phase transformation of Ge anode for LIBs but also enlightened how to improve the cycling stability and capacity retention of Ge-based anodes. It was proposed by the authors that it was possible to suppress the crystallization of $Li_{15}Ge_4$ by fully converting the c-Ge into c-$Li_{15}Ge_4$ at the end of lithiation and cycling at a higher-voltage cut-off.

4.2. Germanium Alloy-Based Anodes for Lithium-Ion Batteries

Since the second half of the 2000s, there has been growing interest in germanium alloy-based anodes for LIBs, due to enhanced properties than individual ones. Assisted by nanostructure and cushion matrix, various germanium alloys displayed good lithium storage performance, such as Sn–Ge alloys,[615] Cu–Ge alloys,[616] Ti–Ge alloys,[617] and others. In 2012, Du's group synthesized Cu–Ge core–shell nanowire arrays as anodes for LIBs via an RF-sputtering technique.[616] Copper nanowire arrays were prepared by cathodic electrodeposition using AAO templates. The Cu–Ge core–shell nanowires were prepared by depositing Ge onto the Cu nanowire array, whose synthesis process is presented in **Figure 17**a. In 2013, Yan and Xi fabricated hybrid Ge–Ti multilayer microtubes from Ge–Ti nano membranes based on a strain-released method,[617] as shown in Figure 17b. According to the reported work,[618,619] nanotubes could be formed from bilayer thin solid films consisting of two materials with different biaxial strains (β_1 and β_2) when the built-in strain gradient over the bilayer was large enough ($\Delta\beta = \beta_2 - \beta_1 > 0.5\%$). The tube-like Ge/Ti nano membranes could improve electronic transportation and stabilize the whole structure, leading to enhanced electrochemical performance. This anode exhibited a reversible discharge capacity as high as 1495 mAh g^{-1} at C/16 and maintained at 930 mAh g^{-1} after 100 cycles. Tin–germanium alloys, combining fast electron transportation of Sn with high specific capacity of Ge, were regarded as a promising anode material for Li-ion batteries. In 2014, Bodnarchuk et al. reported a novel Sn–Ge heterostructures in the form of nanorods fabricated with a colloidal method.[615] The synthesis

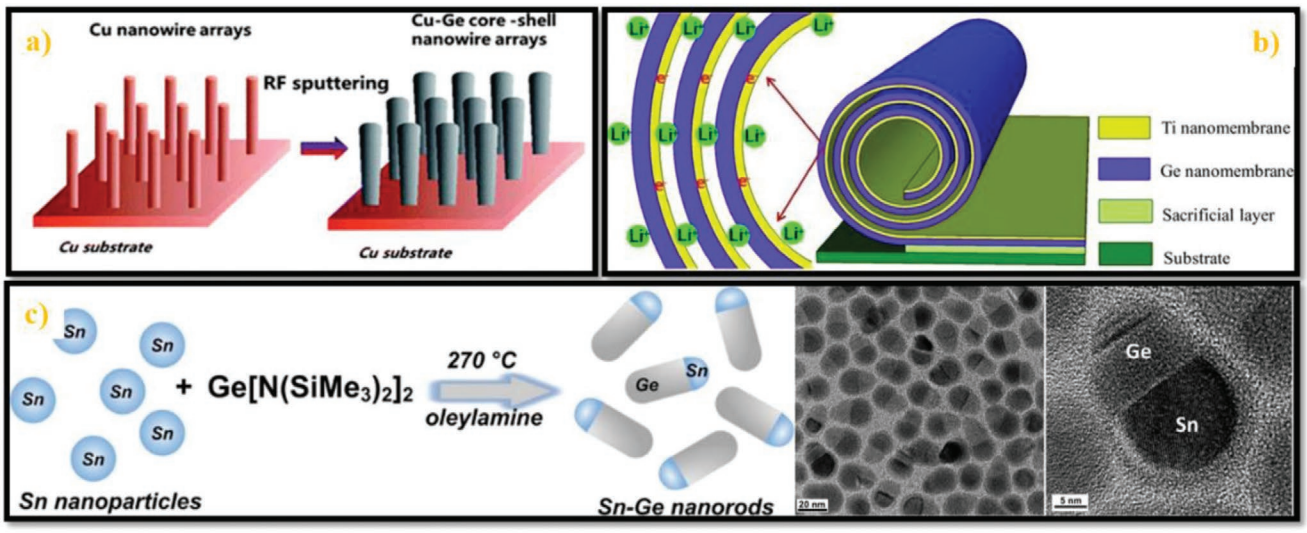

Figure 17. a) Schematic illustration for synthesis of the Cu–Ge 3D electrode. Reproduced with permission.[616] Copyright 2012, Royal Society of Chemistry. b) Schematic illustration of the rolled-up process of the hybrid Ge/Ti multilayer microtubes by the strain-released method. Reproduced with permission.[617] Copyright 2013, Wiley-VCH. c) Outline of the one-pot, solution–liquid–solid growth of colloidal Sn–Ge nanorods using presynthesized Sn nanoparticles as the catalyst, and TEM images of Sn–Ge nanorods. Reproduced with permission.[615] Copyright 2014, American Chemical Society.

of Sn–Ge nanorods was based on a solution–liquid–solid growth (SLS growth) mechanism, where Sn nanoparticles and Ge precursor $Ge[N(SiMe_3)_2]_2$ reacted in oleylamine solvent at low temperatures of from 250 °C to 300 °C (Figure 17c). The as-prepared Sn–Ge nanorods presented a capsule-like shape with the axial length less than 50 nm, as shown in Figure 17c. When applied as anodes for LIBs, this Sn–Ge nanorods kept a reversible capacity of 1520 mAh g^{-1} at the 100th cycle under 1C rate (1C = 1000 mA g^{-1}). Moreover, Sn–Ge nanorods also achieved good rate capability, retaining 80% of the initial capacity with the current density increased from 0.2C to 4C.

4.3. Germanium/Carbonaceous Material Composite Anodes for Lithium-Ion Batteries

It has been demonstrated that carbonaceous material could be the most ideal and effective cushion matrix for volume expansion in tin and antimony systems. In terms of germanium, Ge/carbonaceous and other material composite anodes are one of the most important branches of Ge-based anodes, which have gained the most attention and fruitful achievements. According to our previous taxonomy, Ge/C composite anodes could also be divided into two categories: contact type (embedding and coating designs) and noncontact-type (yolk–shell and other hollow structures).

4.3.1. Rising Stage: 2007–2012

Initially, most studies about Ge/C anodes focused on embedding and coating structure designs. In 2011, Cho's team prepared single crystalline Ge nanowires sheathed with carbon layers as anodes for LIBs and gained good electrochemical performance.[620] Ge nanowires were synthesized by a solid–liquid solution method and coated with carbon layers by pyrolyzing C_2H_2 gas. This Ge/C composite anode exhibited a high initial charge capacity of 963 mAh g^{-1} and maintained 72% reversible capacity after 100 cycles at 0.5C (1C = 800 mA g^{-1}). In 2012, Guo and Wan applied both coating and embedding strategies, where Ge@C nanoparticles were anchored on graphene networks.[621] Germanium NPs were prepared by a reaction between $GeBr_2$ and oleylamine in solution, where the as-obtained Ge NPs were covered with oleylamine, followed by calcination to form Ge@C NPs. Then, Ge@C NPs were embedded on rGO networks by mixing these two materials in ethanol solution and vaporizing the solvent. Due to the double cushion matrix, the Ge@C/rGO nanocomposite anode exhibited enhanced electrochemical performance compared to the one without rGO networks (Ge@C).

4.3.2. Explosive Development Stage: Since 2013

Since 2013, the explosive development of Ge/C composite anodes still didn't change the dominance of contact-type Ge/C anodes. However, noncontact-type Ge/C composites also presented outstanding electrochemical performance as anodes for LIBs.

Contact-Type Germanium/Carbonaceous Material Composite Anodes: A variety of Ge/C nanocomposite anodes with coating and embedding designs were produced recently, including i) using 2D carbon materials (nanotubes, nanowires, and nanofibers) as matrix materials,[622,623] ii) embedding Ge nanoparticles on graphene-based materials,[624,625] iii) constructing Ge@C materials by coating and embedding designs,[626,627] and iv) coating carbonaceous layers on Ge nanowires.[628,629] In the first classification, most researchers focused on loading Ge nanoparticles on carbon nanowires and nanofibers or encapsulating them into carbon nanotubes. Differently, in 2014, Yu's team designed a novel Ge/C composite nanowire where germanium was fully and homogeneously encapsulated in a carbon matrix, via a one-step controlled pyrolysis of organic–inorganic hybrid materials.[623] As illustrated by **Figure 18**a, GeO_2, $NH_2CH_2CH_2NH_2$ (EDA), Fe_2O_3 and H_2O were selected as Ge precursor, carbon source, catalyst, and solvent, respectively. Firstly, 1D organic–inorganic hybrid GeO_x/EDA nanowires were obtained via a hydrothermal process, based on Fe_2O_3-assisted self-assembly mechanism.[630] Due to the existence of H-bonding (N—H···O—Ge), the organic and inorganic units could interconnect with each other and formed multilayered GeO_x/EDA nanowire precursors. After pyrolysis, the final Ge/C nanowires with multilayer structure were prepared. This unique structure realized homogenous encapsulation of 0D Ge nanoparticles in 1D carbon nanowires, leading to enhanced electrochemical performance. Particularly, this Ge/C nanowire anode exhibited a stable cyclability even at a high current density (a reversible capacity of about 770 mAh g^{-1} after 500 cycles at 16 A g^{-1}).

As mentioned previously, Wang's team used VAGN as a matrix to prepare Sn/VAGN composite anodes and gained good electrochemical performance.[385] Similarly, in 2014, Wang's group also extended their strategy to Ge-based anode, where Ge nanoparticles were wrapped by graphene layers and uniformly loaded on both sides of VAGN, denoted as Ge@G/VAGN.[624] The Ge@G/VAGN anode also presented good cycling stability due to its double-buffer structure. In 2015, Park's group reported their latest work about 3D hierarchical Ge/C nanocomposite anode and its great performance of lithium storage.[627] This high-performance anode was fabricated by a facile method, as presented in Figure 18b. GeO_2 nanoparticles were obtained by a sol–gel process and coated with PVP to generate GeO_2/PVP composite. Through a carbonization process, the final 3D-Ge/C nano architecture was obtained, where Ge nanoparticles were covered by carbon and connected with each other to form a continuous 3D porous structure. The formation of this structure was mainly attributed to gas generation during the carbonization process, where CO_2, H_2O, N_2O gases were produced by decomposition of PVP.[631] The rate performance was boosted by the 3D porous structure. It could maintain a reversible capacity of 1122 mAh g^{-1} after 200 cycles at 100C (1C = 1600 mA g^{-1}) and reached a long-cycling life (up to 1000 cycles at 2C). Moreover, a full lithium-ion cell assembled by 3D-Ge/C anode and $LiCoO_2$ cathode also exhibited good cycling stability and rate capability.

As for the fourth classification, Wang's team developed a novel strategy to build Ge nanowires-in graphite tubes (GNIGTs) structure via a one-step CVD process, for the first

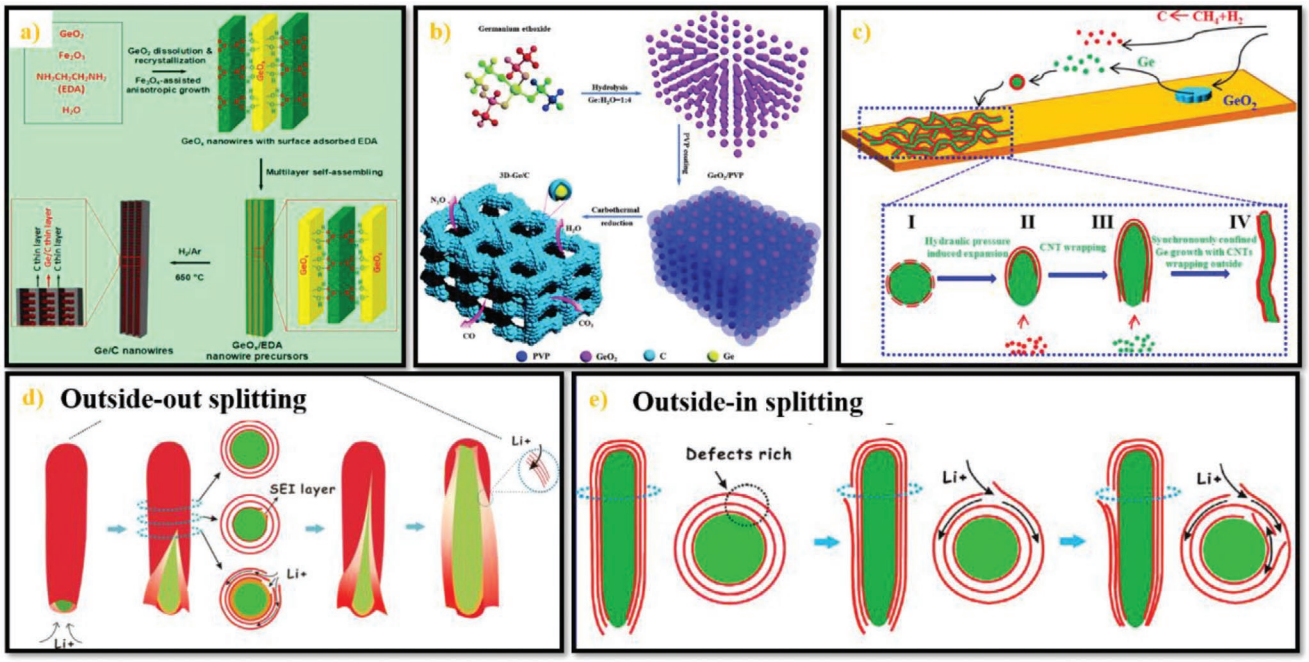

Figure 18. a) Schematic representation of the fabrication of ultrauniform carbon-encapsulated Ge/C composite nanowires from organic–inorganic hybrid GeO_x/EDA nanowires with self-assembled alternating GeO_x and EDA layers. Reproduced with permission.[623] Copyright 2014, American Chemical Society. b) Schematic diagram illustrating the procedure to fabricate 3D-Ge/C. Reproduced with permission.[627] Copyright 2015, Royal Society of Chemistry. c) Illustration of the synergetic-confined-growth of Ge nanowires@Graphite tubes, d) illustration of the proposed inside-out splitting mechanism of a graphite shell and e) outside-in splitting mechanism. Reproduced with permission.[629] Copyright 2015, American Chemical Society.

time in 2015.[629] The synthesis route was started from GeO_2, which was first reduced into Ge source by H_2 under high temperature. Moreover, the Ge clusters could absorb carbon atoms of CH_4, leading to formation of a liquid–solid heterogeneous interface between Ge and C. Consequently, the GNIGTs structure was formed spontaneously based on a synergetic and confined model, which is interpreted in Figure 18c. This GNIGTs anode could retain 88.9% of the specific capacity from the second cycle. Furthermore, the lithium insertion/extraction behavior was also investigated and two types of kinetic mechanisms of graphite shells were proposed, which were referred to as "outside-in" and "inside-out." The inside-out splitting mechanism of the graphite shell originated from interfacial lithiation/expansion and SEI layer formation, which pulled open carbon shell like a zipper (Figure 18d). The outside-in splitting mechanism was attributed to lithium lateral penetration effect across the defects of carbon shell (Figure 18e). According to interpretation by the authors, the splitting graphite shell mechanisms were closely related to the good electrochemical performance of GNIGTs anode, which could not only alleviate pulverization and detachment of germanium by volume change but also enhance the transportation of electrons and lithium ions.

Noncontact-Type Germanium/Carbonaceous Material Composite Anodes: Although only a few reports about noncontact-type Ge/C anodes were published since 2013, all of the work exhibited good results. The typical structures included hollow carbon spheres encapsulating germanium (**Figure 19**a),[632] crumpled N-doped carbon nanotubes encapsulating peapod-like Ge nanoparticles (Figure 19b),[633] carbon nanoboxes encapsulating Ge nanoparticles, (Figure 19c)[634] and 3D nitrogen-doped graphene foam with encapsulated Ge quantum dot/N-doped graphene yolk–shell nano architecture, referred to as Ge–QD@NG/NGF(Figure 19d).[635] Among these studies, the Ge–QD@NG/NGF synthesized by Sun and Yang exhibited the best electrochemical performance. As displayed in Figure 19d, the N-doped graphene was firstly prepared based on Ni foam (NG-NF), through decomposing pyridine and CVD process. GeO_2 nanoparticles were then homogeneously loaded on the N-doped graphene network, forming GeO_2/NG-NF composite. The as-prepared GeO_2/NG-NF was coated with a Ni thin layer via electroplating deposition (GeO_2@Ni/NG-NF). The thin Ni layer acted an important role not only as a catalyst for N-doped graphene growth but also as the sacrificial material for creating internal void space. Thereafter, GeO_2@Ni/NG-NF underwent CVD process, reduction process and acid etching in sequence, obtaining N-doped graphene foam with Ge quantum dot@N-doped graphene yolk–shell nanoarchitecture (Ge–QD@NG/NGF). Finally, the as-prepared composite was coated with a poly(dimethyl siloxane) (PDMS) layer in order to endow the flexibility for the composited anode. Such elaborate design and synthesis enhanced lithium storage performance. This Ge-based composite anode exhibited almost no capacity fading from the 5th to the 1000th cycle, maintaining a reversible capacity of 1200 mAh g^{-1} after 1000 cycles at 1C (1C = 1600 mAh g^{-1}). Furthermore, it could also achieve a reversible capacity of 792 mAh g^{-1} after 200 cycles even at a rate as high as 40C.

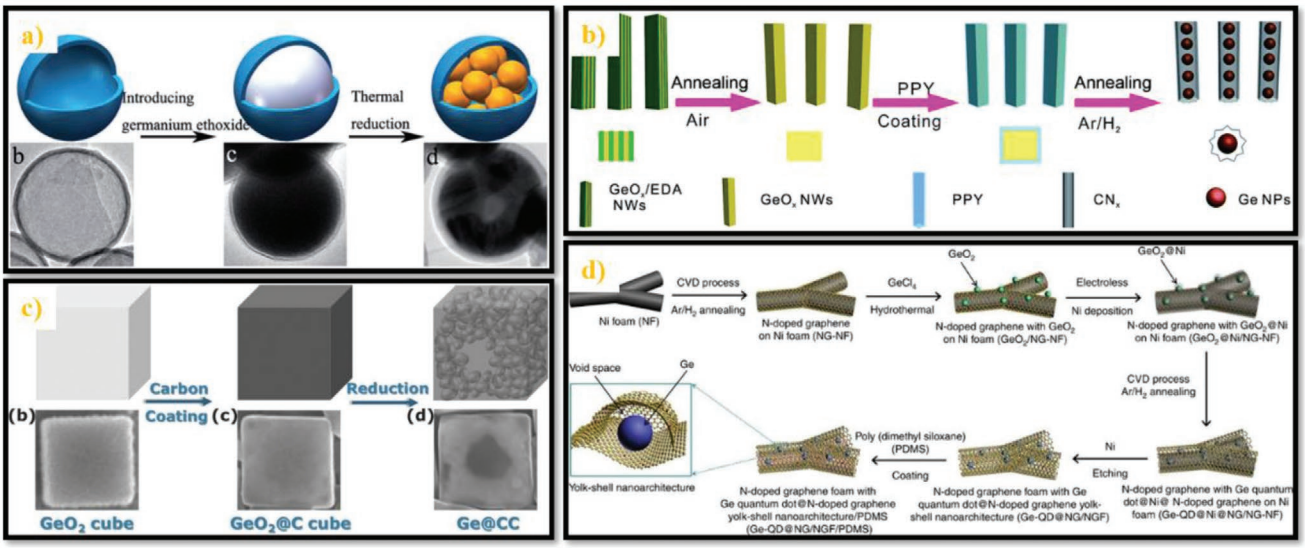

Figure 19. a) Schematic illustration of the formation process to incorporate the germanium into the hollow carbon spheres and corresponding TEM images. Reproduced with permission.[632] Copyright 2015, Royal Society of Chemistry. b) Schematic illustrating the preparation process of the peapod-like Ge/CN_x nanomaterials. Reproduced with permission.[633] Copyright 2016, Royal Society of Chemistry. c) Schematic illustration of the formation process for Ge@CC and corresponding SEM images. Reproduced with permission.[634] Copyright 2015, Wiley-VCH. d) Schematic illustration of the preparation of Ge-QD@NG/NGF/PDMS yolk–shell nanoarchitecture. Reproduced under the terms and conditions of the Creative Commons CC-BY 4.0 International License.[635] Copyright 2017, The Authors, published by Springer Nature.

4.4. Germanium Oxide-Based Anodes for Lithium-Ion Batteries

Compared with elemental germanium, germanium oxide (GeO_2) is a less expensive anode candidate for LIBs and also exhibits a high theoretical capacity of 2152 mAh g^{-1}, based on the following equations.[636,637]

$$GeO_2 + 4Li^+ + 4e^- \rightarrow Ge + 2Ge_2O \quad (49)$$

$$Ge + 4.4Li^+ + 4.4e^- \leftrightarrow 0.2Li_{22}Ge_5 \quad (50)$$

In addition, amorphous germanium oxide (GeO_x) also demonstrated great potential as high-performance anode material for LIBs.[638] Since 2011, germanium oxide-based anodes (both GeO_2 and GeO_x) emerged but rapidly developed as a significant branch of Ge-based anodes in a few years. In this part, the studies of germanium oxide-based anodes for LIBs will be summarized according to four classifications: i) pure germanium oxide anodes,[638,639] ii) germanium oxide/carbonaceous material composite anodes,[640–656] iii) germanium/germanium oxide composite anodes,[657–659] iv) germanium/germanium oxide/carbonaceous material composite anodes.[637,660,661]

4.4.1. Pure Germanium Oxide Anodes

In order to alleviate volumetric effect of germanium and improve the electrochemical performance of electrode, researches about pure germanium oxide anodes are mainly focused on building nanostructures, such as nanoparticles,[662,663] hollow structures,[664,665] and porous structures.[638,639,666] In 2014, Fang et al. reported a simple surfactant-free hydrothermal synthesis method to prepare GeO_x 3D hollow framework.[664] Firstly, Ge nuclei were generated by reducing GeO_4^{2-} which was obtained by dissolution of GeO_2 in NaOH solution. During reduction of GeO_4^{2-}, H_2 bubbles were also formed. Ge nuclei could congregate on the bubble surface in order to reduce surface energy, leading to formation of loose Ge shells around H_2 bubbles. Thereafter, bubbles were amalgamated by the hydrothermal reaction, which allowed shells to connect with each other. Germanium particles were partially oxidized during the process, where GeO_x 3D hollow framework was formed finally as shown in **Figure 20**a. As mentioned in Section 4.1, the inverse opal structure had been successfully applied in elemental Ge anodes and gained good results. In 2018, GeO_2 inverse opal (IO) structure was also prepared and used as a binder and conductive agent-free anode for LIBs.[639] GeO_2 IO materials were fabricated via a sacrificial template method, using PS spheres and germanium ethoxide as templates and Ge precursor, respectively. The as-obtained GeO_2 IO materials (Figure 20b) consisting of highly ordered pores with an average size of about 450 nm, and total thickness reached about 13.4 µm. Such a porous structure provided enough void spaces for volume expansion accommodation and continuous transportation paths for lithium ions. This GeO_2 IO anode achieved a reversible capacity of 714 mAh g^{-1} after 250 cycles at a current density of 150 mAh g^{-1}. Additionally, good cycling performance at high rate was also exhibited.

4.4.2. Germanium Oxide/Carbonaceous Material Composite Anodes

Introducing carbon materials into germanium oxide can obviously enhance its cycling stability and rate capability.

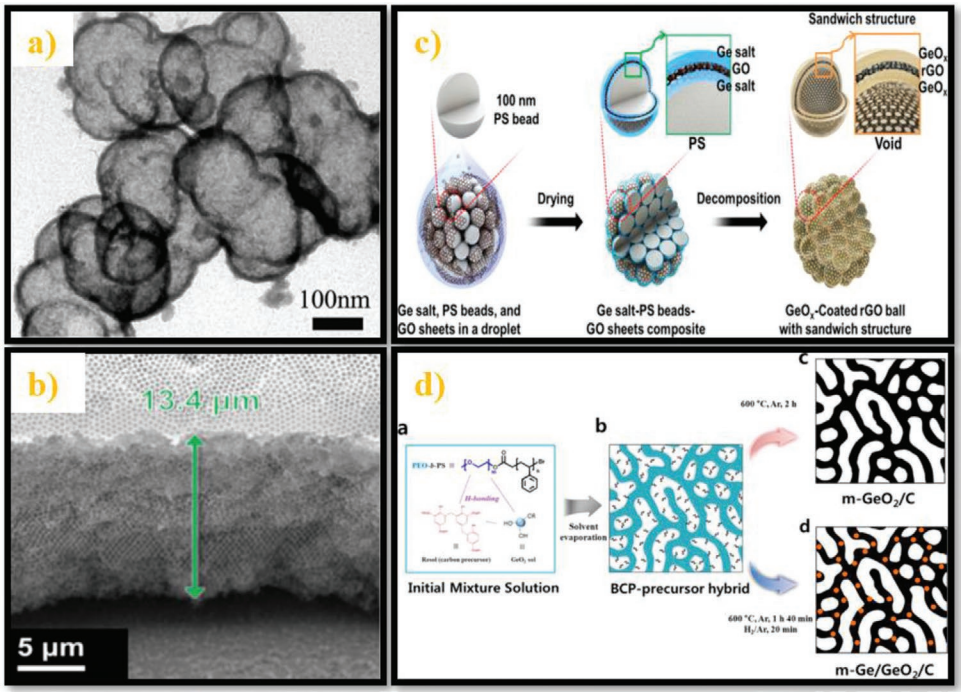

Figure 20. a) TEM image of the GeO_x 3D hollow framework. Reproduced with permission.[664] Copyright 2014, Elsevier Ltd. b) SEM image of GeO_2 IO structure. Reproduced with permission.[639] Copyright 2017, Elsevier Ltd. c) Schematic diagram for the formation mechanism of the amorphous GeO_x-coated rGO composite powder with sandwich structure. Reproduced with permission.[641] Copyright 2015, American Chemical Society. d) Schematic representation of synthesis method for m-GeO_2/C and m-Ge/GeO_2/C. Reproduced with permission.[667] Copyright 2015, American Chemical Society.

Since 2013, many groups fabricated high-performance GeO_2/C anodes inspired by the work from other types of anodes. For example, Yan's team synthesized multilayer GeO_2/graphene tubular nanostructures based on a strain-driven mechanism.[640] Wang's team loaded amorphous GeO_x nanoparticles on vertically aligned graphene nanosheets (VAGN) to build 3D structured GeO_x-based anodes.[646] Moreover, various novel GeO_2/C anodes were also synthesized, where graphene gained much attention. In 2015, Choi and Jung fabricated GeO_x/rGO composite anode where amorphous GeO_x sandwiched rGO with an inside hollow structure (Figure 20c).[641] PS beads were used as templates, and Ge precursor–GO–Ge precursor/PS beads were mixed in a droplet by spray. After thermal reduction process, sandwich-like GeO_x@rGO@GeO_x composites were formed while PS beads were removed to create void space. The unique structure of the composite anode could not only alleviate volumetric effect for long cycling life but also shorten lithium diffusion pathways for enhanced rate performance. Particularly, a capacity of ≈450 mAh g^{-1} at 9 A g^{-1}, and stable cycling over 1600 circles at 9 A g^{-1} with a final reversible capacity of 629 mAh g^{-1} were demonstrated.

4.4.3. Germanium/Germanium Oxide (/Carbonaceous Material) Composite Anodes

Germanium/germanium oxide composites were also studied as LIB anodes in recent years due to high reversible capacity. As for these materials, improvement of electrochemical performance mainly relied on building nanostructures and introducing carbon materials. In 2015, Lee and co-workers synthesized several mesoporous GeO_2-based carbon composites (m-GeO_2, m-GeO_2/C, and m-Ge/GeO_2/C) assisted with block copolymer template.[667] Structure direct agent (PS-*b*-PEO), Ge precursor (germanium ethoxide) and carbon source (phenol-formaldehyde resin) were first mixed into a solution. A small amount of HCl solution was added into the mixture to trigger hydrolysis of germanium ethoxide. After solvent evaporation, the microphase separation of block copolymer led to formation of wormhole-like mesoporous structures. Different GeO_2-based carbon composites were synthesized after calcination at Ar atmosphere with different calcination time lengths. The corresponding synthesis route is presented in Figure 20d. Among these GeO_2-based anodes, the m-Ge/GeO_2/C exhibited the best electrochemical performance, which could retain a reversible capacity of over 1000 mAh g^{-1} at 500 mA g^{-1} after 95 cycles. In order to investigate the reason for the enhanced performance of m-Ge/GeO_2/C anode, CV scan, ex situ XRD and in situ atomic-selective X-ray absorption spectroscopy measurements were carried out. Analysis results indicated that the mesoporous structure and catalytic function of germanium played a synergy effect, which improved the reversibility of the conversion reaction.

4.5. Germanium-Based Compound Anodes for Lithium-Ion Batteries

At the same developing period of germanium oxide-based anodes, germanium-based compounds were also widely studied

as anode candidates for LIBs. Different from tin and antimony which focused on their sulfides and phosphides, new germanium-based compounds, metal germanates, attracted much attention as LIB anodes since 2010s.[668–674] Additionally, several germanium–nonmetal compound anodes also presented good potential as LIB anodes.[675–679]

4.5.1. Metal Germanate Anodes

Due to good thermal stability, electrical, and magnetic properties, various metal germanates have been studied and applied as photocatalysis, chemical sensors, and luminescence devices.[680–682] Recently, lithium storage properties of these materials were investigated, and a variety of metal germanates were studied as LIB anodes, including $Ca_2Ge_7O_{16}$,[683,684] $SrGe_4O_9$,[685] Co_2GeO_4,[686,687] $Zn_2Ge_4O_9$,[674,688–690] and so on. Compared with Ge oxides, metal germanates have some advantages because the crystalline structure could be regarded as composites of GeO_2 and metal oxides. Upon lithiation, the metal oxides are able to accommodate volume change from Ge. Even though, to achieve good electrochemical performance, the metal germanate anodes still need assistance of nanostructures and extra buffer materials. In 2012, Guo and Song fabricated a series of single-crystalline alkaline earth metal germanate nanowires via a low-cost hydrothermal method.[685] The as-prepared alkaline earth metal germanate nanowires included calcium germanate ($Ca_2Ge_7O_{16}$), strontium germanate ($SrGe_4O_9$) and barium germanate ($BaGe_4O_9$), and all of them could be used as anodes for LIBs. The reaction mechanisms between these metal germanates and lithium are presented as follows[684,691]

$Ca_2Ge_7O_{16}$ (theoretical capacity: 990 mAh g^{-1})

$$Ca_2Ge_7O_{16} + 28Li^+ + 28e^- \rightarrow 2CaO + 7Ge + 14Li_2O \quad (51)$$

$$7Ge + 30.8Li^+ + 30.8e^- \leftrightarrow 7Li_{4.4}Ge \quad (52)$$

$SrGe_4O_9$ and $BaGe_4O_9$ (theoretical capacity: 910 mAh g^{-1} and 830 mAh g^{-1})

$$Sr/BaGe_4O_9 + 16Li^+ + 16e^- \rightarrow Sr/BaO + 4Ge + 8Li_2O \quad (53)$$

$$4Ge + 17.6Li^+ + 17.6e^- \leftrightarrow 4Li_{4.4}Ge \quad (54)$$

Particularly, the $Ca_2Ge_7O_{16}$ nanowire anode exhibited the best electrochemical performance among these three type anodes, which retained a reversible capacity of 601 mAh g^{-1} at 100 mA g^{-1} after 100 cycles. Studies on Zinc germanate (Zn_2GeO_4) anodes became favorable recently. In 2015, Hu and Huang synthesized a sandwich-like Zn_2GeO_4/GO nanocomposite through a facile and low-cost approach.[689] Free Zn^{2+} ions were firstly loaded on GO sheets via electrostatic interaction, where GeO_3^{2-} ions were then added into the system by the reaction, forming amorphous Zn_2GeO_4 nanoparticles anchored on GO sheets. The pure Zn_2GeO_4 and Zn_2GeO_4/GO composite presented different electrochemical reactions with lithium, which was described as follows

pure Zn_2GeO_4 (theoretical capacity: 541 mAh g^{-1})

$$Zn_2GeO_4 + 8Li^+ + 8e^- \rightarrow 2Zn + Ge + 4Li_2O \quad (55)$$

$$Ge + 4.4Li^+ + 4.4e^- \leftrightarrow Li_{4.4}Ge \quad (56)$$

$$Zn + Li^+ + e^- \leftrightarrow LiZn \quad (57)$$

Zn_2GeO_4/GO composite (theoretical capacity: 1443 mAh g^{-1})

$$Zn_2GeO_4 + 8Li^+ + 8e^- \rightarrow 2Zn + Ge + 4Li_2O \quad (58)$$

$$Ge + 4.4Li^+ + 4.4e^- \leftrightarrow Li_{4.4}Ge \quad (59)$$

$$Zn + Li^+ + e^- \leftrightarrow LiZn \quad (60)$$

$$Zn + Li_2O \leftrightarrow ZnO + 2Li^+ + 2e^- \quad (61)$$

$$Ge + 2Li_2O \leftrightarrow Ge_2O + 4Li^+ + 4e^- \quad (62)$$

Theoretically, the addition of GO in Zn_2GeO_4 could obviously improve the electrochemical performance of the electrode. The as-prepared Zn_2GeO_4/GO composite anode actually maintained a reversible capacity of 1150 mAh g^{-1} after 100 cycles at a current density of 200 mA g^{-1}. The performance was much better than that of pure Zn_2GeO_4 electrode, which was attributed to a synergistic effect from Zn_2GeO_4 and GO layers.

4.5.2. Germanium–Nonmetal Compound Anodes

Although the number of the studies reported is small, germanium–nonmetal compound anodes are not ignored due to good electrochemical performance. The Ge–nonmetal compounds explored included germanium nitride (Ge_3N_4),[677,692] germanium phosphide (GeP_5),[693] germanium sulfides (GeS and GeS_2),[676,678] germanium selenide/telluride (GeSe, GeTe),[694–696] and germagraphene ($C_{17}Ge$).[675] In 2015, Li et al. reported lithium storage performance of GeP_5 for the first time, which was fabricated by a large-scale mechanical milling method.[679] According to ex situ XRD characterization, the reaction mechanism of GeP_5 is presented as the following equations

$$GeP_5 + 15Li^+ + 15e^- \rightarrow Ge + 5Li_3P \quad (63)$$

$$Ge + 4.4Li^+ + 4.4e^- \leftrightarrow Li_{4.4}Ge \quad (64)$$

Based on the equation, the theoretical capacity of GeP_5 is calculated to be 2289 mAh g^{-1}. The as-prepared GeP_5 anode exhibited initial discharge and charge capacity of 2406 mAh g^{-1} and 2266 mAh g^{-1}, respectively. In order to further improve the electrochemical performance of GeP_5, GeP_5/C composite electrode was synthesized by ball-milling. Because of the amorphous carbon matrix, the GeP_5/C composite anode could reach a capacity of 2127 mAh g^{-1} at a current density of 5 A g^{-1}, and maintained a reversible capacity

of 2300 mAh g^{-1} after 40 cycles (at 0.2 A g^{-1}). In 2019, Yang's team used first-principles calculation method to predict electrochemical performance of germanium doped graphene (denoted as germagraphene, $C_{17}Ge$) LIB anode.[675] The simulation results indicated that the $C_{17}Ge$ could exhibit a specific capacity of 1734 mAh g^{-1} theoretically, based on the following equations

$$C_{17}Ge + 18Li^+ + 18e^- \leftrightarrow Li_{18}C_{17}Ge \quad (65)$$

Moreover, the lattice change of the $C_{17}Ge$ was calculated to be only 0.48% upon lithiation, indicating good cycling stability with respect to the $C_{17}Ge$ anode.

4.6. Germanium-Based Anodes for Sodium-Ion Batteries

As addressed at the beginning of this part, germanium can electrochemically react with sodium to form NaGe alloy, indicating its potential application as anodes for Na-ion batteries. Compared to the prosperity of Ge-based anodes for LIBs, only a few studies focused on SIB Ge-based anodes since the 2010s due to their relative-low capacity. In 2011, Chevrier and Ceder demonstrated the viability of germanium as anodes for SIBs based on density functional theory (DFT) calculations.[88] In 2013, Ge thin film electrodes were synthesized by Veith's[582] and Mullins's team,[697] respectively. The sodium storage property of Ge was proved by experiment for the first time based on Veith's work. The as-prepared Ge thin film anodes could react with Na at low voltage plateaus near 0.15/0.6 V, and exhibited a reversible capacity of 350 mAh g^{-1}. In the following years, studies of Ge-based anodes for SIBs could be divided into two categories generally. On the one hand, nanostructure and buffer matrix were introduced into Ge material to improving cycling stability of the electrode;[698–701] on the other hand, several Ge-based materials were applied as SIB anodes because of their higher capacity than that of pure Ge material.[702–704]

In 2016, Lu's group synthesized germanium@graphene@titanium dioxide core–shell nanofibers (Ge@G@TiO_2 NFs) through electrospinning and following ALD process.[700] Firstly, $GeCl_4$, graphene, and PVP were mixed to prepare the precursor solution, and composite nanofibers were produced via electrospinning. Then, TiO_2 layers were deposited on the surface of as-prepared fibers by ALD technique. After thermal annealing, final Ge@G@TiO_2 nanofibers were obtained. Due to this double-buffer strategy, the electrochemical performance of Ge@G@TiO_2 electrode was clearly enhanced compared with its counterparts (single-buffer or ono-buffer). As SIB anode, the Ge@G@TiO_2 nanofibers maintained a reversible capacity of 190 mAh g^{-1} after 100 cycles at 100 mA g^{-1}. Besides the bare germanium, several Ge-based compounds were also investigated as anodes for SIBs recently, such as germanium oxides,[702] germanium phosphides,[705] and metal germinates.[706,707] In addition, amorphous germanium was found to have a higher sodiation capacity of 590 mAh g^{-1} ($Na_{1.6}Ge$), compared to crystalline Ge (NaGe). In 2015, Li et al. demonstrated good performance of GeP_5/C composite as anode for LIB.[679] Later then, they applied this anode material in SIBs and also achieved good results.[705] According to the following equations, GeP_5 can theoretically reach a capacity of 1888 mAh g^{-1} in SIBs

$$GeP_5 + 16Na^+ + 16e^- \rightarrow 5Na_3P + NaGe \quad (66)$$

$$5Na_3P \leftrightarrow 5P + 15Na^+ + 15e^- \quad (67)$$

$$NaGe \leftrightarrow Ge + Na^+ + e^- \quad (68)$$

The GeP_5 electrode delivered initial discharge/charge capacities of 1351/1245 mAh g^{-1} and kept a 98% retention after 60 cycles (100 mA g^{-1}). Moreover, a full sodium-ion cell with GeP_5/C anode and $Na_3V_2(PO_4)_3$/C cathode exhibited a reversible capacity of ≈800 mAh g^{-1} as well as a high average output voltage of ≈2.65 V.

4.7. Temporary Summary of Germanium-Based Anodes

Compared with tin and antimony-based anodes, the emergence time of germanium-based anodes is the latest. When time entered the new century, Ge-based anodes gradually attracted attention. However, the development of Ge-based anodes still cannot be compared to contemporaneous Sn and Sb-based anodes. As presented by **Figure 21**, the year 2010 is an important turning point regarding the whole development phase of the Ge anodes. In contrast to the weak development momentum of Sn and Sb-based LIB anodes after 2010, the Ge-based LIB anodes inversely embraced an explosive development. As the most two important branches of germanium-based anodes, elemental germanium and germanium/carbon composite anodes gained fruitful achievements. Additionally, germanium alloys, germanium oxides, and germanium-based compounds also exhibited their potential and competitiveness as high-performance anodes for Li-ion batteries. During the last 20-year development, the Ge-based LIB anodes are the protagonists while the progress of Ge-based SIB anodes is limited because of their relative low capacity. Therefore, the Ge-based anodes are the most "unbalanced" type among these three materials. The late beginning time of germanium anodes inversely provides a good opportunity to be inspired and learn from the other two systems. Coupled with the high reversible capacity of germanium, Ge-based materials have become one of the most favorite anodes for LIBs since the 2010s. The synthesis methods and electrochemical performance of representative studies about germanium-based anodes for LIBs and SIBs are summarized in **Table 3**.

5. Conclusions and Perspectives

After fabrication of the first commercialized LIB, high-performance anode materials have always been the pursuit of this research field. Since the 1990s, tin, antimony and germanium-based materials have started to be studied as anodes for LIBs, due to their good lithium storage performance. However, the biggest obstacle of these anodes to realize practical application is the huge volume expansion during their lithiation process, leading to pulverization of electrodes and fast fading of

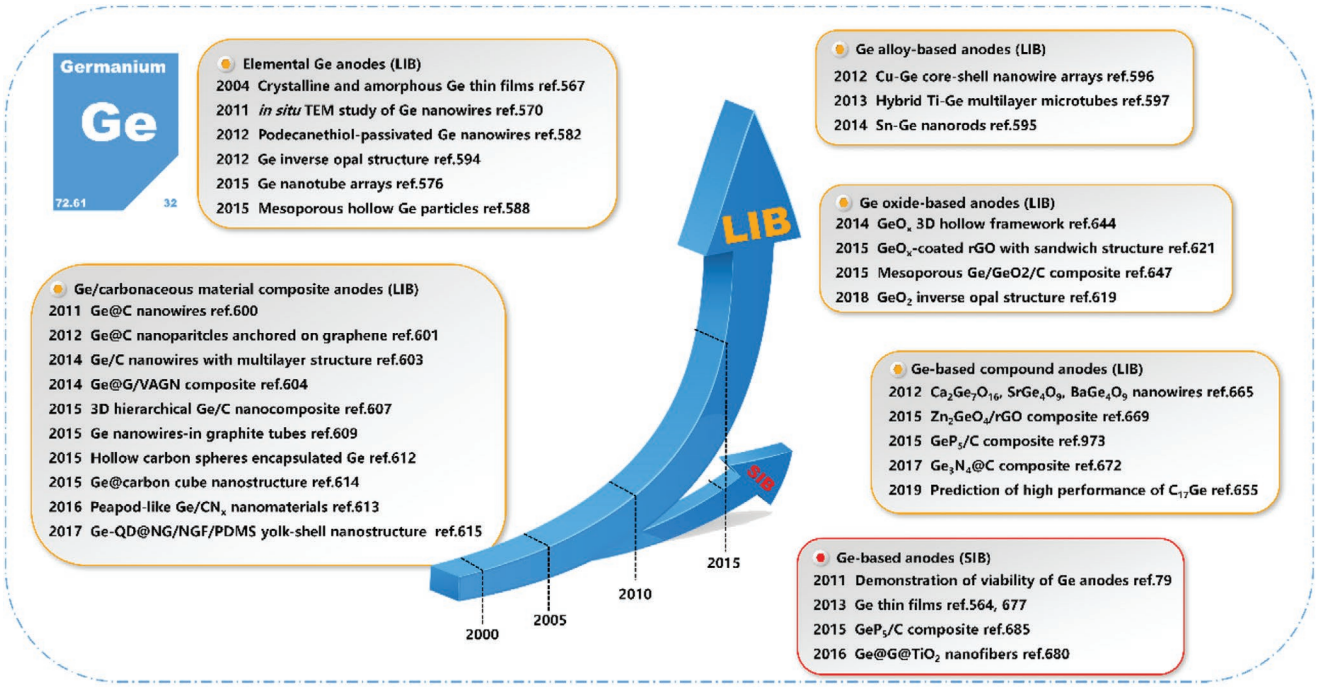

Figure 21. A brief illustration of the development history of germanium-based anodes.

capacities. In the following years, three main strategies tackling this drawback have been generally established, viz. decreasing particle size of active material, constructing void space inside active material, and introducing buffer matrix into active material. Therefore, the electrochemical performance of Sn, Sb, Ge-based LIB anodes has been dramatically enhanced at the end of 2000s. The renaissance of SIBs around 2010 could be regarded as the turning point for Sn, Sb, Ge-based anode materials. The poor sodium storage performance of Si provides a golden opportunity for these nonsilicon-based anodes. It has evolved into a main force for SIBs in a short period, especially for Sn and Sb-based anodes. In this chronicle review, the studies on nonsilicon (Sn, Sb, Ge)-based anodes for lithium/SIBs are summarized from the 1990s to the latest, which almost covered the last 30 years. In every individual part for each material, various types of the specific material are reviewed according to chronological order.

Regarding the tin-based anodes, studies could be dated back to the 1970s. From the 1970s to 1990s, the alloying mechanism between tin and lithium as well as fundamental electrochemical behavior and properties of Li–Sn system were investigated. In following years, five main types of Sn-based anodes for LIBs were developed, including Sn alloy-based anodes, Sn oxide-based anodes, Sn-based compound anodes, Sn/carbonaceous and other material composite anodes, and elemental Sn anodes. In addition, the former four types of anodes were also applied in SIBs since 2010. Generally, the Sn-based anodes presented a relative balance development in both LIB and SIB domains.

i) In terms of number of studies reported, the tin alloy-based anodes (LIB) are the most among all tin-based anodes. The studies of the Sn alloy-based anodes emerged in the middle of the 1990s, and mainly relied on the "active/inactive" mechanism of SnSb alloy to improve cycling stability. From 2000 to 2006, more categories of the Sn alloy were applied as anodes of Li-ion batteries, while some nanostructured Sn alloy anodes were fabricated assisted by new techniques. In the following five years (2007–2011), the Sn alloy-based anodes embraced a fast development period, in which various nanometer-sized and micrometer-sized Sn alloy anodes ae well as Sn/C composite anodes exhibited enhanced electrochemical performance. Since 2012, the development of Sn alloy-based anodes gradually trended to steady, where the three kinds of Sn alloy anodes mentioned in the last stage were still mainstreams. More delicate structures were realized for the Sn alloy-based anodes, resulting in further enhanced lithium storage performance.

ii) The successful application of TCO anode in 1994 opened a gate for a new branch of the Sn-based anodes, tin oxide-based anodes (LIB). Before 2000, reaction mechanism and electrochemical behaviors of the tin oxide anodes were studied. From 2000 to 2009, various tin oxide-based materials with nanostructures and tin oxide/carbon composites attracted most of the attention and gained good electrochemical performance as anodes for LIBs. Since 2010, a series of hollow structured SnO_2 anodes were synthesized through different methods promoted the electrochemical performance of the tin oxide anodes to a new level. Graphene-based materials, as well as noncarbon materials, were widely used as effective buffer matrix for the tin oxide anodes.

iii) In 1998, the lithium storage property of $SnSO_4$ was demonstrated and it followed a multistep reaction mechanism similar to that of tin oxides. From 1998 to 2006, a variety of tin-based compounds, including SnS_2, $SnSO_4$, Sn_4P_3, and $Sn_2P_2O_7$, were successfully applied as anodes for LIBs. Moreover, their reaction mechanisms with lithium were also

Table 3. Summary on representative studies about germanium-based anodes for LIBs and SIBs (ICE: initial coulombic efficiency; *n*: the *n*th cycle).

Material type	Development stage	Representative anode	Synthetic method	ICE	Charge capacity [mAh g^{-1}] (*n*, rate)	Rate capacity [mAh g^{-1}] (rate)	Ref.
			LIBs				
Elemental germanium	Rising stage	a-Ge thin film	Pulsed laser deposition	≈67%	1700 (60, 0.375 A g^{-1})	700 (1500 A g^{-1})	[585]
	(2004–2011)	Ge nanowires	VLS–CVD growth	\	\	\	[588]
	Explosive development stage	Functionalized Ge nanowires	Chemical synthesis	77%	1130 (100, 0.1C)	664 (8C)	[600]
	(since 2012)	Ge nanotube arrays	Template-assisted electrodeposition	77%	1180 (250, 0.2C)	828 (2C)	[594]
		Mesoporous Ge	Redox-transmetalation reaction	89%	1400 (300, 0.5C)	804 (5C)	[606]
Germanium alloy	since 2005	Cu@Ge nanowires	RF-sputtering technique	80%	1419 (40, 0.8 A g^{-1})	734 (96 A g^{-1})	[616]
		Ge–Ti multilayer microtubes	Strain-released method	85%	930 (100, C/16)	\	[617]
		Sn–Ge nanorods	SLS growth	≈46%	1520 (100, 1 A g^{-1})	≈750 (4 A g^{-1})	[615]
Germanium/carbon	Rising stage	Ge@C nanowires	Solid–liquid solution method	91%	693 (100, 0.4 A g^{-1})	700 (4.8 A g^{-1})	[620]
	(2007–2012)	Ge@C/rGO	Solvothermal synthesis	52%	940 (50, 0.05 A g^{-1})	380 (3.6 A g^{-1})	[621]
Contact-type	Explosive development stage	Ge/C nanowires	One-step controlled pyrolysis	82%	770 (500, 16 A g^{-1})	\	[623]
	(since 2012)	3D Ge/C	Sol–gel process and coating	70%	1216 (1000, 3.2 A g^{-1})	429 (640 A g^{-1})	[627]
		GNIGTs	One-step CVD growth	50%	1242 (100, 0.25 A g^{-1})	232 (10 A g^{-1})	[629]
Noncontact-type		Ge@C HCS	Thermal reduction	\	1000 (100, 1.6 A g^{-1})	772 (32 A g^{-1})	[632]
		Peapod-like Ge/CN_x	Solvothermal synthesis	49%	1080 (1200, 0.8 A g^{-1})	874 (12.8 A g^{-1})	[633]
		Ge@CC	Coating and reduction	\	1065 (500, 0.8 A g^{-1})	497 (48 A g^{-1})	[634]
		Ge-QD@NG/NGF	CVD and hydrothermal assembly	76%	1200 (1000, 1.6 A g^{-1})	792 (64 A g^{-1})	[635]
Germanium oxide	2010s	GeO_x 3D hollow framework	Hydrothermal synthesis	≈44%	1000 (50, 0.5 A g^{-1})	850 (4 A g^{-1})	[664]
		GeO_x@rGO@GeO_x	PS templating method	42%	758 (700, 2 A g^{-1})	450 (9 A g^{-1})	[641]
		m-Ge/GeO_2/C	BCP sol–gel process	72%	1000 (95, 0.5 A g^{-1})	428 (8 A g^{-1})	[667]
Metal germanate	2010s	$Ca_2Ge_7O_{16}$ nanowire	Hydrothermal method	18%	601 (100, 0.1 A g^{-1})	\	[685]
		Zn_2GeO_4/GO	Hydrothermal method	35%	1150 (100, 0.2 A g^{-1})	522 (3.2 A g^{-1})	[689]
Ge-based compound	2010s	GeP_5/C	Ball-milling method	95%	2300 (40, 0.2 A g^{-1})	2127 (5 A g^{-1})	[679]
			SIBs				
	2010s	Ge thin film	DC magnetron sputtering	\	350 (15, 1C)	290 (34C)	[582]
		Ge@G@TiO_2 nanofibers	Electrospinning and ALD	≈47%	190 (100, 0.1 A g^{-1})	88 (1 A g^{-1})	[700]
		GeP_5/C	High energy ball-milling	92%	1220 (60, 0.1 A g^{-1})	900 (1.5 A g^{-1})	[705]

investigated via different measurements. Since 2007, many efforts were made in order to improve the electrochemical performance of Sn-based compound anodes, including synthesizing nanostructures and introducing carbon-based materials to improve cycling stability of these anodes.

iv) When assisted by carbon or noncarbon matrix, direct using the pure tin as active material became feasible since about 2000. Due to effective accommodation of volume expansion by matrix, the Sn-based composite anodes could be the most successful Sn-based anodes. During the preliminary stage from 2000 to 2005, most researches of the Sn/C composite anodes focused on contact-type. From 2006 to 2012, the development of contact-type Sn/C composite anodes was obviously accelerated, while the noncontact-type was still at a primary stage. Since 2013, the Sn/C composite anodes embraced a golden development stage, when the quantity of studies witnessed an explosive increase. One important progress in this stage was that a variety of noncontact-type Sn/C composites was fabricated that exhibited great electrochemical performance as anodes of LIBs.

v) Applying bare tin material as anode always faced a huge challenge from severe volume expansion since the birth

of tin-based anodes. Without the cushion matrix, decreasing the absolute size of Sn particles or creating porous Sn structures are other possible options. Until 2007, Sn nanoparticles ranged from 5 to 80 nm were produced as anodes, but the capacity faded quickly after a few cycles due to the nonuniform particle size and agglomeration. In following years, monodisperse Sn nanoparticles and nanoporous Sn material were synthesized, which vastly improved cycling stability of the pure Sn anodes.

vi) After the renaissance of SIBs around 2010, tin-based anodes gained much attention due to their high theoretical capacities. Theoretically, all types of Sn-based anodes for LIBs mentioned above can be applied in SIBs, because Sn active site can electrochemically react with Na ions to form alloys. In the last nine years, tin alloys, tin/carbon (other) composites, tin oxides, and tin-based compounds were all applied as anodes for SIBs. Around 2010, huge amount of work about the Sn-based LIB anodes were reported, which could provide good guidance for Sn-based SIB anodes. As for the tin alloys, tin oxides, and tin-based compounds, creating unique nanostructure and introducing buffer agent were still mainstream strategies to improve the electrochemical performance. During this period, most of the Sn-based composite anodes were contact-type, with carbonaceous materials or titanium oxide as the buffer media.

Antimony is the only one among these three materials which could electrochemically react with lithium or sodium to form alloys with the same molar ratio. Similar to the tin-based anodes, the origin of the antimony-based anodes could also be traced back to the 1970s. Before 2010, studies about the antimony-based LIB anodes mainly focused on antimony alloys and antimony/carbonaceous and other material composites. The research emphasis of the antimony-based anodes was gradually shifted to SIBs after 2010, due to their great sodium storage performance. Antimony alloys, antimony-based composites, antimony oxides, antimony-based compounds as well as pure antimony all presented great potentials as high-performance anodes for SIBs. The development trend of the antimony-based anodes is not as balanced as that of tin-based anodes, which emphasizes more on SIB field since the 2010s.

i) Antimony alloy anodes originated from the last few years of the 1990s. Fundamental studies of various Sb alloys were performed until 2006. A few of Sb alloy-based anodes were also fabricated, which generally relied on the "active/inactive" principle to alleviate volumetric effect of Sb. From 2006 to 2011, different kinds of Sb alloys and Sb alloy/C composites were fabricated with different nanostructures. After 2012, the development momentum of the Sb alloy-based LIB anodes became moderate gradually, which was mainly attributed to the rise of SIBs.

ii) Besides Sb-based alloys, Sb/carbonaceous and other material composite anodes was another main branch of Sb-based anodes for LIBs. Between 2004 and 2010, Sb/C composite electrode was successfully fabricated with Sb nanoparticles uniformly distributed in a carbon matrix. Additionally, non-carbon matrix materials were also developed during this period. Similarly, influenced by the good performance of Sb-based anodes in SIBs, development of Sb/C (other) composite anodes entered a steady stage since 2011.

iii) Since about 2013, various antimony-based materials embraced their explosive developments as anodes for SIBs. Traditional Sb alloys exhibited good sodium storage performance assisted with nanostructures and buffer matrixes. Besides, the reaction mechanism of sodium with different Sb alloys was also investigated.

iv) Antimony/carbonaceous and other material composites are doubtlessly the most favorite and successful Sb-based anodes for SIBs since 2013. From 2013 to 2015, the Sb/C hybrid anodes achieved great progress during this short period, especially the Sb/C composite fibers. Since 2016, the quantity of the studies about Sb/C (or other materials) composite anodes gained further development and fruitful progress. Hollow structures were widely applied in both contact and noncontact-type Sb-based composite electrodes. Moreover, several Sb composite anodes could be applied in full cells and exhibited good electrochemical performance.

v) Although antimony oxides were studied as LIB anodes as early as 1999, they didn't receive much attention in the following years. Until the 2010s, antimony oxides were once again investigated as anodes for SIBs due to high theoretical capacities. Combination of nanostructured antimony oxides and carbon materials exhibited great advantages for improving the electrochemical performance of Sb oxide-based anodes in SIBs. It became a mainstream strategy since the 2010s.

vi) The rising of the antimony oxide-based SIB anodes also inspired the development of other antimony–chalcogen compounds as anodes for SIBs since the 2010s. Antimony sulfide, selenide, and telluride were modified by nanostructures or compositing with carbon materials, in order to improve their electrochemical performance. In addition, other Sb-based compounds were also applied as anodes for Na-ion batteries, including antimony oxychloride, antimony phosphate, antimony–niobium pentoxide, and antimony tungstate.

vii) Compared with pure tin anodes, the application of elemental antimony anodes made much more achievements. Attempts of using bare Sb materials as anodes for LIBs started from 2004. In following years, various Sb anodes with delicate nanostructure design were synthesized successively, where cycling stability of the pure Sb anodes were clearly improved. Since the 2010s, more elemental Sb anodes were designed pertinently for applications in SIBs, including monodisperse nanoparticles and hollow nanostructures.

Although the origin of the germanium-based anodes could be dated back to the 1980s, the development history is still the shortest among these three materials. During the first ten years of the 21st century, Ge-based anodes didn't attract much attention. Until around 2010, the great lithium storage property and other advantages of Ge materials were actually realized by researchers. Therefore, since 2010, Ge-based LIB anodes entered a fast development stage in a few years. Pure germanium materials, germanium alloys, germanium/carbon (other) composites, germanium oxides, and other germanium-based compounds all exhibited huge potential as high-performance

anodes for LIBs. Different from the rise of the Sn or Sb-based SIB anodes after about 2010, the development of Ge-based SIB anodes was limited by the relative-low specific capacity. Hence, the studies on the Ge-based anodes were significantly unbalanced regarding the applications in the LIBs and SIBs during their development history.

i) Elemental germanium anodes (LIB) are the most successful compared with pure Sn and Sb anodes. From 2004 to 2011, Ge thin films, nanowires, nanotubes, and porous materials were fabricated, which demonstrated good electrochemical performance. Since 2012, studies of the pure Ge anodes embraced an explosive progress, where various hollow structural and porous Ge anodes were successfully synthesized with simple and cost-effective routes.
ii) Germanium alloy-based anodes (LIB) emerged after 2005 and made much progress due to nanostructure construction strategy. Since 2012, a variety of high-performance Ge alloy-based anodes were synthesized, including nanowire arrays, microtubes, and nanorods.
iii) Germanium/carbonaceous material composite anodes were the first major branch of Ge-based anodes and gained the most attention and fruitful achievements in the last decade. From 2007 to 2012, most studies about the Ge/C anodes focused on embedding and coating designs (contact-type). Since 2013, contact-type Ge/C hybrid anodes still held the dominance during this explosive development stage, while the noncontact-type Ge/C anodes gradually emerged. Germanium nanoparticles were encapsulated into different carbon materials, forming various yolk–shell architectures to accommodate the volume expansion of Ge during cycling.
iv) Because of high theoretical capacity and low cost, germanium oxides were studied as anodes for Li-ion batteries since 2011 and rapidly developed into a significant branch of the Ge-based anodes within a few years. In the last few years, three different types of germanium oxide-based LIB anodes were explored, including pure germanium oxide anodes, germanium oxide/C composite anodes, and germanium/germanium oxide/carbon composite anodes.
v) In comparison to tin and antimony anodes, the categories of the germanium-based compound anodes are expanded significantly, including various metal germanates and Ge–nonmetal compounds. The lithium storage property of the metal germanate was investigated in around 2010. Thereafter, a series of metal germanates were studied as anodes for LIBs, including calcium, strontium, barium, zinc, copper and cobalt germanates. In addition, the Ge–nonmetal compounds also exhibited good performance as LIB anodes, such as germanium nitride, phosphide, sulfide, selenide, and telluride.
vi) In contrast to the flourish of the Ge-based LIB anodes, the applications of the Ge-based anodes in SIB domain are limited due to their low theoretical capacities. In the first few years of the 2010s, studies about the Ge-based SIB anodes were mainly concentrated on fundamental researches of electrochemical behaviors. In the following years, nanostructure and buffer matrix were introduced into Ge material to improve cycling stability; while some new Ge-based anodes were found with higher theoretical capacities.

Originated as early as the 1970s, nonsilicon (Sn, Sb, Ge)-based anodes developed from nothing into a prosperous situation at the end of 2010s. By reviewing the total development process of the tin, antimony, germanium-based anodes, it can be divided into four periods. Before 1990, at the era without commercialized Li-ion battery, fundamental researches about alloying mechanisms between Sn, Sb, Ge, and lithium paved the way for later practical applications. From 1990 to 2000, the commercialization of LIB stimulated studies for searching anodes with better electrochemical performance. During this period, feasibilities of the Sn, Sb and Ge anodes for LIBs were demonstrated in succession, and initial Sn, Sb and Ge-based anodes were prepared. From 2000 to 2010, the development of the Sn and Sb-based anodes stepped into a fast stage. Various types of Sn and Sb-based anodes appeared, and their electrochemical performance was clearly enhanced assisted with nanostructures and buffer matrixes. The year of 2010 is regarded as the turning point for all these three anode materials. Due to good sodium storage performance of the Sn and Sb-based anodes, the renaissance of SIB shifted their application emphasis since 2010. Moreover, the Ge-based anodes finally embraced a golden period and gained explosive development. As illustrated by **Figure 22**, the development of the Sn, Sb, and Ge-based anodes is a process of learning and inspiring from each other. The development process is also a history of fighting against the serious volume expansion and other drawbacks. Until now, the electrochemical performance of the Sn, Sb and Ge-based anodes in both LIBs and SIBs are dramatically improved and close to the level of practical applications.

A few years ago, a chronicle perspective review about Si-based LIB anodes was published by Zuo et al.[64] The development history of Si-based anodes was divided into four stages: preliminary stage (1990–2000), rise stage (2001–2005), rapid development stage (2006–2010), and explosive development stage (2011–2015). In every single timeframe, related studies about 0D (nanoparticle), 1D (nanowire), 2D (thinfilm), 3D (porous and hollow structures), and Si-based anodes for LIBs were reviewed. In comparison, the development trends of

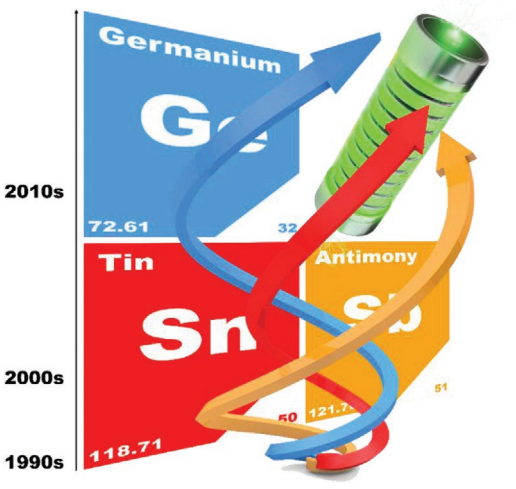

Figure 22. Schematic diagram of the development trends for Sn, Sb, Ge-based anodes.

nonsilicon-based anodes in this review share several similarities and differences with that of silicon-based anodes, as expressed below.

Similarities:

i) Due to the inherent drawback of alloy-type anodes, volume expansion during cycling, the developments of both silicon-based and nonsilicon-based (Sn, Sb, Ge) anodes always revolved around a permanent theme: how to alleviate the negative effect of the volume expansion. Until now, decreasing particle size, creating inner space and introducing buffer matrix have been generally accepted as the three most effective strategies to solve this issue. Based on the same objective, many studies about nonsilicon-based anodes drew experience from those about silicon-based anodes.
ii) In the past 30 years, the studies about both silicon-based and nonsilicon-based (Sn, Sb, Ge) anodes underwent two similar turning points regarding the concepts. The first turning point was around 2005. At that time, the development of nanotechnology and new material boosted the anode research into a new era, in which how to improve electrochemical performance of these anodes (Si, Sn, Sb, Ge) was the prime pursuit of most of studies. Countless anodes materials with delicate nanostructure and good electrochemical performance have been fabricated in the following ten years. Probably from 2015, because of the huge market demand for the next-generation LIBs, a consideration of how to facilitate these alloy-type anodes to real applications started to attract more and more attentions in academia. A large number of related studies began to focus on facile and scalable synthesis methods as well as low-cost and readily available materials instead of fantastic structures.

Differences:

i) Unlike the "single-line" development of silicon-based anodes, the development of nonsilicon-based anodes appeared bifurcation at about 2010, which was mainly related to the renaissance of SIBs. Due to the inferior alloying ability of Si with Na, Sn, Sb, Ge-based anodes embraced a great opportunity to explore their application boundary. After about ten-year development, nonsilicon-based anodes have become very promising candidates for future applications in SIBs.
ii) Due to the ultrahigh theoretical capacity of silicon, the studies about Si-based anodes mainly focused on nanostructured silicon and silicon/carbon composite materials. In terms of Sn, Sb, Ge-based anodes, the related studies exhibited more diversity in the kind of alternative materials, including sulfides, phosphides, selenides, tellurides, and metal germanates.

Although the Sn, Sb, Ge-based materials have exhibited huge potential as high-performance anodes for both LIBs and SIBs, the real application of these anodes still needs more time. Before the real application, there are several critical concerns need to be addressed properly. Firstly, a suitable material needs to be selected from such many candidates. For now, the Sn, Sb, Ge/C composite is the most ideal anode for future applications due to its stable cyclability. Secondly, the balance between industrial feasibility of fabrication method and actual usability of electrochemical performance is also a critical issue. In most of the present studies, the reported fabrication methods are not suitable to real industrial production although the Sn, Sb, Ge-based anodes display good electrochemical performance. Thirdly, reasonable areal mass loading of the electrode has been regarded as a necessary condition to realize decent energy output in real battery applications.[708] However, few of studies about Sn, Sb, Ge-based anodes paid attention to this important issue. Fourthly, the cost problem would be a big obstacle to commercialize the Sn, Sb, Ge-based anodes. How to decrease the cost of material and production of these anodes is a challenge to both academia and industry. Compared with Si-based anodes, the advantage of Sn, Sb, Ge-based anodes is their applicability in SIBs. Compared with LIBs, the advantages of SIBs are the low cost and abundance of sodium source as well as the application potential in large-scale energy storage devices. Therefore, it could be predicted that the Sn, Sb, Ge-based anodes will have great application potential in the SIB-based energy storage facilities in the future.

In addition, potassium-ion batteries (PIBs) have attracted tremendous attention recently due to their low cost, fast ionic conductivity in electrolyte, and high operating voltage.[709] In recent years, Sn, Sb, Ge-based materials have been demonstrated to be anode candidates for PIBs.[710–714] However, due to the larger-radius of K ions, these anodes face big challenges of sluggish K^+ diffusion kinetics and huge volume change during potassiation/depotassiation processes. On the basis of previous studies about LIBs and SIBs, rational structure engineering and composite electrode design are still effective strategies for Sn, Sb, Ge-based anodes to improve their electrochemical performance in PIBs. For examples, few-layered SnS_2 nanosheets supported on reduced graphene oxide (SnS_2@rGO) were fabricated by Xia and co-workers, which presented 73% capacity retention after 300 cycles as anode for PIB.[715] Wang and co-workers prepared a novel type of Sb/C composite anode where Sb nanoparticles were uniformly encapsulated by an interconnecting carbon sphere network (Sb@CSN).[714] The Sb@CSN anode retained a high reversible capacity of 504 mAh g^{-1} after 220 cycles, corresponding to a capacity decay of 0.06% per cycle from the 10th to 100th cycle. In terms of Ge-based material, He and co-workers reported a pure germanium PIB anode with nanoporous structures which were prepared by a facile chemical dealloying process.[716] This porous Ge anode delivered a stable capacity of 120 mAh g^{-1} over 400 cycles due to the shortened K-ion diffusion pathway and sufficient space for volume expansion. All these studies proved a good application prospect of Sn, Sb, Ge-based anodes for PIBs. We believe that there is more potency with the Sn, Sb and Ge-based anodes to be used in rechargeable battery devices. The continuous studies on these materials will strongly advance the realization of next-generation, high-performance rechargeable batteries.

Acknowledgements

This research was funded by the National Key R&D Program of China (Grant No. 2016YFB0100100), Natural Science Foundation of China (51702335, 21773279), the CAS-EU S&T cooperation partner program (174433KYSB20150013), and Key Laboratory of Bio-based Polymeric

Materials of Zhejiang Province. S.L. acknowledges the China Scholarship Council (CSC) for funding and Mr. Suijing Shi for help on schematic diagrams. This project received funding from the European Union's Horizon 2020 research and innovation program under the Marie Sklodowska-Curie grant agreement No 655881. P.M-B. acknowledges funding by the International Research Training Group 2022 Alberta/Technical University of Munich International Graduate School for Environmentally Responsible Functional Hybrid Materials (ATUMS).

Conflict of Interest

The authors declare no conflict of interest.

Keywords

antimony, germanium, lithium-ion batteries, nonsilicon anodes, sodium-ion batteries, tin

Received: March 21, 2020
Revised: April 8, 2020
Published online:

[1] C. Choi, D. S. Ashby, D. M. Butts, R. H. DeBlock, Q. Wei, J. Lau, B. Dunn, *Nat. Rev. Mater.* **2019**, 1.
[2] Y. Liu, Y. Zhu, Y. Cui, *Nat. Energy* **2019**, *4*, 540.
[3] G. Harper, R. Sommerville, E. Kendrick, L. Driscoll, P. Slater, R. Stolkin, A. Walton, P. Christensen, O. Heidrich, S. Lambert, A. Abbott, K. Ryder, L. Gaines, P. Anderson, *Nature* **2019**, *575*, 75.
[4] M. Chen, X. Ma, B. Chen, R. Arsenault, P. Karlson, N. Simon, Y. Wang, *Joule* **2019**, *3*, 2622.
[5] E. Pomerantseva, F. Bonaccorso, X. Feng, Y. Cui, Y. Gogotsi, *Science* **2019**, *366*, eaan8285.
[6] Y. Yang, G. Zheng, Y. Cui, *Energy Environ. Sci.* **2013**, *6*, 1552.
[7] H. Pan, Y.-S. Hu, L. Chen, *Energy Environ. Sci.* **2013**, *6*, 2338.
[8] Z. Yang, J. Zhang, M. C. W. Kintner-Meyer, X. Lu, D. Choi, J. P. Lemmon, J. Liu, *Chem. Rev.* **2011**, *111*, 3577.
[9] B. Dunn, H. Kamath, J.-M. Tarascon, *Science* **2011**, *334*, 928.
[10] H. Ibrahim, A. Ilinca, J. Perron, *Renewable Sustainable Energy Rev.* **2008**, *12*, 1221.
[11] V. Etacheri, R. Marom, R. Elazari, G. Salitra, D. Aurbach, *Energy Environ. Sci.* **2011**, *4*, 3243.
[12] M. Winter, B. Barnett, K. Xu, *Chem. Rev.* **2018**, *118*, 11433.
[13] H. Bauman, *Limited-Cycle Secondary Battery Using Lithium Anode*, Lockheed Missiles and Space Co. Inc., Sunnyvale CA **1964**.
[14] H. F. Bauman, *Lithium Anode Limited Cycle Secondary Battery*, Lockheed Missiles and Space Co. Inc., Mechanical And Mathematical Science Lab, Polo Alto CA **1963**.
[15] M. B. Rao, K. R. Hill, *Evaluation of Rechargeable Lithium-Copper Chloride Organic Electrolyte Battery System*, Mallory (PR) And Co. Inc., Lab for Physical Science, Burlington MA **1967**.
[16] N. K. R. Gupta, *Electrochemical Characterization of Systems for Secondary Battery Application Second Quarterly Report, Aug.–Oct. 1966*, National Aeronautics and Space Administration, **1966**.
[17] H. F. Bauman, J. E. Chilton, W. J. Conner, G. M. Cook, *New Cathode-Anode Couples Using Non-Aqueous Electrolyte*, Lockheed Missiles and Space Co. Inc., Sunnyvale CA **1963**.
[18] K. R. R. Hill, *Research and Development of a High Capacity, Non-Aqueous Secondary Battery Final Report, Oct. 1964–Dec. 1965*, National Aeronautics and Space Administration, **1965**.
[19] A. V. Fraioli, W. A. Barber, A. M. Feldman, *US3551205A*, **1970**.
[20] J. R. Moser, *US3660163A*, **1972**.
[21] A. A. Schneider, J. R. Moser, *US3674562A*, **1972**.
[22] M. Hughes, N. A. Hampson, S. A. G. R. Karunathilaka, *J. Power Sources* **1984**, *12*, 83.
[23] M. S. Whittingham, *Science* **1976**, *192*, 1126.
[24] M. S. Whittingham, F. R. Gamble, *Mater. Res. Bull.* **1975**, *10*, 363.
[25] B. M. L. Rao, R. W. Francis, H. A. Christopher, *J. Electrochem. Soc.* **1977**, *124*, 1490.
[26] K. Mizushima, P. C. Jones, P. J. Wiseman, J. B. Goodenough, *Mater. Res. Bull.* **1980**, *15*, 783.
[27] K. Mizushima, P. C. Jones, P. J. Wiseman, J. B. Goodenough, *Solid State Ionics* **1981**, *3-4*, 171.
[28] J. B. Goodenough, K. Mizuchima, *US4302518A*, **1981**.
[29] M. M. Thackeray, W. I. F. David, P. G. Bruce, J. B. Goodenough, *Mater. Res. Bull.* **1983**, *18*, 461.
[30] M. M. Thackeray, P. J. Johnson, L. A. de Picciotto, P. G. Bruce, J. B. Goodenough, *Mater. Res. Bull.* **1984**, *19*, 179.
[31] J. Goodenough, M. Thackeray, W. David, P. Bruce, *Rev. Chim. Miner.* **1984**, *21*, 435.
[32] R. Kanno, Y. Takeda, T. Ichikawa, K. Nakanishi, O. Yamamoto, *J. Power Sources* **1989**, *26*, 535.
[33] M. Mohri, N. Yanagisawa, Y. Tajima, H. Tanaka, T. Mitate, S. Nakajima, M. Yoshida, Y. Yoshimoto, T. Suzuki, H. Wada, *J. Power Sources* **1989**, *26*, 545.
[34] R. Fong, U. von Sacken, J. R. Dahn, *J. Electrochem. Soc.* **1990**, *137*, 2009.
[35] Y. Takasu, M. Shiinoki, Y. Matsuda, *J. Electrochem. Soc.* **1984**, *131*, 959.
[36] A. N. Dey, *J. Electrochem. Soc.* **1985**, *132*, 2290.
[37] J. R. MacCallum, J. S. McKechnie, C. A. Vincent, *Mater. Res. Bull.* **1983**, *18*, 743.
[38] L. W. Shacklette, J. E. Toth, N. S. Murthy, R. H. Baughman, *J. Electrochem. Soc.* **1985**, *132*, 1529.
[39] A. Yoshino, *Angew. Chem., Int. Ed.* **2012**, *51*, 5798.
[40] A. Yoshino, K. Sanechika, T. Nakajima, *US4668595A*, **1987**.
[41] H. Awano, in *Lithium-Ion Batter. Sci. Technol.* (Eds: M. Yoshio, R. J. Brodd, A. Kozawa), Springer New York, New York, NY **2009**, pp. 299–313.
[42] *Nat. Energy* **2019**, *4*, 893, https://www.nature.com/articles/s41560-019-0503-2.
[43] Y.-F. Y. Yao, J. T. Kummer, *J. Inorg. Nucl. Chem.* **1967**, *29*, 2453.
[44] J. Sudworth, A. R. Tiley, *Sodium Sulphur Battery*, Springer Science & Business Media, Berlin **1985**.
[45] T. Oshima, M. Kajita, A. Okuno, *Int. J. Appl. Ceram. Technol.* **2004**, *1*, 269.
[46] R. J. Bones, D. A. Teagle, S. D. Brooker, F. L. Cullen, *J. Electrochem. Soc.* **1989**, *136*, 1274.
[47] C.-H. Dustmann, *J. Power Sources* **2004**, *127*, 85.
[48] N. Yabuuchi, K. Kubota, M. Dahbi, S. Komaba, *Chem. Rev.* **2014**, *114*, 11636.
[49] G. H. Newman, L. P. Klemann, *J. Electrochem. Soc.* **1980**, *127*, 2097.
[50] C. Delmas, J. Braconnier, A. Maazaz, P. Hagenmuller, *Rev. Chim. Miner.* **1982**, *19*, 343.
[51] C. Delmas, J.-J. Braconnier, C. Fouassier, P. Hagenmuller, *Solid State Ionics* **1981**, *3-4*, 165.
[52] K. M. Abraham, *Solid State Ionics.* **1982**, *7*, 199.
[53] P. Ge, M. Fouletier, *Solid State Ionics* **1988**, *28-30*, 1172.
[54] M. M. Doeff, Y. Ma, S. J. Visco, L. C. D. Jonghe, *J. Electrochem. Soc.* **1993**, *140*, L169.
[55] S.-W. Kim, D.-H. Seo, X. Ma, G. Ceder, K. Kang, *Adv. Energy Mater.* **2012**, *2*, 710.
[56] V. Palomares, P. Serras, I. Villaluenga, K. B. Hueso, J. Carretero-González, T. Rojo, *Energy Environ. Sci.* **2012**, *5*, 5884.
[57] M. D. Slater, D. Kim, E. Lee, C. S. Johnson, *Adv. Funct. Mater.* **2013**, *23*, 947.
[58] C. Vaalma, D. Buchholz, M. Weil, S. Passerini, *Nat. Rev. Mater.* **2018**, *3*, 18013.

[59] M. Winter, J. O. Besenhard, M. E. Spahr, P. Novák, *Adv. Mater.* **1998**, *10*, 725.
[60] A. K. Shukla, T. P. Kumar, *Curr. Sci.* **2008**, *94*, 314.
[61] W.-J. Zhang, *J. Power Sources* **2011**, *196*, 13.
[62] V. Aravindan, Y.-S. Lee, S. Madhavi, *Adv. Energy Mater.* **2015**, *5*, 1402225.
[63] C.-M. Park, J.-H. Kim, H. Kim, H.-J. Sohn, *Chem. Soc. Rev.* **2010**, *39*, 3115.
[64] X. Zuo, J. Zhu, P. Müller-Buschbaum, Y.-J. Cheng, *Nano Energy* **2017**, *31*, 113.
[65] J. S. Chen, X. W. (David) Lou, *Small* **2013**, *9*, 1877.
[66] M. V. Reddy, G. V. Subba Rao, B. V. R. Chowdari, *Chem. Rev.* **2013**, *113*, 5364.
[67] M. G. Kim, J. Cho, *Adv. Funct. Mater.* **2009**, *19*, 1497.
[68] L. Ji, Z. Lin, M. Alcoutlabi, X. Zhang, *Energy Environ. Sci.* **2011**, *4*, 2682.
[69] M. He, K. Kravchyk, M. Walter, M. V. Kovalenko, *Nano Lett.* **2014**, *14*, 1255.
[70] J.-Y. Liao, A. Manthiram, *Adv. Energy Mater.* **2014**, *4*, 1400403.
[71] Y. Zhong, X. Li, Y. Zhang, R. Li, M. Cai, X. Sun, *Appl. Surf. Sci.* **2015**, *332*, 192.
[72] L. Wang, S. Kitamura, T. Sonoda, K. Obata, S. Tanase, T. Sakai, *J. Electrochem. Soc.* **2003**, *150*, A1346.
[73] J. Yin, M. Wada, S. Yoshida, K. Ishihara, S. Tanase, T. Sakai, *J. Electrochem. Soc.* **2003**, *150*, A1129.
[74] X. W. Lou, C. M. Li, L. A. Archer, *Adv. Mater.* **2009**, *21*, 2536.
[75] Y. Chen, Q. Z. Huang, J. Wang, Q. Wang, J. M. Xue, *J. Mater. Chem.* **2011**, *21*, 17448.
[76] H. Morito, T. Yamada, T. Ikeda, H. Yamane, *J. Alloys Compd.* **2009**, *480*, 723.
[77] S. Komaba, Y. Matsuura, T. Ishikawa, N. Yabuuchi, W. Murata, S. Kuze, *Electrochem. Commun.* **2012**, *21*, 65.
[78] L. D. Ellis, B. N. Wilkes, T. D. Hatchard, M. N. Obrovac, *J. Electrochem. Soc.* **2014**, *161*, A416.
[79] M. Lao, Y. Zhang, W. Luo, Q. Yan, W. Sun, S. X. Dou, *Adv. Mater.* **2017**, *29*, 1700622.
[80] Q. Wang, C. Zhao, Y. Lu, Y. Li, Y. Zheng, Y. Qi, X. Rong, L. Jiang, X. Qi, Y. Shao, D. Pan, B. Li, Y.-S. Hu, L. Chen, *Small* **2017**, *13*, 1701835.
[81] A. N. Dey, *J. Electrochem. Soc.* **1971**, *118*, 1547.
[82] G. Masing, G. Tammann, *Z. Anorg. Chem.* **1910**, *67*, 183.
[83] C. J. Wen, R. A. Huggins, *J. Solid State Chem.* **1980**, *35*, 376.
[84] J. Wang, I. D. Raistrick, R. A. Huggins, *J. Electrochem. Soc.* **1986**, *133*, 457.
[85] A. Anani, S. Crouch-Baker, R. A. Huggins, *J. Electrochem. Soc.* **1987**, *134*, 3098.
[86] Z. Moser, W. Gasior, F. Sommer, G. Schwitzgebel, B. Predel, *Metall. Trans. B* **1986**, *17*, 791.
[87] O. Mao, R. A. Dunlap, J. R. Dahn, *J. Electrochem. Soc.* **1999**, *146*, 405.
[88] V. L. Chevrier, G. Ceder, *J. Electrochem. Soc.* **2011**, *158*, A1011.
[89] X.-L. Wu, Y.-G. Guo, L.-J. Wan, *Chem. - Asian J.* **2013**, *8*, 1948.
[90] J. Yang, M. Winter, J. O. Besenhard, *Solid State Ionics.* **1996**, *90*, 281.
[91] O. Crosnier, T. Brousse, D. M. Schleich, *Ionics* **1999**, *5*, 311.
[92] K. D. Kepler, J. T. Vaughey, M. M. Thackeray, *Electrochem. Solid-State Lett.* **1999**, *2*, 307.
[93] O. Mao, J. R. Dahn, *J. Electrochem. Soc.* **1999**, *146*, 414.
[94] O. Mao, J. R. Dahn, *J. Electrochem. Soc.* **1999**, *146*, 423.
[95] J. O. Besenhard, J. Yang, M. Winter, *J. Power Sources* **1997**, *68*, 87.
[96] R. Hu, H. Liu, M. Zeng, J. Liu, M. Zhu, *Chin. Sci. Bull.* **2012**, *57*, 4119.
[97] C. Julien, J. P. Pereira-Ramos, A. Momchilov, *New Trends in Intercalation Compounds for Energy Storage*, Springer Science & Business Media, Berlin **2012**.
[98] L. Liu, F. Xie, J. Lyu, T. Zhao, T. Li, B. G. Choi, *J. Power Sources* **2016**, *321*, 11.
[99] J. Yang, M. Wachtler, M. Winter, J. O. Besenhard, *Electrochem. Solid-State Lett.* **1999**, *2*, 161.
[100] I. Rom, M. Wachtler, I. Papst, M. Schmied, J. O. Besenhard, F. Hofer, M. Winter, *Solid State Ionics.* **2001**, *143*, 329.
[101] J. Yang, Y. Takeda, Q. Li, N. Imanishi, O. Yamamoto, *J. Power Sources* **2000**, *90*, 64.
[102] L. Fang, B. V. R. Chowdari, *J. Power Sources* **2001**, *97–98*, 181.
[103] H. Kim, Y.-J. Kim, D. G. Kim, H.-J. Sohn, T. Kang, *Solid State Ionics.* **2001**, *144*, 41.
[104] Y. Xia, T. Sakai, T. Fujieda, M. Wada, H. Yoshinaga, *J. Electrochem. Soc.* **2001**, *148*, A471.
[105] Y. Xia, T. Sakai, T. Fujieda, M. Wada, H. Yoshinaga, *Electrochem. Solid-State Lett.* **2001**, *4*, A9.
[106] W. Pu, X. He, J. Ren, C. Wan, C. Jiang, *Electrochim. Acta* **2005**, *50*, 4140.
[107] C. Arbizzani, M. Lazzari, M. Mastragostino, *J. Electrochem. Soc.* **2005**, *152*, A289.
[108] J. Wolfenstine, S. Campos, D. Foster, J. Read, W. K. Behl, *J. Power Sources* **2002**, *109*, 230.
[109] J. G. Ren, W. H. Pu, X. M. He, C. R. Wan, C. Y. Jiang, *J. Mater. Sci. Technol.* **2005**, *21*, 770.
[110] J. Ren, X. He, C. Jiang, C. Wan, *Acta Metall. Sin.* **2006**, *42*, 727.
[111] K. Wang, X. He, L. Wang, J. Ren, C. Jiang, C. Wan, *J. Electrochem. Soc.* **2006**, *153*, A1859.
[112] T. Sarakonsri, T. Apirattanawan, S. Tungprasurt, T. Tunkasiri, *J. Mater. Sci.* **2006**, *41*, 4749.
[113] N. Tamura, R. Ohshita, M. Fujimoto, S. Fujitani, M. Kamino, I. Yonezu, *J. Power Sources* **2002**, *107*, 48.
[114] H.-C. Shin, M. Liu, *Adv. Funct. Mater.* **2005**, *15*, 582.
[115] N. Tamura, R. Ohshita, M. Fujimoto, M. Kamino, S. Fujitani, *J. Electrochem. Soc.* **2003**, *150*, A679.
[116] J. Hassoun, S. Panero, B. Scrosati, *J. Power Sources* **2006**, *160*, 1336.
[117] X.-Q. Cheng, P.-F. Shi, *J. Alloys Compd.* **2005**, *391*, 241.
[118] J.-H. Ahn, Y.-J. Kim, G. Wang, M. Lindsay, H. K. Liu, S. Dou, *Mater. Trans.* **2002**, *43*, 63.
[119] H.-Y. Lee, S.-W. Jang, S.-M. Lee, S.-J. Lee, H.-K. Baik, *J. Power Sources* **2002**, *112*, 8.
[120] Y.-L. Kim, H.-Y. Lee, S.-W. Jang, S.-J. Lee, H.-K. Baik, Y.-S. Yoon, Y.-S. Park, S.-M. Lee, *Solid State Ionics.* **2003**, *160*, 235.
[121] N. Tamura, M. Fujimoto, M. Kamino, S. Fujitani, *Electrochim. Acta* **2004**, *49*, 1949.
[122] N. Tamura, Y. Kato, A. Mikami, M. Kamino, S. Matsuta, S. Fujitani, *J. Electrochem. Soc.* **2006**, *153*, A2227.
[123] N. Tamura, Y. Kato, A. Mikami, M. Kamino, S. Matsuta, S. Fujitani, *J. Electrochem. Soc.* **2006**, *153*, A1626.
[124] J. Zhang, Y. Xia, *J. Electrochem. Soc.* **2006**, *153*, A1466.
[125] A. V. Trifonova, A. A. Momchilov, B. L. Puresheva, I. Abrahams, *Solid State Ionics.* **2001**, *143*, 319.
[126] M. Wada, J. T. Yin, S. Tanase, T. Sakai, *J. Jpn. Inst. Met.* **2004**, *68*, 46.
[127] J. Yin, M. Wada, S. Tanase, T. Sakai, *J. Electrochem. Soc.* **2004**, *151*, A583.
[128] D. G. Kim, H. Kim, H.-J. Sohn, T. Kang, *J. Power Sources* **2002**, *104*, 221.
[129] H.-C. Shin, J. Dong, M. Liu, *Adv. Mater.* **2003**, *15*, 1610.
[130] Q. F. Dong, C. Z. Wu, M. G. Jin, Z. C. Huang, M. S. Zheng, J. K. You, Z. G. Lin, *Solid State Ionics.* **2004**, *167*, 49.
[131] H. Mukaibo, T. Momma, T. Osaka, *J. Power Sources* **2005**, *146*, 457.
[132] H. Mukaibo, T. Sumi, T. Yokoshima, T. Momma, T. Osaka, *Electrochem. Solid-State Lett.* **2003**, *6*, A218.

[133] J. Yin, M. Wada, S. Tanase, T. Sakai, *J. Electrochem. Soc.* **2004**, *151*, A867.
[134] J. Yin, M. Wada, Y. Kitano, S. Tanase, O. Kajita, T. Sakai, *J. Electrochem. Soc.* **2005**, *152*, A1341.
[135] M. Wada, J. T. Yin, S. Yoshida, K. Ishihara, S. Tanase, T. Sakai, *J. Jpn. Inst. Met.* **2003**, *67*, 424.
[136] G. X. Wang, L. Sun, D. H. Bradhurst, S. X. Dou, H. K. Liu, *J. Alloys Compd.* **2000**, *299*, L12.
[137] E. Rönnebro, J. Yin, A. Kitano, M. Wada, S. Tanase, T. Sakai, *J. Electrochem. Soc.* **2005**, *152*, A152.
[138] A. Finke, P. Poizot, C. Guéry, J.-M. Tarascon, *J. Electrochem. Soc.* **2005**, *152*, A2364.
[139] H. Mukaibo, T. Momma, M. Mohamedi, T. Osaka, *J. Electrochem. Soc.* **2005**, *152*, A560.
[140] A. Bonakdarpour, K. C. Hewitt, R. L. Turner, J. R. Dahn, *J. Electrochem. Soc.* **2004**, *151*, A470.
[141] J. Xie, G. S. Cao, X. B. Zhao, Y. D. Zhong, M. J. Zhao, *J. Electrochem. Soc.* **2004**, *151*, A1905.
[142] X.-L. Wang, W.-Q. Han, J. Chen, J. Graetz, *ACS Appl. Mater. Interfaces* **2010**, *2*, 1548.
[143] J. Ren, X. He, L. Wang, W. Pu, C. Jiang, C. Wan, *Electrochim. Acta* **2007**, *52*, 2447.
[144] Z. Du, S. Zhang, Y. Xing, X. Wu, *J. Power Sources* **2011**, *196*, 9780.
[145] C. Yang, D. Zhang, Y. Zhao, Y. Lu, L. Wang, J. B. Goodenough, *J. Power Sources* **2011**, *196*, 10673.
[146] M. Tian, W. Wang, S.-H. Lee, Y.-C. Lee, R. Yang, *J. Power Sources* **2011**, *196*, 10207.
[147] S. Zhang, Z. Du, R. Lin, T. Jiang, G. Liu, X. Wu, D. Weng, *Adv. Mater.* **2010**, *22*, 5378.
[148] Z. Du, S. Zhang, *J. Phys. Chem. C* **2011**, *115*, 23603.
[149] M. G. Kim, S. Sim, J. Cho, *Adv. Mater.* **2010**, *22*, 5154.
[150] S.-W. Woo, N. Okada, M. Kotobuki, K. Sasajima, H. Munakata, K. Kajihara, K. Kanamura, *Electrochim. Acta* **2010**, *55*, 8030.
[151] S. Chen, P. Chen, M. Wu, D. Pan, Y. Wang, *Electrochem. Commun.* **2010**, *12*, 1302.
[152] S. Stølen, F. Grønvold, *J. Chem. Thermodyn.* **1999**, *31*, 379.
[153] J. Yang, Y. Takeda, N. Imanishi, J. Y. Xie, O. Yamamoto, *Solid State Ionics.* **2000**, *133*, 189.
[154] L. Simonin, U. Lafont, E. M. Kelder, *J. Power Sources* **2008**, *180*, 859.
[155] R. Z. Hu, Y. Zhang, M. Zhu, *Electrochim. Acta* **2008**, *53*, 3377.
[156] L. Huang, H.-B. Wei, F.-S. Ke, X.-Y. Fan, J.-T. Li, S.-G. Sun, *Electrochim. Acta* **2009**, *54*, 2693.
[157] L. Trahey, J. T. Vaughey, H. H. Kung, M. M. Thackeray, *J. Electrochem. Soc.* **2009**, *156*, A385.
[158] L.-J. Xue, Y.-F. Xu, L. Huang, F.-S. Ke, Y. He, Y.-X. Wang, G.-Z. Wei, J.-T. Li, S.-G. Sun, *Electrochim. Acta* **2011**, *56*, 5979.
[159] L. Xue, Z. Fu, Y. Yao, T. Huang, A. Yu, *Electrochim. Acta* **2010**, *55*, 7310.
[160] F.-S. Ke, L. Huang, J.-S. Cai, S.-G. Sun, *Electrochim. Acta* **2007**, *52*, 6741.
[161] F.-S. Ke, L. Huang, H.-B. Wei, J.-S. Cai, X.-Y. Fan, F.-Z. Yang, S.-G. Sun, *J. Power Sources* **2007**, *170*, 450.
[162] Y. Liu, J. Y. Xie, J. Yang, *J. Power Sources* **2003**, *119–121*, 572.
[163] A. Ulus, Y. Rosenberg, L. Burstein, E. Peled, *J. Electrochem. Soc.* **2002**, *149*, A635.
[164] W. Cui, F. Wang, J. Wang, H. Liu, C. Wang, Y. Xia, *J. Power Sources* **2011**, *196*, 3633.
[165] S. Liu, Q. Li, Y. Chen, F. Zhang, *J. Alloys Compd.* **2009**, *478*, 694.
[166] W. Cui, F. Li, H. Liu, C. Wang, Y. Xia, *J. Mater. Chem.* **2009**, *19*, 7202.
[167] C.-M. Park, K.-J. Jeon, *Chem. Commun.* **2011**, *47*, 2122.
[168] F. Nacimiento, R. Alcántara, J. L. Tirado, *J. Electrochem. Soc.* **2010**, *157*, A666.
[169] Y. Kwon, H. Kim, S.-G. Doo, J. Cho, *Chem. Mater.* **2007**, *19*, 982.
[170] J. Hassoun, G. Derrien, S. Panero, B. Scrosati, *Electrochim. Acta* **2009**, *54*, 4441.
[171] N. Jayaprakash, N. Kalaiselvi, C. H. Doh, *J. Appl. Electrochem.* **2007**, *37*, 567.
[172] Z. Wang, W. Tian, X. Liu, R. Yang, X. Li, *J. Solid State Chem.* **2007**, *180*, 3360.
[173] J.-H. Jeong, D.-W. Jung, B.-S. Kong, J. Lee, E.-S. Oh, *J. Ceram. Process. Res.* **2011**, *12*, S105.
[174] T. Huang, Y. Yao, Z. Wei, Z. Liu, A. Yu, *Electrochim. Acta* **2010**, *56*, 476.
[175] C. Zhai, N. Du, H. Zhang, J. Yu, P. Wu, C. Xiao, D. Yang, *Nanoscale* **2011**, *3*, 1798.
[176] M.-S. Park, S. A. Needham, G.-X. Wang, Y.-M. Kang, J.-S. Park, S.-X. Dou, H.-K. Liu, *Chem. Mater.* **2007**, *19*, 2406.
[177] H.-R. Jung, W.-J. Lee, *J. Electrochem. Soc.* **2011**, *158*, A644.
[178] L. Huang, J.-S. Cai, Y. He, F.-S. Ke, S.-G. Sun, *Electrochem. Commun.* **2009**, *11*, 950.
[179] G. Derrien, J. Hassoun, S. Panero, B. Scrosati, *Adv. Mater.* **2007**, *19*, 2336.
[180] K. S. Novoselov, A. K. Geim, S. V. Morozov, D. Jiang, Y. Zhang, S. V. Dubonos, I. V. Grigorieva, A. A. Firsov, *Science* **2004**, *306*, 666.
[181] K. S. Novoselov, A. K. Geim, S. V. Morozov, D. Jiang, M. I. Katsnelson, I. V. Grigorieva, S. V. Dubonos, A. A. Firsov, *Nature* **2005**, *438*, 197.
[182] F. Akbar, M. Kolahdouz, Sh. Larimian, B. Radfar, H. H. Radamson, *J. Mater. Sci.: Mater. Electron.* **2015**, *26*, 4347.
[183] M. Liang, B. Luo, L. Zhi, *Int. J. Energy Res.* **2009**, *33*, 1161.
[184] P. Lian, X. Zhu, S. Liang, Z. Li, W. Yang, H. Wang, *Electrochim. Acta* **2010**, *55*, 3909.
[185] B. Wang, X.-L. Wu, C.-Y. Shu, Y.-G. Guo, C.-R. Wang, *J. Mater. Chem.* **2010**, *20*, 10661.
[186] L. Ji, A. J. Medford, X. Zhang, *J. Mater. Chem.* **2009**, *19*, 5593.
[187] Z. Lin, L. Ji, M. D. Woodroof, X. Zhang, *J. Power Sources* **2010**, *195*, 5025.
[188] E. Frackowiak, S. Gautier, H. Gaucher, S. Bonnamy, F. Beguin, *Carbon* **1999**, *37*, 61.
[189] B. Gao, A. Kleinhammes, X. P. Tang, C. Bower, L. Fleming, Y. Wu, O. Zhou, *Chem. Phys. Lett.* **1999**, *307*, 153.
[190] G. T. Wu, C. S. Wang, X. B. Zhang, H. S. Yang, Z. F. Qi, P. M. He, W. Z. Li, *J. Electrochem. Soc.* **1999**, *146*, 1696.
[191] X.-Y. Fan, Q.-C. Zhuang, G.-Z. Wei, L. Huang, Q.-F. Dong, S.-G. Sun, *J. Appl. Electrochem.* **2009**, *39*, 1323.
[192] K. Ui, S. Kikuchi, Y. Jimba, N. Kumagai, *J. Power Sources* **2011**, *196*, 3916.
[193] H. Groult, H. El Ghallali, A. Barhoun, E. Briot, L. Perrigaud, S. Hernandorena, F. Lantelme, *Electrochim. Acta* **2010**, *55*, 1926.
[194] H. Zhao, C. Yin, H. Guo, J. He, W. Qiu, Y. Li, *J. Power Sources* **2007**, *174*, 916.
[195] H. Groult, H. El Ghallali, A. Barhoun, E. Briot, C. M. Julien, F. Lantelme, S. Borensztjan, *Electrochim. Acta* **2011**, *56*, 2656.
[196] R. Zhang, M. S. Whittingham, *Electrochem. Solid-State Lett.* **2010**, *13*, A184.
[197] J.-T. Li, S.-R. Chen, F.-S. Ke, G.-Z. Wei, L. Huang, S.-G. Sun, *J. Electroanal. Chem.* **2010**, *649*, 171.
[198] X. H. Hou, S. J. Hu, H. W. Yu, L. Z. Zhao, Q. Ru, C. L. Tan, W. S. Li, *Mater. Sci. Forum* **2009**, *610–613*, 506.
[199] S.-I. Lee, S. Yoon, C.-M. Park, J.-M. Lee, H. Kim, D. Im, S.-G. Doo, H.-J. Sohn, *Electrochim. Acta* **2008**, *54*, 364.
[200] J.-T. Li, J. Swiatowska, A. Seyeux, L. Huang, V. Maurice, S.-G. Sun, P. Marcus, *J. Power Sources* **2010**, *195*, 8251.
[201] R. Hu, Q. Shi, H. Wang, M. Zeng, M. Zhu, *J. Phys. Chem. C* **2009**, *113*, 18953.
[202] R. Z. Hu, L. Zhang, X. Liu, M. Q. Zeng, M. Zhu, *Electrochem. Commun.* **2008**, *10*, 1109.
[203] R. Hu, M. Zeng, C. Y. V. Li, M. Zhu, *J. Power Sources* **2009**, *188*, 268.

[204] M. Tian, W. Wang, Y. Wei, R. Yang, *J. Power Sources* **2012**, *211*, 46.
[205] H. Zhang, T. Shi, D. J. Wetzel, R. G. Nuzzo, P. V. Braun, *Adv. Mater.* **2016**, *28*, 742.
[206] X. Yu, Y.-J. Lee, R. Furstenberg, J. O. White, P. V. Braun, *Adv. Mater.* **2007**, *19*, 1689.
[207] H. Zhang, X. Yu, P. V. Braun, *Nat. Nanotechnol.* **2011**, *6*, 277.
[208] H. Zhang, P. V. Braun, *Nano Lett.* **2012**, *12*, 2778.
[209] J. H. Pikul, H. G. Zhang, J. Cho, P. V. Braun, W. P. King, *Nat. Commun.* **2013**, *4*, 1732.
[210] L. M. Qi, J. Li, J. M. Ma, *Adv. Mater.* **2002**, *14*, 300.
[211] J. Yu, H. Guo, S. A. Davis, S. Mann, *Adv. Funct. Mater.* **2006**, *16*, 2035.
[212] M.-H. Park, Y. Cho, K. Kim, J. Kim, M. Liu, J. Cho, *Angew. Chem., Int. Ed.* **2011**, *50*, 9647.
[213] X. Y. Gao, J. S. Zhang, L. Zhang, *Adv. Mater.* **2002**, *14*, 290.
[214] Y. Tang, L. Yang, S. Fang, Z. Qiu, *Electrochim. Acta* **2009**, *54*, 6244.
[215] J. Ye, H. Zhang, R. Yang, X. Li, L. Qi, *Small* **2010**, *6*, 296.
[216] F. Caruso, R. A. Caruso, H. Möhwald, *Science* **1998**, *282*, 1111.
[217] H. Ma, F. Cheng, J. Chen, J. Zhao, C. Li, Z. Tao, J. Liang, *Adv. Mater.* **2007**, *19*, 4067.
[218] K. P. Velikov, A. van Blaaderen, *Langmuir* **2001**, *17*, 4779.
[219] H. Chun Zeng, *J. Mater. Chem.* **2006**, *16*, 649.
[220] Q. Peng, X.-Y. Sun, J. C. Spagnola, C. Saquing, S. A. Khan, R. J. Spontak, G. N. Parsons, *ACS Nano* **2009**, *3*, 546.
[221] A. V. Evteev, E. V. Levchenko, I. V. Belova, G. E. Murch, *J. Nano Res.* **2009**, *7*, 11.
[222] W. Wang, M. Dahl, Y. Yin, *Chem. Mater.* **2013**, *25*, 1179.
[223] G. D. Park, Y. C. Kang, *Small* **2018**, *14*, 1703957.
[224] S. Wang, M. He, M. Walter, F. Krumeich, K. V. Kravchyk, M. V. Kovalenko, *Nanoscale* **2018**, *10*, 6827.
[225] M. He, M. Walter, K. V. Kravchyk, R. Erni, R. Widmer, M. V. Kovalenko, *Nanoscale* **2015**, *7*, 455.
[226] M. V. Kovalenko, H. Meng, K. Kravchyk, M. Walter, *US20150147650A1*, **2015**.
[227] M. V. Kovalenko, H. Meng, K. Kravchyk, M. Walter, *US20170155140A1*, **2017**.
[228] M. V. Kovalenko, M. Walter, *EP3124137A1*, **2017**.
[229] M. V. Kovalenko, M. Bodarchuk, K. kravchyk, *WO2014083135A1*, **2014**.
[230] M. Walter, S. Doswald, M. V. Kovalenko, *J. Mater. Chem. A* **2016**, *4*, 7053.
[231] M. He, L. Protesescu, R. Caputo, F. Krumeich, M. V. Kovalenko, *Chem. Mater.* **2015**, *27*, 635.
[232] X.-Y. Fan, Y.-X. Shi, J.-J. Wang, J. Wang, X.-Y. Shi, L. Xu, L. Gou, D.-L. Li, *Solid State Ionics.* **2013**, *237*, 1.
[233] D.-H. Nam, R.-H. Kim, C.-L. Lee, H.-S. Kwon, *J. Electrochem. Soc.* **2012**, *159*, A1822.
[234] S. Sengupta, A. Patra, A. Mitra, S. Jena, K. Das, S. B. Majumder, S. Das, *Appl. Surf. Sci.* **2018**, *441*, 965.
[235] X. Dong, W. Liu, X. Chen, J. Yan, N. Li, S. Shi, S. Zhang, X. Yang, *Chem. Eng. J.* **2018**, *350*, 791.
[236] C. Tan, G. Qi, Y. Li, J. Guo, X. Wang, D. Kong, H. Wang, S. Zhang, *Int. J. Electrochem. Sci.* **2013**, *8*, 1966.
[237] F.-S. Ke, L. Huang, L. Jamison, L.-J. Xue, G.-Z. Wei, J.-T. Li, X.-D. Zhou, S.-G. Sun, *Nano Energy* **2013**, *2*, 595.
[238] H.-C. Shin, M. Liu, *Chem. Mater.* **2004**, *16*, 5460.
[239] R. Li, X. Sun, X. Zhou, M. Cai, X. Sun, *J. Phys. Chem. C* **2007**, *111*, 9130.
[240] Y. Wang, H. C. Zeng, J. Y. Lee, *Adv. Mater.* **2006**, *18*, 645.
[241] Y. Wang, M. Wu, Z. Jiao, J. Y. Lee, *Chem. Mater.* **2009**, *21*, 3210.
[242] H. Peng, R. Li, J. Hu, W. Deng, F. Pan, *ACS Appl. Mater. Interfaces* **2016**, *8*, 12221.
[243] A. Birrozzi, F. Maroni, R. Raccichini, R. Tossici, R. Marassi, F. Nobili, *J. Power Sources* **2015**, *294*, 248.
[244] H. Zhang, M. Zhang, M. Zhang, L. Zhang, A. Zhang, Y. Zhou, P. Wu, Y. Tang, *J. Colloid Interface Sci.* **2017**, *501*, 267.
[245] C. Wu, J. Maier, Y. Yu, *Adv. Funct. Mater.* **2015**, *25*, 3488.
[246] X. Chen, Q. Ru, Z. Wang, X. Hou, S. Hu, *Mater. Lett.* **2017**, *191*, 218.
[247] H. Yang, L. Li, *J. Alloys Compd.* **2014**, *584*, 76.
[248] H. Shi, Z. Fang, X. Zhang, F. Li, Y. Tang, Y. Zhou, P. Wu, G. Yu, *Nano Lett.* **2018**, *18*, 3193.
[249] X. Li, Y. Zhong, M. Cai, M. P. Balogh, D. Wang, Y. Zhang, R. Li, X. Sun, *Electrochim. Acta* **2013**, *89*, 387.
[250] C. Suryanarayana, *Prog. Mater. Sci.* **2001**, *46*, 1.
[251] M.-G. Park, D.-H. Lee, H. Jung, J.-H. Choi, C.-M. Park, *ACS Nano* **2018**, *12*, 2955.
[252] X.-M. Zheng, L. Huang, Y. Xiao, H. Su, G. Xu, F. Fu, J.-T. Li, S.-G. Sun, *Chem. Commun.* **2012**, *48*, 6854.
[253] X.-M. Zheng, Y. Xiao, L. Huang, F.-S. Ke, Y. He, J.-T. Li, G.-Z. Wei, S.-G. Sun, *Electrochem. Commun.* **2009**, *11*, 1803.
[254] X.-M. Zheng, P.-Y. Zhang, L.-K. Wang, S. Tao, Y.-X. Wang, L. Huang, J.-T. Li, S.-G. Sun, *Electrochim. Acta* **2017**, *247*, 314.
[255] Y.-X. Wang, L. Huang, Y.-Q. Chang, F.-S. Ke, J.-T. Li, S.-G. Sun, *Electrochem. Commun.* **2010**, *12*, 1226.
[256] M. Fehse, A. Darwiche, M. T. Sougrati, E. M. Kelder, A. V. Chadwick, M. Alfredsson, L. Monconduit, L. Stievano, *Chem. Mater.* **2017**, *29*, 10446.
[257] P. Antitomaso, B. Fraisse, L. Stievano, S. Biscaglia, D. Ayme-Perrot, P. Girard, M. T. Sougrati, L. Monconduit, *J. Mater. Chem. A* **2017**, *5*, 6546.
[258] J. Song Chen, L. A. Archer, X. W. (David) Lou, *J. Mater. Chem.* **2011**, *21*, 9912.
[259] K. Sakaushi, Y. Oaki, H. Uchiyama, E. Hosono, H. Zhou, H. Imai, *Small* **2010**, *6*, 776.
[260] Y. J. Chen, X. Y. Xue, Y. G. Wang, T. H. Wang, *Appl. Phys. Lett.* **2005**, *87*, 233503.
[261] L. Li, J. Huang, T. Wang, H. Zhang, Y. Liu, J. Li, *Biosens. Bioelectron.* **2010**, *25*, 2436.
[262] Y. Idota, M. Mishima, Y. Miyaki, T. Kubota, T. Miyasaka, *US5780181A*, **1998**.
[263] Y. Idota, T. Kubota, A. Matsufuji, Y. Maekawa, T. Miyasaka, *Science* **1997**, *276*, 1395.
[264] S. Kirklin, B. Meredig, C. Wolverton, *Adv. Energy Mater.* **2013**, *3*, 252.
[265] I. A. Courtney, J. R. Dahn, *J. Electrochem. Soc.* **1997**, *144*, 2943.
[266] I. A. Courtney, J. R. Dahn, *J. Electrochem. Soc.* **1997**, *144*, 2045.
[267] N. Li, C. R. Martin, *J. Electrochem. Soc.* **2001**, *148*, A164.
[268] N. Li, C. R. Martin, B. Scrosati, *Electrochem. Solid-State Lett.* **1999**, *3*, 316.
[269] N. Li, C. R. Martin, B. Scrosati, *J. Power Sources* **2001**, *97–98*, 240.
[270] H. Kim, J. Cho, *J. Mater. Chem.* **2008**, *18*, 771.
[271] Y.-D. Ko, J.-G. Kang, J.-G. Park, S. Lee, D.-W. Kim, *Nanotechnology* **2009**, *20*, 455701.
[272] J. Liu, Y. Li, X. Huang, R. Ding, Y. Hu, J. Jiang, L. Liao, *J. Mater. Chem.* **2009**, *19*, 1859.
[273] P. Meduri, C. Pendyala, V. Kumar, G. U. Sumanasekera, M. K. Sunkara, *Nano Lett.* **2009**, *9*, 612.
[274] Z. Ying, Q. Wan, H. Cao, Z. T. Song, S. L. Feng, *Appl. Phys. Lett.* **2005**, *87*, 113108.
[275] D. Deng, J. Y. Lee, *Chem. Mater.* **2008**, *20*, 1841.
[276] Y. Liu, J. Dong, M. Liu, *Adv. Mater.* **2004**, *16*, 353.
[277] X. W. Lou, Y. Wang, C. Yuan, J. Y. Lee, L. A. Archer, *Adv. Mater.* **2006**, *18*, 2325.
[278] H. G. Yang, H. C. Zeng, *Angew. Chem., Int. Ed.* **2004**, *43*, 5930.
[279] Z. Ping Guo, G. Dong Du, Y. Nuli, M. Faiz Hassan, H. Kun Liu, *J. Mater. Chem.* **2009**, *19*, 3253.
[280] R. Zhang, J. Y. Lee, Z. L. Liu, *J. Power Sources* **2002**, *112*, 596.
[281] Y. Wang, J. Yang Lee, *Electrochem. Commun.* **2003**, *5*, 292.

[282] Y. Wang, J. Y. Lee, B.-H. Chen, *Electrochem. Solid-State Lett.* **2003**, *6*, A19.
[283] Y. Wang, J. Y. Lee, *J. Power Sources* **2005**, *144*, 220.
[284] J. C. Meyer, A. K. Geim, M. I. Katsnelson, K. S. Novoselov, T. J. Booth, S. Roth, *Nature* **2007**, *446*, 60.
[285] X. Li, X. Wang, L. Zhang, S. Lee, H. Dai, *Science* **2008**, *319*, 1229.
[286] X. Li, G. Zhang, X. Bai, X. Sun, X. Wang, E. Wang, H. Dai, *Nat. Nanotechnol.* **2008**, *3*, 538.
[287] F. Li, J. Song, H. Yang, S. Gan, Q. Zhang, D. Han, A. Ivaska, L. Niu, *Nanotechnology* **2009**, *20*, 455602.
[288] S.-M. Paek, E. Yoo, I. Honma, *Nano Lett.* **2009**, *9*, 72.
[289] J. Yao, X. Shen, B. Wang, H. Liu, G. Wang, *Electrochem. Commun.* **2009**, *11*, 1849.
[290] G. Chen, Z. Wang, D. Xia, *Chem. Mater.* **2008**, *20*, 6951.
[291] N. Du, H. Zhang, B. Chen, X. Ma, X. Huang, J. Tu, D. Yang, *Mater. Res. Bull.* **2009**, *44*, 211.
[292] Y. Fu, R. Ma, Y. Shu, Z. Cao, X. Ma, *Mater. Lett.* **2009**, *63*, 1946.
[293] Z. Wen, Q. Wang, Q. Zhang, J. Li, *Adv. Funct. Mater.* **2007**, *17*, 2772.
[294] J. Xie, V. K. Varadan, *Mater. Chem. Phys.* **2005**, *91*, 274.
[295] H.-X. Zhang, C. Feng, Y.-C. Zhai, K.-L. Jiang, Q.-Q. Li, S.-S. Fan, *Adv. Mater.* **2009**, *21*, 2299.
[296] M. H. Chen, Z. C. Huang, G. T. Wu, G. M. Zhu, J. K. You, Z. G. Lin, *Mater. Res. Bull.* **2003**, *38*, 831.
[297] J. Bao, C. Tie, Z. Xu, Z. Suo, Q. Zhou, J. Hong, *Adv. Mater.* **2002**, *14*, 1483.
[298] J. Bao, K. Wang, Z. Xu, H. Zhang, Z. Lu, *Chem. Commun.* **2003**, *0*, 208.
[299] K. Kim, S. H. Lee, W. Yi, J. Kim, J. W. Choi, Y. Park, J.-I. Jin, *Adv. Mater.* **2003**, *15*, 1618.
[300] Z. Liu, Y. Bando, M. Mitome, J. Zhan, *Phys. Rev. Lett.* **2004**, *93*, 095504.
[301] L. Zhao, L. Gao, *Carbon* **2004**, *42*, 3269.
[302] Z. Zhu, D. Su, G. Weinberg, R. E. Jentoft, R. Schlögl, *Small* **2005**, *1*, 107.
[303] X. Zhou, L. Yu, X. Wen (David) Lou, *Nanoscale* **2016**, *8*, 8384.
[304] Z. Wang, D. Luan, F. Y. C. Boey, X. W. (David) Lou, *J. Am. Chem. Soc.* **2011**, *133*, 4738.
[305] Z. Wang, Z. C. Wang, S. Madhavi, X. W. (David) Lou, *Chem. - Eur. J.* **2012**, *18*, 7561.
[306] Z. Wang, L. Zhou, X. W. (David) Lou, *Adv. Mater.* **2012**, *24*, 1903.
[307] J. S. Cho, Y. C. Kang, *Small* **2015**, *11*, 4673.
[308] G. Dae Park, J. Hwa Kim, Y. Chan Kang, *Nanoscale* **2018**, *10*, 13531.
[309] L.-S. Zhang, L.-Y. Jiang, H.-J. Yan, W. D. Wang, W. Wang, W.-G. Song, Y.-G. Guo, L.-J. Wan, *J. Mater. Chem.* **2010**, *20*, 5462.
[310] L.-S. Zhong, J.-S. Hu, Z.-M. Cui, L.-J. Wan, W.-G. Song, *Chem. Mater.* **2007**, *19*, 4557.
[311] X. Sui, X. Huang, Y. Wu, R. Ren, H. Pu, J. Chang, G. Zhou, S. Mao, J. Chen, *ACS Appl. Mater. Interfaces* **2018**, *10*, 26170.
[312] Z. Wang, D. Song, J. Si, Y. Jiang, Y. Yang, Y. Jiang, S. Huang, Z. Chen, B. Zhao, *Electrochim. Acta* **2018**, *292*, 72.
[313] W. Yao, S. Wu, L. Zhan, Y. Wang, *Chem. Eng. J.* **2019**, *361*, 329.
[314] B. Zhao, Z. Wang, S. Wang, J. Jiang, J. Si, S. Huang, Z. Chen, W. Li, Y. Jiang, *Nanoscale* **2018**, *10*, 16116.
[315] B. Luo, L. Zhi, *Energy Environ. Sci.* **2015**, *8*, 456.
[316] Y. Li, H. Zhang, P. Kang Shen, *Nano Energy* **2015**, *13*, 563.
[317] Y. Li, Z. Li, P. K. Shen, *Adv. Mater.* **2013**, *25*, 2474.
[318] D. Ahn, X. Xiao, Y. Li, A. K. Sachdev, H. W. Park, A. Yu, Z. Chen, *J. Power Sources* **2012**, *212*, 66.
[319] Z. Liu, R. Guo, M. Zheng, F. Li, B. Wang, T. Li, Y. Luo, *Ceram. Int.* **2018**, *44*, 11757.
[320] J. Zhang, Z. Ma, W. Jiang, Y. Zou, Y. Wang, C. Lu, *J. Electroanal. Chem.* **2016**, *767*, 49.
[321] N. H. Zhao, L. C. Yang, P. Zhang, G. J. Wang, B. Wang, B. D. Yao, Y. P. Wu, *Mater. Lett.* **2010**, *64*, 972.
[322] C. A. Bonino, L. Ji, Z. Lin, O. Toprakci, X. Zhang, S. A. Khan, *ACS Appl. Mater. Interfaces* **2011**, *3*, 2534.
[323] L. Ji, Z. Lin, B. Guo, A. J. Medford, X. Zhang, *Chem. - Eur. J.* **2010**, *16*, 11543.
[324] J. Kong, Z. Liu, Z. Yang, H. Ru Tan, S. Xiong, S. Yee Wong, X. Li, X. Lu, *Nanoscale* **2012**, *4*, 525.
[325] B. Cao, Z. Liu, C. Xu, J. Huang, H. Fang, Y. Chen, *J. Power Sources* **2019**, *414*, 233.
[326] X. Chen, K. Kierzek, K. Wilgosz, J. Machnikowski, J. Gong, J. Feng, T. Tang, R. J. Kalenczuk, H. Chen, P. K. Chu, E. Mijowska, *J. Power Sources* **2012**, *216*, 475.
[327] S. Ding, D. Zhang, H. Bin Wu, Z. Zhang, X. W. (David) Lou, *Nanoscale* **2012**, *4*, 3651.
[328] H. Zhang, L. Li, Z. Li, W. Zhong, H. Liao, Z. Li, *Appl. Surf. Sci.* **2018**, *442*, 65.
[329] G. F. Ortiz, I. Hanzu, P. Lavela, P. Knauth, J. L. Tirado, T. Djenizian, *Chem. Mater.* **2010**, *22*, 1926.
[330] D. Wexler, Z. Guo, H.-K. Liu, G. Du, P. Zhang, Y. Li, M. Chen, *Faculty of Health and Behavioural Sciences – Papers (Archive)* **2010**, 5689.
[331] X.-Y. Xue, B. He, S. Yuan, L.-L. Xing, Z.-H. Chen, C. Ma, *Nanotechnology* **2011**, *22*, 395702.
[332] J. Zhu, G. Zhang, S. Gu, B. Lu, *Electrochim. Acta* **2014**, *150*, 308.
[333] D. Qi, H. Chu, K. Wang, X. Li, J. Huang, *ChemistrySelect* **2018**, *3*, 12469.
[334] H. Yang, H. Wu, K. Zhang, Y. Chen, M. Lu, S. Lin, *J. Nanosci. Nanotechnol.* **2018**, *18*, 7811.
[335] Y. Ding, B. Liu, J. Zou, H. Liu, T. Xin, L. Xia, Y. Wang, *Mater. Res. Bull.* **2018**, *106*, 7.
[336] T. Li, T. Xin, Y. Ding, J. Zou, H. Liu, B. Liu, Y. Wang, *J. Solid State Electrochem.* **2019**, *23*, 379.
[337] Y.-S. Hu, L. Kienle, Y.-G. Guo, J. Maier, *Adv. Mater.* **2006**, *18*, 1421.
[338] L. Kavan, M. Kalbáč, M. Zukalová, I. Exnar, V. Lorenzen, R. Nesper, M. Graetzel, *Chem. Mater.* **2004**, *16*, 477.
[339] T. Momma, N. Shiraishi, A. Yoshizawa, T. Osaka, A. Gedanken, J. Zhu, L. Sominski, *J. Power Sources* **2001**, *97-98*, 198.
[340] M. Nagayama, T. Morita, H. Ikuta, M. Wakihara, M. Takano, S. Kawasaki, *Solid State Ionics.* **1998**, *106*, 33.
[341] B. León, J. I. Corredor, J. L. Tirado, C. Pérez-Vicente, *J. Electrochem. Soc.* **2006**, *153*, A1829.
[342] J. Yang Lee, Y. Xiao, Z. Liu, *Solid State Ionics.* **2000**, *133*, 25.
[343] Y.-U. Kim, C. K. Lee, H.-J. Sohn, T. Kang, *J. Electrochem. Soc.* **2004**, *151*, A933.
[344] Y. Li, J. P. Tu, H. M. Wu, Y. F. Yuan, D. Q. Shi, *Mater. Sci. Eng., B* **2006**, *128*, 75.
[345] A. Y. Shenouda, H. K. Liu, *J. Power Sources* **2008**, *185*, 1386.
[346] Y. W. Xiao, J. Y. Lee, A. S. Yu, Z. L. Liu, *J. Electrochem. Soc.* **1999**, *146*, 3623.
[347] R. Alcántara, J. L. Tirado, J. C. Jumas, L. Monconduit, J. Olivier-Fourcade, *J. Power Sources* **2002**, *109*, 308.
[348] D. C. C. Silva, O. Crosnier, G. Ouvrard, J. Greedan, A. Safa-Sefat, L. F. Nazar, *Electrochem. Solid-State Lett.* **2003**, *6*, A162.
[349] D. C. S. Souza, V. Pralong, A. J. Jacobson, L. F. Nazar, *Science* **2002**, *296*, 2012.
[350] S. Lee, J. Cho, *Chem. Commun.* **2010**, *46*, 2444.
[351] P. Wu, N. Du, H. Zhang, J. Liu, L. Chang, L. Wang, D. Yang, J.-Z. Jiang, *Nanoscale* **2012**, *4*, 4002.
[352] J. Lu, C. Nan, L. Li, Q. Peng, Y. Li, *Nano Res.* **2013**, *6*, 55.
[353] S. Liu, H. Zhang, L. Xu, L. Ma, *J. Cryst. Growth* **2016**, *438*, 31.
[354] Y. Ding, Z.-F. Li, E. V. Timofeeva, C. U. Segre, *Adv. Energy Mater.* **2018**, *8*, 1702134.
[355] Y. Fang, X. Xu, Y. Du, X. Zhu, X. Zhou, J. Bao, *J. Mater. Chem. A* **2018**, *6*, 11244.
[356] X. Jin, H. Huang, A. Wu, S. Gao, M. Lei, J. Zhao, X. Gao, G. Cao, *ACS Nano* **2018**, *12*, 8037.

[357] Q. Liu, J. Ye, Z. Chen, Q. Hao, C. Xu, J. Hou, *J. Colloid Interface Sci.* **2019**, *537*, 588.
[358] J. Choi, W.-S. Kim, K.-H. Kim, S.-H. Hong, *J. Mater. Chem. A* **2018**, *6*, 17437.
[359] J. Hassoun, G. Derrien, S. Panero, B. Scrosati, *Adv. Mater.* **2008**, *20*, 3169.
[360] X. Li, A. Dhanabalan, L. Gu, C. Wang, *Adv. Energy Mater.* **2012**, *2*, 238.
[361] Y. Yu, L. Gu, C. Wang, A. Dhanabalan, P. A. van Aken, J. Maier, *Angew. Chem., Int. Ed.* **2009**, *48*, 6485.
[362] Y. Yu, L. Gu, C. Zhu, P. A. van Aken, J. Maier, *J. Am. Chem. Soc.* **2009**, *131*, 15984.
[363] R. Alcántara, P. Lavela, G. F. Ortiz, J. L. Tirado, R. Stoyanova, E. Zhecheva, C. Merino, *Carbon* **2004**, *42*, 2153.
[364] L. Balan, J. Ghanbaja, P. Willmann, D. Billaud, *Carbon* **2005**, *43*, 2311.
[365] Á. Caballero, J. Morales, L. Sánchez, *Electrochem. Solid-State Lett.* **2005**, *8*, A464.
[366] M. Egashira, H. Takatsuji, S. Okada, J. Yamaki, *J. Power Sources* **2002**, *107*, 56.
[367] I. Grigoriants, A. Soffer, G. Salitra, D. Aurbach, *J. Power Sources* **2005**, *146*, 185.
[368] I. Grigoriants, L. Sominski, H. Li, I. Ifargan, D. Aurbach, A. Gedanken, *Chem. Commun.* **2005**, *0*, 921.
[369] Y. S. Jung, K. T. Lee, J. H. Ryu, D. Im, S. M. Oh, *J. Electrochem. Soc.* **2005**, *152*, A1452.
[370] I. Kim, G. E. Blomgren, P. N. Kumta, *Electrochem. Solid-State Lett.* **2004**, *7*, A44.
[371] Y. Liu, J. Y. Xie, Y. Takeda, J. Yang, *J. Appl. Electrochem.* **2002**, *32*, 687.
[372] M. Noh, Y. Kwon, H. Lee, J. Cho, Y. Kim, M. G. Kim, *Chem. Mater.* **2005**, *17*, 1926.
[373] B. Veeraraghavan, A. Durairajan, B. Haran, B. Popov, R. Guidotti, *J. Electrochem. Soc.* **2002**, *149*, A675.
[374] G. X. Wang, J.-H. Ahn, M. J. Lindsay, L. Sun, D. H. Bradhurst, S. X. Dou, H. K. Liu, *J. Power Sources* **2001**, *97-98*, 211.
[375] G. X. Wang, J. Yao, J.-H. Ahn, H. K. Liu, S. X. Dou, *J. Appl. Electrochem.* **2004**, *34*, 187.
[376] Y. Wang, J. Y. Lee, T. C. Deivaraj, *J. Electrochem. Soc.* **2004**, *151*, A1804.
[377] K. T. Lee, Y. S. Jung, S. M. Oh, *J. Am. Chem. Soc.* **2003**, *125*, 5652.
[378] K.-C. Hsu, C.-E. Liu, P.-C. Chen, C.-Y. Lee, H.-T. Chiu, *J. Mater. Chem.* **2012**, *22*, 21533.
[379] Y. Zou, Y. Wang, *ACS Nano* **2011**, *5*, 8108.
[380] B. Luo, B. Wang, X. Li, Y. Jia, M. Liang, L. Zhi, *Adv. Mater.* **2012**, *24*, 3538.
[381] B. Luo, B. Wang, M. Liang, J. Ning, X. Li, L. Zhi, *Adv. Mater.* **2012**, *24*, 1405.
[382] G. Wang, B. Wang, X. Wang, J. Park, S. Dou, H. Ahn, K. Kim, *J. Mater. Chem.* **2009**, *19*, 8378.
[383] W.-M. Zhang, J.-S. Hu, Y.-G. Guo, S.-F. Zheng, L.-S. Zhong, W.-G. Song, L.-J. Wan, *Adv. Mater.* **2008**, *20*, 1160.
[384] W. Stöber, A. Fink, E. Bohn, *J. Colloid Interface Sci.* **1968**, *26*, 62.
[385] N. Li, H. Song, H. Cui, C. Wang, *Nano Energy* **2014**, *3*, 102.
[386] H. Ying, F. Xin, W. Han, *Adv. Mater. Interfaces* **2016**, *3*, 1600498.
[387] N. Li, H. Song, H. Cui, G. Yang, C. Wang, *J. Mater. Chem. A* **2014**, *2*, 2526.
[388] Y. Xu, Q. Liu, Y. Zhu, Y. Liu, A. Langrock, M. R. Zachariah, C. Wang, *Nano Lett.* **2013**, *13*, 470.
[389] N. Zhang, Q. Zhao, X. Han, J. Yang, J. Chen, *Nanoscale* **2014**, *6*, 2827.
[390] Z. Zhu, S. Wang, J. Du, Q. Jin, T. Zhang, F. Cheng, J. Chen, *Nano Lett.* **2014**, *14*, 153.
[391] Y. Zhang, L. Jiang, C. Wang, *Nanoscale* **2015**, *7*, 11940.
[392] D. H. Youn, A. Heller, C. B. Mullins, *Chem. Mater.* **2016**, *28*, 1343.
[393] R. E. A. Ardhi, G. Liu, M. X. Tran, C. Hudaya, J. Y. Kim, H. Yu, J. K. Lee, *ACS Nano* **2018**, *12*, 5588.
[394] W. Shockley, M. Sparks, G. K. Teal, *Phys. Rev.* **1951**, *83*, 151.
[395] W. Shockley, *Bell Syst. Tech. J.* **1949**, *28*, 435.
[396] F. S. Goucher, G. L. Pearson, M. Sparks, G. K. Teal, W. Shockley, *Phys. Rev.* **1951**, *81*, 637.
[397] W. Ni, Y. Wang, R. Xu, *Part. Part. Syst. Charact.* **2013**, *30*, 873.
[398] W. Ni, J. Cheng, L. Shi, X. Li, B. Wang, Q. Guan, L. Huang, G. Gu, H. Li, *J. Mater. Chem. A* **2014**, *2*, 19122.
[399] Y. J. Hong, Y. C. Kang, *Small* **2015**, *11*, 2157.
[400] H. Zhang, X. Huang, O. Noonan, L. Zhou, C. Yu, *Adv. Funct. Mater.* **2017**, *27*, 1606023.
[401] Z. Wang, J. Liu, F. Wang, S. Chen, H. Luo, X. Yu, *J. Phys. Chem. C* **2010**, *114*, 13577.
[402] J.-Y. Liao, B.-X. Lei, H.-Y. Chen, D.-B. Kuang, C.-Y. Su, *Energy Environ. Sci.* **2012**, *5*, 5750.
[403] A. Tolosa, M. Widmaier, B. Krüner, J. M. Griffin, V. Presser, *Sustainable Energy Fuels* **2018**, *2*, 215.
[404] J. Zhu, G. Hu, J. Zhang, *Mater. Lett.* **2016**, *185*, 565.
[405] L. Wei, K. Zhang, Z. Tao, J. Chen, *J. Alloys Compd.* **2015**, *644*, 742.
[406] J. Lin, J.-M. Lim, D. H. Youn, K. Kawashima, J.-H. Kim, Y. Liu, H. Guo, G. Henkelman, A. Heller, C. B. Mullins, *ACS Nano* **2017**, *11*, 10347.
[407] T. Zhang, L. J. Fu, J. Gao, Y. P. Wu, R. Holze, H. Q. Wu, *J. Power Sources* **2007**, *174*, 770.
[408] K. Kravchyk, L. Protesescu, M. I. Bodnarchuk, F. Krumeich, M. Yarema, M. Walter, C. Guntlin, M. V. Kovalenko, *J. Am. Chem. Soc.* **2013**, *135*, 4199.
[409] S. Ryu, H. C. Shim, J. T. Song, I. Kim, H. Ryoo, S. Hyun, J. Oh, *Part. Part. Syst. Charact.* **2019**, *36*, 1800331.
[410] L. Baggetto, H.-Y. Hah, J.-C. Jumas, C. E. Johnson, J. A. Johnson, J. K. Keum, C. A. Bridges, G. M. Veith, *J. Power Sources* **2014**, *267*, 329.
[411] S. Fan, T. Sun, X. Rui, Q. Yan, H. H. Hng, *J. Power Sources* **2012**, *201*, 288.
[412] L. Xiao, Y. Cao, J. Xiao, W. Wang, L. Kovarik, Z. Nie, J. Liu, *Chem. Commun.* **2012**, *48*, 3321.
[413] L. Ji, W. Zhou, V. Chabot, A. Yu, X. Xiao, *ACS Appl. Mater. Interfaces* **2015**, *7*, 24895.
[414] J. Li, J. Pu, Z. Liu, J. Wang, W. Wu, H. Zhang, H. Ma, *ACS Appl. Mater. Interfaces* **2017**, *9*, 25250.
[415] W. Ma, K. Yin, H. Gao, J. Niu, Z. Peng, Z. Zhang, *Nano Energy* **2018**, *54*, 349.
[416] M. Fehse, M. T. Sougrati, A. Darwiche, V. Gabaudan, C. La Fontaine, L. Monconduit, L. Stievano, *J. Mater. Chem. A* **2018**, *6*, 8724.
[417] M. Wang, Z. Yang, J. Wang, W. Li, L. Gu, Y. Yu, *Small* **2015**, *11*, 5381.
[418] J. S. Thorne, R. A. Dunlap, M. N. Obrovac, *Electrochim. Acta* **2013**, *112*, 133.
[419] J. Liu, Y. Wen, P. A. van Aken, J. Maier, Y. Yu, *Nano Lett.* **2014**, *14*, 6387.
[420] L. O. Vogt, C. Villevieille, *J. Electrochem. Soc.* **2016**, *163*, A1306.
[421] B. Huang, J. Yang, Y. Li, S. Xiao, Q. Chen, *Mater. Lett.* **2018**, *210*, 321.
[422] H. Usui, Y. Domi, S. Ohshima, H. Sakaguchi, *Electrochim. Acta* **2017**, *246*, 280.
[423] L. O. Vogt, C. Villevieille, *J. Mater. Chem. A* **2016**, *4*, 19116.
[424] W. Chen, D. Deng, *ACS Sustainable Chem. Eng.* **2015**, *3*, 63.
[425] W. Chen, D. Deng, *Carbon* **2015**, *87*, 70.
[426] J.-S. Choi, H.-J. Lee, J.-K. Ha, K.-K. Cho, *J. Nanosci. Nanotechnol.* **2018**, *18*, 6459.
[427] M. K. Datta, R. Epur, P. Saha, K. Kadakia, S. K. Park, P. N. Kumta, *J. Power Sources* **2013**, *225*, 316.
[428] W. Dong, S. Yang, B. Liang, D. Shen, W. Sun, Y. Liu, Y. Zhao, X. Wang, X. Wu, *ChemistrySelect* **2017**, *2*, 11739.
[429] Y. Liu, N. Zhang, L. Jiao, J. Chen, *Adv. Mater.* **2015**, *27*, 6702.

[430] S. Li, Z. Wang, J. Liu, L. Yang, Y. Guo, L. Cheng, M. Lei, W. Wang, *ACS Appl. Mater. Interfaces* **2016**, *8*, 19438.
[431] C. He, S. Wu, N. Zhao, C. Shi, E. Liu, J. Li, *ACS Nano* **2013**, *7*, 4459.
[432] J. Zhou, J. Qin, X. Zhang, C. Shi, E. Liu, J. Li, N. Zhao, C. He, *ACS Nano* **2015**, *9*, 3837.
[433] M. Mao, F. Yan, C. Cui, J. Ma, M. Zhang, T. Wang, C. Wang, *Nano Lett.* **2017**, *17*, 3830.
[434] D. Ma, Y. Li, H. Mi, S. Luo, P. Zhang, Z. Lin, J. Li, H. Zhang, *Angew. Chem., Int. Ed.* **2018**, *57*, 8901.
[435] J. Liu, P. Kopold, C. Wu, P. A. van Aken, J. Maier, Y. Yu, *Energy Environ. Sci.* **2015**, *8*, 3531.
[436] J. Park, J.-W. Park, J.-H. Han, S.-W. Lee, K.-Y. Lee, H.-S. Ryu, K.-W. Kim, G. Wang, J.-H. Ahn, H.-J. Ahn, *Mater. Res. Bull.* **2014**, *58*, 186.
[437] M. Shimizu, H. Usui, H. Sakaguchi, *J. Power Sources* **2014**, *248*, 378.
[438] Y. Kim, K.-H. Ha, S. M. Oh, K. T. Lee, *Chem. - Eur. J.* **2014**, *20*, 11980.
[439] Z. Li, J. Ding, D. Mitlin, *Acc. Chem. Res.* **2015**, *48*, 1657.
[440] B. Qin, H. Zhang, T. Diemant, D. Geiger, R. Raccichini, R. J. Behm, U. Kaiser, A. Varzi, S. Passerini, *ACS Appl. Mater. Interfaces* **2017**, *9*, 26797.
[441] Y.-X. Wang, Y.-G. Lim, M.-S. Park, S.-L. Chou, J. Ho Kim, H.-K. Liu, S.-X. Dou, Y.-J. Kim, *J. Mater. Chem. A* **2014**, *2*, 529.
[442] X. Kang, X. Sun, B. Han, *Adv. Mater.* **2016**, *28*, 1011.
[443] Y. Xu, B. Peng, F. M. Mulder, *Adv. Energy Mater.* **2018**, *8*, 1701847.
[444] J. Qian, Y. Xiong, Y. Cao, X. Ai, H. Yang, *Nano Lett.* **2014**, *14*, 1865.
[445] S. C. Jung, J.-H. Choi, Y.-K. Han, *J. Mater. Chem. A.* **2018**, *6*, 1772.
[446] Y. Kim, Y. Kim, A. Choi, S. Woo, D. Mok, N.-S. Choi, Y. S. Jung, J. H. Ryu, S. M. Oh, K. T. Lee, *Adv. Mater.* **2014**, *26*, 4139.
[447] B. Qu, C. Ma, G. Ji, C. Xu, J. Xu, Y. S. Meng, T. Wang, J. Y. Lee, *Adv. Mater.* **2014**, *26*, 3854.
[448] E. Cho, K. Song, M. H. Park, K.-W. Nam, Y.-M. Kang, *Small* **2016**, *12*, 2510.
[449] X. Yang, R.-Y. Zhang, J. Zhao, Z.-X. Wei, D.-X. Wang, X.-F. Bie, Y. Gao, J. Wang, F. Du, G. Chen, *Adv. Energy Mater.* **2018**, *8*, 1701827.
[450] C. Ma, J. Xu, J. Alvarado, B. Qu, J. Somerville, J. Y. Lee, Y. S. Meng, *Chem. Mater.* **2015**, *27*, 5633.
[451] Y. Kim, Y. Park, A. Choi, N.-S. Choi, J. Kim, J. Lee, J. H. Ryu, S. M. Oh, K. T. Lee, *Adv. Mater.* **2013**, *25*, 3045.
[452] J. Qian, X. Wu, Y. Cao, X. Ai, H. Yang, *Angew. Chem., Int. Ed.* **2013**, *52*, 4633.
[453] J. W. Wang, X. H. Liu, S. X. Mao, J. Y. Huang, *Nano Lett.* **2012**, *12*, 5897.
[454] E. Pan, Y. Jin, C. Zhao, M. Jia, Q. Chang, R. Zhang, M. Jia, *Appl. Surf. Sci.* **2019**, *475*, 12.
[455] H. Chen, B. Zhang, J. Zhang, W. Yu, J. Zheng, Z. Ding, H. Li, L. Ming, D. A. M. Bengono, S. Chen, H. Tong, *Front. Chem.* **2018**, *6*, 629.
[456] Y. Wang, Y. Zhang, J. Shi, A. Pan, F. Jiang, S. Liang, G. Cao, *J. Mater. Chem. A* **2018**, *6*, 18286.
[457] S. Zhang, H. Zhao, M. Wang, Z. Li, J. Mi, *Electrochim. Acta* **2018**, *279*, 186.
[458] A.-R. Park, C.-M. Park, *ACS Nano* **2017**, *11*, 6074.
[459] X. Yang, R. Zhang, N. Chen, X. Meng, P. Yang, C. Wang, Y. Zhang, Y. Wei, G. Chen, F. Du, *Chem. - Eur. J.* **2016**, *22*, 1445.
[460] X. Ren, J. Wang, D. Zhu, Q. Li, W. Tian, L. Wang, J. Zhang, L. Miao, P. K. Chu, K. Huo, *Nano Energy* **2018**, *54*, 322.
[461] Y. Kim, Y. Kim, Y. Park, Y. Nam Jo, Y.-J. Kim, N.-S. Choi, K. Tae Lee, *Chem. Commun.* **2015**, *51*, 50.
[462] Z. Zhang, X. Zhao, J. Li, *Mater. Lett.* **2016**, *162*, 169.
[463] L. Wu, P. Lu, R. Quhe, Q. Wang, C. Yang, P. Guan, K. Yang, *J. Mater. Chem. A* **2018**, *6*, 7933.
[464] G. Dae Park, J.-H. Lee, Y. Chan Kang, *Nanoscale* **2016**, *8*, 11889.
[465] J.-U. Seo, G.-K. Seong, C.-M. Park, *Sci. Rep.* **2015**, *5*, 7969.
[466] J. Zhang, Y.-X. Yin, Y.-G. Guo, *ACS Appl. Mater. Interfaces* **2015**, *7*, 27838.
[467] M. V. Kovalenko, W. Heiss, E. V. Shevchenko, J.-S. Lee, H. Schwinghammer, A. P. Alivisatos, D. V. Talapin, *J. Am. Chem. Soc.* **2007**, *129*, 11354.
[468] T. H. Hsieh, H. Lin, J. Liu, W. Duan, A. Bansil, L. Fu, *Nat. Commun.* **2012**, *3*, 982.
[469] K. V. Mitrofanov, A. V. Kolobov, P. Fons, M. Krbal, T. Shintani, J. Tominaga, T. Uruga, *Phys. Rev. B* **2014**, *90*, 134101.
[470] Z. Wang, Q. Su, H. Deng, W. He, J. Lin, Y. Q. Fu, *J. Mater. Chem. A* **2014**, *2*, 13976.
[471] M. Mortazavi, Q. Ye, N. Birbilis, N. V. Medhekar, *J. Power Sources* **2015**, *285*, 29.
[472] D. Liu, Z. jiao Liu, X. Li, W. Xie, Q. Wang, Q. Liu, Y. Fu, D. He, *Small* **2017**, *13*, 1702000.
[473] W. Weppner, R. A. Huggins, *J. Electrochem. Soc.* **1977**, *124*, 1569.
[474] W. Weppner, R. A. Huggins, *J. Electrochem. Soc.* **1978**, *125*, 7.
[475] Y. Guo, H. Li, T. Zhai, *Adv. Mater.* **2017**, *29*, 1700007.
[476] R. Alcántara, F. J. Fernández-Madrigal, P. Lavela, J. L. Tirado, J. C. Jumas, J. Olivier-Fourcade, *J. Mater. Chem.* **1999**, *9*, 2517.
[477] V. Pralong, J.-B. Leriche, B. Beaudoin, E. Naudin, M. Morcrette, J.-M. Tarascon, *Solid State Ionics.* **2004**, *166*, 295.
[478] C. S. Johnson, J. T. Vaughey, M. M. Thackeray, T. Sarakonsri, S. A. Hackney, L. Fransson, K. Edström, J. O. Thomas, *Electrochem. Commun.* **2000**, *2*, 595.
[479] D. Larcher, L. Y. Beaulieu, O. Mao, A. E. George, J. R. Dahn, *J. Electrochem. Soc.* **2000**, *147*, 1703.
[480] X. Zhao, G. Cao, T. Li, *J. Mater. Sci. Lett.* **2000**, *19*, 851.
[481] F. J. Fernández-Madrigal, P. Lavela, C. Pérez-Vicente, J. L. Tirado, *J. Electroanal. Chem.* **2001**, *501*, 205.
[482] H. Honda, H. Sakaguchi, I. Tanaka, T. Esaka, *J. Power Sources* **2003**, *123*, 216.
[483] J. T. Vaughey, L. Fransson, H. A. Swinger, K. Edström, M. M. Thackeray, *J. Power Sources* **2003**, *119-121*, 64.
[484] L. J. Zhang, X. B. Zhao, X. B. Jiang, C. P. Lv, G. S. Cao, *J. Power Sources* **2001**, *94*, 92.
[485] S.-W. Song, R. P. Reade, E. J. Cairns, J. T. Vaughey, M. M. Thackeray, K. A. Striebel, *J. Electrochem. Soc.* **2004**, *151*, A1012.
[486] L. Huang, X.-M. Zheng, Y.-S. Wu, L.-J. Xue, F.-S. Ke, G.-Z. Wei, S.-G. Sun, *Electrochem. Commun.* **2009**, *11*, 585.
[487] J. Zhu, T. Sun, J. Chen, W. Shi, X. Zhang, X. Lou, S. Mhaisalkar, H. H. Hng, F. Boey, J. Ma, Q. Yan, *Chem. Mater.* **2010**, *22*, 5333.
[488] S. Saadat, Y. Y. Tay, J. Zhu, P. F. Teh, S. Maleksaeedi, M. M. Shahjamali, M. Shakerzadeh, M. Srinivasan, B. Y. Tay, H. H. Hng, J. Ma, Q. Yan, *Chem. Mater.* **2011**, *23*, 1032.
[489] C.-M. Park, H.-J. Sohn, *Adv. Mater.* **2010**, *22*, 47.
[490] J. Xu, H. Wu, F. Wang, Y. Xia, G. Zheng, *Adv. Energy Mater.* **2013**, *3*, 286.
[491] J. M. Mosby, A. L. Prieto, *J. Am. Chem. Soc.* **2008**, *130*, 10656.
[492] E. D. Jackson, J. M. Mosby, A. L. Prieto, *Electrochim. Acta* **2016**, *214*, 253.
[493] E. D. Jackson, A. L. Prieto, *ACS Appl. Mater. Interfaces* **2016**, *8*, 30379.
[494] M. C. Schulze, R. K. Schulze, A. L. Prieto, *J. Mater. Chem. A* **2018**,*6*,12708.
[495] D. Kim, J. Chang, J. Park, J. J. Pak, *J. Mater. Sci.: Mater. Electron.* **2011**, *22*, 703.
[496] A. Dailly, J. Ghanbaja, P. Willmann, D. Billaud, *J. Power Sources* **2004**, *125*, 70.
[497] A. Dailly, L. Balan, J. Ghanbaja, P. Willmann, D. Billaud, *Carbon* **2005**, *43*, 1001.
[498] J. Hassoun, G. Derrien, S. Panero, B. Scrosati, *J. Power Sources* **2008**, *183*, 339.
[499] C.-M. Park, H.-J. Sohn, *Chem. Mater.* **2008**, *20*, 3169.

[500] S. Yoon, A. Manthiram, *Chem. Mater.* **2009**, *21*, 3898.
[501] Z. Chen, Y. Cao, J. Qian, X. Ai, H. Yang, *J. Phys. Chem. C* **2010**, *114*, 15196.
[502] C.-M. Park, H.-J. Sohn, *J. Electrochem. Soc.* **2010**, *157*, A46.
[503] Z. Yi, Q. Han, S. Ju, Y. Wu, Y. Cheng, L. Wang, *J. Electrochem. Soc.* **2016**, *163*, A2641.
[504] H. Wang, X. Yang, Q. Wu, Q. Zhang, H. Chen, H. Jing, J. Wang, S.-B. Mi, A. L. Rogach, C. Niu, *ACS Nano* **2018**, *12*, 3406.
[505] B. Gao, S. Sinha, L. Fleming, O. Zhou, *Adv. Mater.* **2001**, *13*, 816.
[506] N. Yan, F. Wang, H. Zhong, Y. Li, Y. Wang, L. Hu, Q. Chen, *Sci. Rep.* **2013**, *3*, 1568.
[507] S.-Z. Liang, X.-Y. Wang, Y.-G. Xia, S.-L. Xia, E. Metwalli, B. Qiu, Q. Ji, S.-S. Yin, S. Xie, K. Fang, L.-Y. Zheng, M.-M. Wang, X.-X. Zuo, R.-J. Li, Z.-P. Liu, J. Zhu, P. Müller-Buschbaum, Y.-J. Cheng, *Acta Metall. Sin. (Engl. Lett.)* **2018**, *31*, 910.
[508] J. Liu, Z. Yang, J. Wang, L. Gu, J. Maier, Y. Yu, *Nano Energy* **2015**, *16*, 389.
[509] J. Qin, T. Wang, D. Liu, E. Liu, N. Zhao, C. Shi, F. He, L. Ma, C. He, *Adv. Mater.* **2018**, *30*, 1704670.
[510] P. Wu, A. Zhang, L. Peng, F. Zhao, Y. Tang, Y. Zhou, G. Yu, *ACS Nano* **2018**, *12*, 759.
[511] Y. Zhu, X. Han, Y. Xu, Y. Liu, S. Zheng, K. Xu, L. Hu, C. Wang, *ACS Nano* **2013**, *7*, 6378.
[512] L. Wu, X. Hu, J. Qian, F. Pei, F. Wu, R. Mao, X. Ai, H. Yang, Y. Cao, *Energy Environ. Sci.* **2014**, *7*, 323.
[513] X. Zhou, Y. Zhong, M. Yang, M. Hu, J. Wei, Z. Zhou, *Chem. Commun.* **2014**, *50*, 12888.
[514] C. Yang, W. Li, Z. Yang, L. Gu, Y. Yu, *Nano Energy* **2015**, *18*, 12.
[515] L. Wu, H. Lu, L. Xiao, X. Ai, H. Yang, Y. Cao, *J. Mater. Chem. A* **2015**, *3*, 5708.
[516] N. Zhang, Y. Liu, Y. Lu, X. Han, F. Cheng, J. Chen, *Nano Res.* **2015**, *8*, 3384.
[517] C. Nithya, S. Gopukumar, *J. Mater. Chem. A* **2014**, *2*, 10516.
[518] Y.-L. Ding, C. Wu, P. Kopold, P. A. van Aken, J. Maier, Y. Yu, *Small* **2015**, *11*, 6026.
[519] W. Zhang, Y. Liu, C. Chen, Z. Li, Y. Huang, X. Hu, *Small* **2015**, *11*, 3822.
[520] Z. Liu, X.-Y. Yu, X. Wen (David) Lou, U. Paik, *Energy Environ. Sci.* **2016**, *9*, 2314.
[521] N. Wang, Z. Bai, Y. Qian, J. Yang, *Adv. Mater.* **2016**, *28*, 4126.
[522] W. Luo, F. Li, J.-J. Gaumet, P. Magri, S. Diliberto, L. Zhou, L. Mai, *Adv. Energy Mater.* **2018**, *8*, 1703237.
[523] J. Liu, L. Yu, C. Wu, Y. Wen, K. Yin, F.-K. Chiang, R. Hu, J. Liu, L. Sun, L. Gu, J. Maier, Y. Yu, M. Zhu, *Nano Lett.* **2017**, *17*, 2034.
[524] J. Song, P. Yan, L. Luo, X. Qi, X. Rong, J. Zheng, B. Xiao, S. Feng, C. Wang, Y.-S. Hu, Y. Lin, V. L. Sprenkle, X. Li, *Nano Energy* **2017**, *40*, 504.
[525] N. Wang, Z. Bai, Y. Qian, J. Yang, *ACS Appl. Mater. Interfaces* **2017**, *9*, 447.
[526] H. Li, X. Huang, L. Chen, *Solid State Ionics.* **1999**, *123*, 189.
[527] M.-Z. Xue, Z.-W. Fu, *Electrochem. Commun.* **2006**, *8*, 1250.
[528] H. Bryngelsson, J. Eskhult, K. Edström, L. Nyholm, *Electrochim. Acta* **2007**, *53*, 1062.
[529] H. Bryngelsson, J. Eskhult, L. Nyholm, M. Herranen, O. Alm, K. Edström, *Chem. Mater.* **2007**, *19*, 1170.
[530] L. Simonin, U. Lafont, N. Tabrizi, A. Schmidt-Ott, E. M. Kelder, *J. Power Sources* **2007**, *174*, 805.
[531] Z. Wang, Y. Cheng, Q. Li, L. Chang, L. Wang, *J. Power Sources* **2018**, *389*, 214.
[532] Q. Sun, Q.-Q. Ren, H. Li, Z.-W. Fu, *Electrochem. Commun.* **2011**, *13*, 1462.
[533] K. Li, H. Liu, G. Wang, *Arabian J. Sci. Eng.* **2014**, *39*, 6589.
[534] X. Zhou, X. Liu, Y. Xu, Y. Liu, Z. Dai, J. Bao, *J. Phys. Chem. C* **2014**, *118*, 23527.
[535] K.-S. Hong, D.-H. Nam, S.-J. Lim, D. Sohn, T.-H. Kim, H. Kwon, *ACS Appl. Mater. Interfaces* **2015**, *7*, 17264.
[536] N. Li, S. Liao, Y. Sun, H. W. Song, C. X. Wang, *J. Mater. Chem. A* **2015**, *3*, 5820.
[537] D.-H. Nam, K.-S. Hong, S.-J. Lim, M.-J. Kim, H.-S. Kwon, *Small* **2015**, *11*, 2885.
[538] W. Li, K. Wang, S. Cheng, K. Jiang, *J. Mater. Chem. A* **2017**, *5*, 1160.
[539] J. Pan, N. Wang, Y. Zhou, X. Yang, W. Zhou, Y. Qian, J. Yang, *Nano Res.* **2017**, *10*, 1794.
[540] G.-Z. Wang, J.-M. Feng, L. Dong, X.-F. Li, D.-J. Li, *J. Alloys Compd.* **2017**, *693*, 141.
[541] G.-Z. Wang, J.-M. Feng, L. Dong, X.-F. Li, D.-J. Li, *Electrochim. Acta* **2017**, *240*, 203.
[542] Z. Yi, Q. Han, X. Li, Y. Wu, Y. Cheng, L. Wang, *Chem. Eng. J.* **2017**, *315*, 101.
[543] L. Yang, Y. Huang, X. Li, J. Sheng, F. Li, Z. Xie, Z. Zhou, *ChemElectroChem* **2018**, *5*, 2522.
[544] S. Gandi, S. R. Chinta, P. Ghoshal, B. R. Ravuri, *J. Non-Cryst. Solids* **2019**, *506*, 80.
[545] C.-M. Park, Y. Hwa, N.-E. Sung, H.-J. Sohn, *J. Mater. Chem.* **2010**, *20*, 1097.
[546] J. Kong, H. Wei, D. Xia, P. Yu, *Mater. Lett.* **2016**, *179*, 114.
[547] Z. Yi, Q. Han, Y. Cheng, Y. Wu, L. Wang, *Chem. Commun.* **2016**, *52*, 7691.
[548] M.-Z. Xue, Z.-W. Fu, *J. Alloys Compd.* **2008**, *458*, 351.
[549] K.-H. Nam, C.-M. Park, *J. Mater. Chem. A* **2016**, *4*, 8562.
[550] H. Kim, M. Kim, Y. H. Yoon, Q. H. Nguyen, I. T. Kim, J. Hur, S. G. Lee, *Electrochim. Acta* **2019**, *293*, 8.
[551] D. Y. W. Yu, P. V. Prikhodchenko, C. W. Mason, S. K. Batabyal, J. Gun, S. Sladkevich, A. G. Medvedev, O. Lev, *Nat. Commun.* **2013**, *4*, 1.
[552] H. Hou, M. Jing, Z. Huang, Y. Yang, Y. Zhang, J. Chen, Z. Wu, X. Ji, *ACS Appl. Mater. Interfaces* **2015**, *7*, 19362.
[553] J. Xie, L. Liu, J. Xia, Y. Zhang, M. Li, Y. Ouyang, S. Nie, X. Wang, *Nano-Micro Lett.* **2018**, *10*, 12.
[554] W. Luo, A. Calas, C. Tang, F. Li, L. Zhou, L. Mai, *ACS Appl. Mater. Interfaces* **2016**, *8*, 35219.
[555] W. Zhao, C. M. Li, *J. Colloid Interface Sci.* **2017**, *488*, 356.
[556] K. P. Lakshmi, K. J. Janas, M. M. Shaijumon, *Carbon* **2018**, *131*, 86.
[557] J. Pan, S. Chen, Q. Fu, Y. Sun, Y. Zhang, N. Lin, P. Gao, J. Yang, Y. Qian, *ACS Nano* **2018**, *12*, 12869.
[558] L. Wang, X. Bi, S. Yang, *J. Mater. Chem. A* **2018**, *6*, 6225.
[559] P. Wang, S. Xie, Y. She, W. Fan, M. K. H. Leung, H. Wang, *ChemistrySelect* **2019**, *4*, 1078.
[560] S. Su, G. Cao, X. Zhao, *Chin. Sci. Bull.* **2004**, *49*, 1882.
[561] H. Kim, J. Cho, *Chem. Mater.* **2008**, *20*, 1679.
[562] Y. Gao, W. Tian, C. Huo, K. Zhang, S. Guo, S. Zhang, X. Song, L. Jiang, K. Huo, H. Zeng, *J. Mater. Chem. A* **2019**, *7*, 3238.
[563] A. Darwiche, C. Marino, M. T. Sougrati, B. Fraisse, L. Stievano, L. Monconduit, *J. Am. Chem. Soc.* **2012**, *134*, 20805.
[564] H. Hou, M. Jing, Y. Yang, Y. Zhu, L. Fang, W. Song, C. Pan, X. Yang, X. Ji, *ACS Appl. Mater. Interfaces* **2014**, *6*, 16189.
[565] H. Hou, M. Jing, Y. Yang, Y. Zhang, Y. Zhu, W. Song, X. Yang, X. Ji, *J. Mater. Chem. A* **2015**, *3*, 2971.
[566] H. Hou, M. Jing, Y. Zhang, J. Chen, Z. Huang, X. Ji, *J. Mater. Chem. A* **2015**, *3*, 17549.
[567] M. Walter, R. Erni, M. V. Kovalenko, *Sci. Rep.* **2015**, *5*, 8418.
[568] Y. Yang, X. Yang, Y. Zhang, H. Hou, M. Jing, Y. Zhu, L. Fang, Q. Chen, X. Ji, *J. Power Sources* **2015**, *282*, 358.
[569] S. Liu, J. Feng, X. Bian, J. Liu, H. Xu, *Energy Environ. Sci.* **2016**, *9*, 1229.
[570] O. Ruiz, M. Cochrane, M. Li, Y. Yan, K. Ma, J. Fu, Z. Wang, S. H. Tolbert, V. B. Shenoy, E. Detsi, *Adv. Energy Mater.* **2018**, *8*, 1801781.

[571] L. Baggetto, P. Ganesh, C.-N. Sun, R. A. Meisner, T. A. Zawodzinski, G. M. Veith, *J. Mater. Chem. A* **2013**, *1*, 7985.
[572] P. K. Allan, J. M. Griffin, A. Darwiche, O. J. Borkiewicz, K. M. Wiaderek, K. W. Chapman, A. J. Morris, P. J. Chupas, L. Monconduit, C. P. Grey, *J. Am. Chem. Soc.* **2016**, *138*, 2352.
[573] D. Larcher, S. Beattie, M. Morcrette, K. Edström, J.-C. Jumas, J.-M. Tarascon, *J. Mater. Chem.* **2007**, *17*, 3759.
[574] Y. Liu, S. Zhang, T. Zhu, *ChemElectroChem* **2014**, *1*, 706.
[575] L. Baggetto, P. H. L. Notten, *J. Electrochem. Soc.* **2009**, *156*, A169.
[576] X. Xiao, X. Li, S. Zheng, J. Shao, H. Xue, H. Pang, *Adv. Mater. Interfaces* **2017**, *4*, 1600798.
[577] C. S. Fuller, J. C. Severiens, *Phys. Rev.* **1954**, *96*, 21.
[578] D. Wang, Y.-L. Chang, Q. Wang, J. Cao, D. B. Farmer, R. G. Gordon, H. Dai, *J. Am. Chem. Soc.* **2004**, *126*, 11602.
[579] M. R. S. John, A. J. Furgala, A. F. Sammells, *J. Electrochem. Soc.* **1982**, *129*, 246.
[580] C. van der Marel, A. B. van Oosten, W. Geertsma, W. van der Lugt, *J. Phys. F: Met. Phys.* **1982**, *12*, L129.
[581] J. Sangster, A. D. Pelton, *J. Phase Equilib.* **1997**, *18*, 289.
[582] L. Baggetto, J. K. Keum, J. F. Browning, G. M. Veith, *Electrochem. Commun.* **2013**, *34*, 41.
[583] L. Y. Lim, N. Liu, Y. Cui, M. F. Toney, *Chem. Mater.* **2014**, *26*, 3739.
[584] Z. Hu, S. Zhang, C. Zhang, G. Cui, *Coord. Chem. Rev.* **2016**, *326*, 34.
[585] J. Graetz, C. C. Ahn, R. Yazami, B. Fultz, *J. Electrochem. Soc.* **2004**, *151*, A698.
[586] C. K. Chan, X. F. Zhang, Y. Cui, *Nano Lett.* **2008**, *8*, 307.
[587] Y.-D. Ko, J.-G. Kang, G.-H. Lee, J.-G. Park, K.-S. Park, Y.-H. Jin, D.-W. Kim, *Nanoscale* **2011**, *3*, 3371.
[588] X. H. Liu, S. Huang, S. T. Picraux, J. Li, T. Zhu, J. Y. Huang, *Nano Lett.* **2011**, *11*, 3991.
[589] M.-H. Park, K. Kim, J. Kim, J. Cho, *Adv. Mater.* **2010**, *22*, 415.
[590] L. C. Yang, Q. S. Gao, L. Li, Y. Tang, Y. P. Wu, *Electrochem. Commun.* **2010**, *12*, 418.
[591] A. M. Chockla, K. C. Klavetter, C. B. Mullins, B. A. Korgel, *ACS Appl. Mater. Interfaces* **2012**, *4*, 4658.
[592] G. Flynn, K. Palaniappan, M. Sheehan, T. Kennedy, K. M. Ryan, *Nanotechnology* **2017**, *28*, 255603.
[593] Y. Xiao, M. Cao, L. Ren, C. Hu, *Nanoscale* **2012**, *4*, 7469.
[594] X. Liu, J. Hao, X. Liu, C. Chi, N. Li, F. Endres, Y. Zhang, Y. Li, J. Zhao, *Chem. Commun.* **2015**, *51*, 2064.
[595] K. C. Klavetter, S. M. Wood, Y.-M. Lin, J. L. Snider, N. C. Davy, A. M. Chockla, D. K. Romanovicz, B. A. Korgel, J.-W. Lee, A. Heller, C. B. Mullins, *J. Power Sources* **2013**, *238*, 123.
[596] L. Wang, K. Bao, Z. Lou, G. Liang, Q. Zhou, *Dalton Trans.* **2016**, *45*, 2814.
[597] N. Lin, T. Li, Y. Han, Q. Zhang, T. Xu, Y. Qian, *ACS Appl. Mater. Interfaces* **2018**, *10*, 8399.
[598] K. Mishra, X.-C. Liu, F.-S. Ke, X.-D. Zhou, *Composites, Part B* **2019**, *163*, 158.
[599] J. Gu, S. M. Collins, A. I. Carim, X. Hao, B. M. Bartlett, S. Maldonado, *Nano Lett.* **2012**, *12*, 4617.
[600] F.-W. Yuan, H.-J. Yang, H.-Y. Tuan, *ACS Nano* **2012**, *6*, 9932.
[601] T. Kennedy, E. Mullane, H. Geaney, M. Osiak, C. O'Dwyer, K. M. Ryan, *Nano Lett.* **2014**, *14*, 716.
[602] E. Mullane, T. Kennedy, H. Geaney, C. Dickinson, K. M. Ryan, *Chem. Mater.* **2013**, *25*, 1816.
[603] J. Hao, Y. Yang, J. Zhao, X. Liu, F. Endres, C. Chi, B. Wang, X. Liu, Y. Li, *Nanoscale* **2017**, *9*, 8481.
[604] C. Kim, G. Song, L. Luo, J. Y. Cheong, S.-H. Cho, D. Kwon, S. Choi, J.-W. Jung, C.-M. Wang, I.-D. Kim, S. Park, *ACS Nano* **2018**, *12*, 8169.
[605] N. K. Mahenderkar, Y.-C. Liu, J. A. Koza, J. A. Switzer, *ACS Nano* **2014**, *8*, 9524.
[606] S. Choi, J. Kim, N.-S. Choi, M. G. Kim, S. Park, *ACS Nano* **2015**, *9*, 2203.
[607] L. Li, K. Hau Seng, C. Feng, H. Kun Liu, Z. Guo, *J. Mater. Chem. A* **2013**, *1*, 7666.
[608] D. K. Yi, D.-Y. Kim, *Nano Lett.* **2003**, *3*, 207.
[609] D. K. Yi, E.-M. Seo, D.-Y. Kim, *Langmuir* **2002**, *18*, 5321.
[610] T. Suezaki, J. I. L. Chen, T. Hatayama, T. Fuyuki, G. A. Ozin, *Appl. Phys. Lett.* **2010**, *96*, 242102.
[611] N. Tachikawa, K. Yamauchi, E. Takashima, J.-W. Park, K. Dokko, M. Watanabe, *Chem. Commun.* **2011**, *47*, 8157.
[612] T. Song, Y. Jeon, M. Samal, H. Han, H. Park, J. Ha, D. Kee Yi, J.-M. Choi, H. Chang, Y.-M. Choi, U. Paik, *Energy Environ. Sci.* **2012**, *5*, 9028.
[613] L. Y. Lim, S. Fan, H. H. Hng, M. F. Toney, *J. Phys. Chem. C* **2015**, *119*, 22772.
[614] L. Y. Lim, S. Fan, H. H. Hng, M. F. Toney, *Adv. Energy Mater.* **2015**, *5*, 1500599.
[615] M. I. Bodnarchuk, K. V. Kravchyk, F. Krumeich, S. Wang, M. V. Kovalenko, *ACS Nano* **2014**, *8*, 2360.
[616] J. Wang, N. Du, H. Zhang, J. Yu, D. Yang, *J. Mater. Chem.* **2012**, *22*, 1511.
[617] C. Yan, W. Xi, W. Si, J. Deng, O. G. Schmidt, *Adv. Mater.* **2013**, *25*, 539.
[618] O. G. Schmidt, K. Eberl, *Nature* **2001**, *410*, 168.
[619] G. P. Nikishkov, *J. Appl. Phys.* **2003**, *94*, 5333.
[620] M.-H. Seo, M. Park, K. Tae Lee, K. Kim, J. Kim, J. Cho, *Energy Environ. Sci.* **2011**, *4*, 425.
[621] D.-J. Xue, S. Xin, Y. Yan, K.-C. Jiang, Y.-X. Yin, Y.-G. Guo, L.-J. Wan, *J. Am. Chem. Soc.* **2012**, *134*, 2512.
[622] J. Hao, L. Pan, H. Zhang, C. Chi, Q. Guo, J. Zhao, Y. Yang, X. Liu, X. Ma, Y. Li, *Chem. Eng. J.* **2018**, *346*, 427.
[623] J. Liu, K. Song, C. Zhu, C.-C. Chen, P. A. van Aken, J. Maier, Y. Yu, *ACS Nano* **2014**, *8*, 7051.
[624] S. Jin, N. Li, H. Cui, C. Wang, *ACS Appl. Mater. Interfaces* **2014**, *6*, 19397.
[625] B. Wang, J. Jin, K. Rui, C. Zhu, Z. Wen, *J. Power Sources* **2018**, *396*, 124.
[626] X. Sun, X. Lu, S. Huang, L. Xi, L. Liu, B. Liu, Q. Weng, L. Zhang, O. G. Schmidt, *ACS Appl. Mater. Interfaces* **2017**, *9*, 38556.
[627] D. Tung Ngo, H. T. T. Le, C. Kim, J.-Y. Lee, J. G. Fisher, I.-D. Kim, C.-J. Park, *Energy Environ. Sci.* **2015**, *8*, 3577.
[628] C. Wang, J. Ju, Y. Yang, Y. Tang, J. Lin, Z. Shi, R. P. S. Han, F. Huang, *J. Mater. Chem. A* **2013**, *1*, 8897.
[629] Y. Sun, S. Jin, G. Yang, J. Wang, C. Wang, *ACS Nano* **2015**, *9*, 3479.
[630] Q. Gao, P. Chen, Y. Zhang, Y. Tang, *Adv. Mater.* **2008**, *20*, 1837.
[631] D. T. Ngo, R. S. Kalubarme, H. T. T. Le, J. G. Fisher, C.-N. Park, I.-D. Kim, C.-J. Park, *Adv. Funct. Mater.* **2014**, *24*, 5291.
[632] D. Li, C. Feng, H. kun Liu, Z. Guo, *J. Mater. Chem. A* **2015**, *3*, 978.
[633] K. Huo, L. Wang, C. Peng, X. Peng, Y. Li, Q. Li, Z. Jin, P. K. Chu, *J. Mater. Chem. A* **2016**, *4*, 7585.
[634] D. Li, H. Wang, H. K. Liu, Z. Guo, *Adv. Energy Mater.* **2016**, *6*, 1501666.
[635] R. Mo, D. Rooney, K. Sun, H. Y. Yang, *Nat. Commun.* **2017**, *8*, 13949.
[636] J. K. Feng, M. O. Lai, L. Lu, *Electrochim. Acta* **2012**, *62*, 103.
[637] K. H. Seng, M. Park, Z. P. Guo, H. K. Liu, J. Cho, *Nano Lett.* **2013**, *13*, 1230.
[638] X.-L. Wang, W.-Q. Han, H. Chen, J. Bai, T. A. Tyson, X.-Q. Yu, X.-J. Wang, X.-Q. Yang, *J. Am. Chem. Soc.* **2011**, *133*, 20692.
[639] D. McNulty, H. Geaney, D. Buckley, C. O'Dwyer, *Nano Energy* **2018**, *43*, 11.
[640] Y. Chen, C. Yan, O. G. Schmidt, *Adv. Energy Mater.* **2013**, *3*, 1269.
[641] S. H. Choi, K. Y. Jung, Y. C. Kang, *ACS Appl. Mater. Interfaces* **2015**, *7*, 13952.

[642] K. J. Harry, D. T. Hallinan, D. Y. Parkinson, A. A. MacDowell, N. P. Balsara, *Nat. Mater.* **2014**, *13*, 69.
[643] A. Jahel, A. Darwiche, C. Matei Ghimbeu, C. Vix-Guterl, L. Monconduit, *J. Power Sources* **2014**, *269*, 755.
[644] F. Jia, L. Song, W. Wei, P. Qu, M. Xu, *New J. Chem.* **2015**, *39*, 689.
[645] H. Jia, R. Kloepsch, X. He, J. Pablo Badillo, M. Winter, T. Placke, *J. Mater. Chem. A* **2014**, *2*, 17545.
[646] S. Jin, N. Li, H. Cui, C. Wang, *Nano Energy* **2013**, *2*, 1128.
[647] D. Lv, M. L. Gordin, R. Yi, T. Xu, J. Song, Y.-B. Jiang, D. Choi, D. Wang, *Adv. Funct. Mater.* **2014**, *24*, 1059.
[648] A. G. Medvedev, A. A. Mikhaylov, D. A. Grishanov, D. Y. W. Yu, J. Gun, S. Sladkevich, O. Lev, P. V. Prikhodchenko, *ACS Appl. Mater. Interfaces* **2017**, *9*, 9152.
[649] L. Mei, M. Mao, S. Chou, H. Liu, S. Dou, D. H. L. Ng, J. Ma, *J. Mater. Chem. A* **2015**, *3*, 21699.
[650] H. Qiu, L. Zeng, T. Lan, X. Ding, M. Wei, *J. Mater. Chem. A* **2015**, *3*, 1619.
[651] H. Song, B. Zhao, X. Xu, S. Yan, Y. Shi, *Mater. Sci. Eng., B* **2017**, *225*, 122.
[652] D. Tung Ngo, R. S. Kalubarme, H. T. T. Le, C.-N. Park, C.-J. Park, *Nanoscale* **2015**, *7*, 2552.
[653] D. Tung Ngo, H. T. T. Le, R. S. Kalubarme, J.-Y. Lee, C.-N. Park, C.-J. Park, *J. Mater. Chem. A* **2015**, *3*, 21722.
[654] W. Wei, L. Guo, *Part. Part. Syst. Charact.* **2013**, *30*, 658.
[655] W. Wei, A. Tian, F. Jia, K. Wang, P. Qu, M. Xu, *RSC Adv.* **2016**, *6*, 87440.
[656] X. Wei, W. Li, L. Zeng, Y. Yu, *Part. Part. Syst. Charact.* **2016**, *33*, 524.
[657] R. Xu, S. Wu, Y. Du, Z. Zhang, *Chem. Eng. J.* **2016**, *296*, 349.
[658] S. Yan, H. Song, S. Lin, H. Wu, Y. Shi, J. Yao, *Adv. Funct. Mater.* **2019**, *29*, 1807946.
[659] S. Yoon, S.-H. Jung, K.-N. Jung, S.-G. Woo, W. Cho, Y.-N. Jo, K. Y. Cho, *Electrochim. Acta* **2016**, *188*, 120.
[660] F. Pantò, Y. Fan, S. Stelitano, E. Fazio, S. Patanè, P. Frontera, P. Antonucci, N. Pinna, S. Santangelo, *Adv. Funct. Mater.* **2018**, *28*, 1800938.
[661] L. Zeng, X. Huang, X. Chen, C. Zheng, Q. Qian, Q. Chen, M. Wei, *ACS Appl. Mater. Interfaces* **2016**, *8*, 232.
[662] X. Li, J. Liang, Z. Hou, Y. Zhu, Y. Wang, Y. Qian, *Chem. Commun.* **2014**, *50*, 13956.
[663] J. Zhao, L. Yang, J. A. McLeod, L. Liu, *Sci. Rep.* **2015**, *5*, 17779.
[664] Z. Fang, T. Qiang, J. Fang, Y. Song, Q. Ma, M. Ye, F. Qiang, B. Geng, *Electrochim. Acta* **2015**, *151*, 453.
[665] S.-Y. Lim, W. Jang, S. Yun, W.-S. Yoon, J.-Y. Choi, D. Whang, *Mater. Res. Bull.* **2019**, *110*, 24.
[666] H. Song, B. Zhao, S. Yan, K. Li, X. Xu, Y. Shi, *J. Nanosci. Nanotechnol.* **2017**, *17*, 9036.
[667] J. Hwang, C. Jo, M. G. Kim, J. Chun, E. Lim, S. Kim, S. Jeong, Y. Kim, J. Lee, *ACS Nano* **2015**, *9*, 5299.
[668] M. M. Rahman, I. Sultana, T. Yang, Z. Chen, N. Sharma, A. M. Glushenkov, Y. Chen, *Angew. Chem.* **2016**, *128*, 16293.
[669] L. Wang, X. Zhang, G. Shen, X. Peng, M. Zhang, J. Xu, *Nanotechnology* **2016**, *27*, 095602.
[670] W. Wang, J. Qin, M. Cao, *ACS Appl. Mater. Interfaces* **2016**, *8*, 1388.
[671] W. Wei, F. Jia, K. Wang, B. Luo, P. Qu, M. Xu, *Mater. Lett.* **2017**, *196*, 157.
[672] Y. Wei, L. Huang, J. He, Y. Guo, R. Qin, H. Li, T. Zhai, *Adv. Energy Mater.* **2018**, *8*, 1703635.
[673] S. Wu, R. Wang, Z. Wang, Z. Lin, *Nanoscale* **2014**, *6*, 8350.
[674] R. Yi, J. Feng, D. Lv, M. L. Gordin, S. Chen, D. Choi, D. Wang, *Nano Energy* **2013**, *2*, 498.
[675] J. Hu, C. Ouyang, S. A. Yang, H. Ying Yang, *Nanoscale Horiz.* **2019**, *4*, 457.
[676] Y. Jae Cho, H. Soon Im, Y. Myung, C. Hyun Kim, H. Sung Kim, S. Hyuk Back, Y. Rok Lim, C. Su Jung, D. Myung Jang, J. Park, E. Hee Cha, S. Ho Choo, M. Seob Song, W. Il Cho, *Chem. Commun.* **2013**, *49*, 4661.
[677] C. Kim, G. Hwang, J.-W. Jung, S.-H. Cho, J. Y. Cheong, S. Shin, S. Park, I.-D. Kim, *Adv. Funct. Mater.* **2017**, *27*, 1605975.
[678] Y. Kim, H. Hwang, K. Lawler, S. W. Martin, J. Cho, *Electrochim. Acta* **2008**, *53*, 5058.
[679] W. Li, H. Li, Z. Lu, L. Gan, L. Ke, T. Zhai, H. Zhou, *Energy Environ. Sci.* **2015**, *8*, 3629.
[680] M.-Y. Tsai, C.-Y. Yu, C.-C. Wang, T.-P. Perng, *Cryst. Growth Des.* **2008**, *8*, 2264.
[681] C. Yan, P. S. Lee, *J. Phys. Chem. C* **2009**, *113*, 14135.
[682] C. Yan, P. S. Lee, *J. Phys. Chem. C* **2010**, *114*, 265.
[683] W. Li, D. Chen, G. Shen, *J. Mater. Chem. A* **2015**, *3*, 20673.
[684] W. Li, X. Wang, B. Liu, S. Luo, Z. Liu, X. Hou, Q. Xiang, D. Chen, G. Shen, *Chem. - Eur. J.* **2013**, *19*, 8650.
[685] W. Li, Y.-X. Yin, S. Xin, W.-G. Song, Y.-G. Guo, *Energy Environ. Sci.* **2012**, *5*, 8007.
[686] X. Ge, S. Song, H. Zhang, *CrystEngComm* **2012**, *14*, 7306.
[687] S. Jin, G. Yang, H. Song, H. Cui, C. Wang, *ACS Appl. Mater. Interfaces* **2015**, *7*, 24932.
[688] J. K. Feng, M. O. Lai, L. Lu, *Electrochem. Commun.* **2011**, *13*, 287.
[689] F. Zou, X. Hu, L. Qie, Y. Jiang, X. Xiong, Y. Qiao, Y. Huang, *Nanoscale* **2014**, *6*, 924.
[690] F. Zou, X. Hu, Y. Sun, W. Luo, F. Xia, L. Qie, Y. Jiang, Y. Huang, *Chem. - Eur. J.* **2013**, *19*, 6027.
[691] W. Li, X. Wang, B. Liu, J. Xu, B. Liang, T. Luo, S. Luo, D. Chen, G. Shen, *Nanoscale* **2013**, *5*, 10291.
[692] N. Pereira, M. Balasubramanian, L. Dupont, J. McBreen, L. C. Klein, G. G. Amatucci, *J. Electrochem. Soc.* **2003**, *150*, A1118.
[693] K. C. Klavetter, J. P. de Souza, A. Heller, C. Buddie Mullins, *J. Mater. Chem. A* **2015**, *3*, 5829.
[694] P. R. Abel, K. C. Klavetter, A. Heller, C. B. Mullins, *J. Phys. Chem. C* **2014**, *118*, 17407.
[695] K.-H. Nam, G.-K. Sung, J.-H. Choi, J.-S. Youn, K.-J. Jeon, C.-M. Park, *J. Mater. Chem. A* **2019**, *7*, 3278.
[696] X. Wang, B. Wang, M. Meyerson, C. B. Mullins, Y. Fu, L. Zhu, L. Chen, *Int. J. Mech. Sci.* **2018**, *144*, 158.
[697] P. R. Abel, Y.-M. Lin, T. de Souza, C.-Y. Chou, A. Gupta, J. B. Goodenough, G. S. Hwang, A. Heller, C. B. Mullins, *J. Phys. Chem. C* **2013**, *117*, 18885.
[698] A. Kohandehghan, K. Cui, M. Kupsta, J. Ding, E. Memarzadeh Lotfabad, W. P. Kalisvaart, D. Mitlin, *Nano Lett.* **2014**, *14*, 5873.
[699] C. Yue, Y. Yu, S. Sun, X. He, B. Chen, W. Lin, B. Xu, M. Zheng, S. Wu, J. Li, J. Kang, L. Lin, *Adv. Funct. Mater.* **2015**, *25*, 1386.
[700] X. Wang, L. Fan, D. Gong, J. Zhu, Q. Zhang, B. Lu, *Adv. Funct. Mater.* **2016**, *26*, 1104.
[701] Q. Li, Z. Zhang, S. Dong, C. Li, X. Ge, Z. Li, J. Ma, L. Yin, *Part. Part. Syst. Charact.* **2017**, *34*, 1600115.
[702] K. Shen, N. Lin, T. Xu, Y. Han, Y. Qian, *R. Soc. Open Sci.* **2018**, *5*, 171477.
[703] Y. Zhou, M. Zhao, Z. Wen Chen, X. Mei Shi, Q. Jiang, *Phys. Chem. Chem. Phys.* **2018**, *20*, 30290.
[704] H. Wu, W. Liu, L. Zheng, D. Zhu, N. Du, C. Xiao, L. Su, L. Wang, *ChemistryOpen* **2019**, *8*, 298.
[705] W. Li, L. Ke, Y. Wei, S. Guo, L. Gan, H. Li, T. Zhai, H. Zhou, *J. Mater. Chem. A* **2017**, *5*, 4413.
[706] M. Li, Z. Zhang, X. Ge, Z. Wei, Y. Yao, H. Chen, C. Wang, F. Du, G. Chen, *Chem. Eng. J.* **2018**, *331*, 203.
[707] J. Han, J. Qin, L. Guo, K. Qin, N. Zhao, C. Shi, E. Liu, F. He, L. Ma, C. He, *Appl. Surf. Sci.* **2018**, *427*, 670.
[708] M. F. L. D. Volder, S. H. Tawfick, R. H. Baughman, A. J. Hart, *Science* **2013**, *339*, 535.

[709] W. Zhang, Y. Liu, Z. Guo, *Sci. Adv.* **2019**, *5*, eaav7412.
[710] Z. Huang, Z. Chen, S. Ding, C. Chen, M. Zhang, *Mater. Lett.* **2018**, *219*, 19.
[711] G. Suo, D. Li, L. Feng, X. Hou, Y. Yang, W. (Alex) Wang, *J. Electroanal. Chem.* **2019**, *833*, 113.
[712] Y.-S. Xu, S.-Y. Duan, Y.-G. Sun, D.-S. Bin, X.-S. Tao, D. Zhang, Y. Liu, A.-M. Cao, L.-J. Wan, *J. Mater. Chem. A* **2019**, *7*, 4334.
[713] Z. Yi, N. Lin, W. Zhang, W. Wang, Y. Zhu, Y. Qian, *Nanoscale* **2018**, *10*, 13236.
[714] J. Zheng, Y. Yang, X. Fan, G. Ji, X. Ji, H. Wang, S. Hou, M. R. Zachariah, C. Wang, *Energy Environ. Sci.* **2019**, *12*, 615.
[715] L. Fang, J. Xu, S. Sun, B. Lin, Q. Guo, D. Luo, H. Xia, *Small* **2019**, *15*, 1804806.
[716] Q. Yang, Z. Wang, W. Xi, G. He, *Electrochem. Commun.* **2019**, *101*, 68.